year ??

VELOCITY AND ATTENUATION DISPERSION IN CARBONATE SEDIMENTS, KANEOHE BAY, OAHU

A THESIS SUBMITTED TO THE GRADUATE DIVISION OF THE
UNIVERSITY OF HAWAI'I IN PARTIAL FULFILLMENT
OF THE REQUIREMENTS FOR THE DEGREE OF

MASTER OF SCIENCE

IN

GEOLOGY AND GEOPHYSICS

By

Stefano F. Baffi

1999

THESIS COMMITTEE

Roy H. Wilkens, Chairman
Fred K. Dunnebier
Gerard J. Fryer

We certify that we have read this thesis and that, in our opinion, it is satisfactory in scope and quality as a thesis for the degree of Master of Science in Geology and Geophysics.

THESIS COMMITTEE

_____

Chairman

_____

_____

ACKNOWLEDGEMENTS

The first and biggest thank goes to my family, who allowed me to be here and write this thesis. Then, I am very grateful to my advisor Dr. Roy H. Wilkens, whose wise and explicative help always put me out of difficult things and inexperience. A great thanks to my committee members, Dr. Fred K. Dunnebier and Dr. Gerard J. Fryer.

Thank to Dr. Mike Richardson and to all the staff at the Naval Research Laboratory for providing most of the core data, to Dr. Janet Becker who helped me a lot in a better understanding of the mathematics involved in this project, and to Dr. Horst Brandes for allowing me to use his laboratory facility at the Civil Engineering Department.

Finally, thanks to Carola for being the way she is and being always there.

ABSTRACT

New composite transducer materials were used to obtain compressional and shear waveform signals in carbonate sediments in Kaneohe Bay, Oahu, in a continuous frequency interval between 20 and 100 kHz with a 1μm sampling rate. The acoustic tests, coupled with short diver core sampling, were performed in sediments that are primarily calcite composed, but different in grain size, environment energy, and sorting. Horizontal spacing between the transducers was fixed at 0.30 meters approximately.

After spectral analysis of the waveforms, effective attenuation was calculated from both the in-situ data and from the core samples at ultrasonic frequency (400 kHz), by using pulse techniques. Compressional wave velocity dispersion, slight but constant, was found in the coarser sediments with dispersion gradients decreasing from 0.14 to 0.09 m/sec-kHz with decreasing grain size. The finer sediments (clays and muds) show very little variability, with a velocity gradient of 0.04 m/sec-kHz. Attenuation has the same variability pattern, ranging from 40 to about 100 dB/m for the sandy materials and from 11 to 18 dB/m for the finer sediments.

The Biot-Stoll theory was tested on these data and a mathematical model was implemented to determine if a model fit to the observed wave dispersion could yield reasonable attenuation and sediment properties and, conversely, if the constraining inputs derived from cores and literature could correctly predict in-situ wave dispersion and attenuation. The last objective was the determination of the exponent (n) in the discussed attenuation-frequency relationship, within the investigated frequency interval.

In-situ compressional wave velocities were simulated with the actual core estimations, leading to a general agreement with the in-situ wave velocity data, but the overall dispersion was not matched. Good agreement with the in-situ dispersion was obtained for permeability values different than those estimated from the core analysis. Such modeling approaches showed a clear difference between in-situ and simulated attenuation, since the model outputs intrinsic attenuation and the in-situ data represent effective attenuation. A third modeling approach attempted to determine if "scattering" effects could be reduced within a reasonable range of sediment properties, but the compressional wave dispersion could not be matched for a corresponding fit of the in-situ effective attenuation.

The frequency dependence of the modeled intrinsic attenuation for the sandy sediments also showed good agreement with the in-situ data, with exponents in the attenuation-frequency relationship equal to 0.43 and to 0.51, thus excluding a linear dependence of frequency over the investigated frequency interval. Simulations for the finer sediments did not produce satisfactory results, due to the very low variations of attenuation and wave velocity in such materials.

In addition, energy loss due to "scattering" effects is remarkably high in the wave velocity fits for the sandy sediments, and is reduced for simulations using the core data. Control of grain size and sorting on permeability and of biological and hydrodynamic processes on the global geoacoustic response of these sediments seems to be the primary factor influencing the observed differences between in-situ and simulated data.

TABLE OF CONTENTS

LIST OF TABLES

LIST OF FIGURES

LIST OF SYMBOLS

Symbol	Significance [Unit]
α	Effective or Intrinsic Attenuation Factor [dB/m ; Nepers/m]
α_{ref}	Reference Attenuation Factor [dB/m ; Nepers/m]
ΔG	Specific Gravity Difference
$\Delta t_{arrivals}$	Time Interval between First Arrivals at Near and Far Receivers [μsec]
ϕ	Porosity
γ	Seawater Specific Weight [64 lb/ft]
η	Pore Fluid Viscosity [Pa-sec]
κ	Flow Correction Factor
μ_b	Frame Shear Modulus (Real and Imaginary) [Pa]
ρ	Sediment Saturated Density [kg/m^3]
ρ_b	Sediment Bulk Density [kg/m^3]
ρ_g	Grain Density [kg/m^3]
ρ_f	Pore Fluid Density [kg/m^3]
σ_{frame}	Frame Poisson's Ratio
$\sigma_{mineral}$	Mineral Poisson's Ratio
τ_{vert}	Vertical Stress [Pa]
ω	Angular Frequency [radians]
ζ	Divergence of Displacement Vectors u and U Times the Medium Porosity
a'	Structure Factor [1-3]
a	Pore-Size Parameter [m]
A_s	Averaged Amplitude in Sediment
A_w	Averaged Amplitude in Seawater

Symbol	Significance [Unit]
C	Biot's Complex Elastic Coefficient [Pa]
D	Biot's Complex Elastic Coefficient
D_m	Median on Grain Size Distribution Curve (also D_{50})
D_{10}	Effective Grain Size
e	Void Ratio, Vector Displacement Difference
f	Frequency [Hz]
f_{ref}	Reference Frequency [Hz]
$F(\kappa)$	Complex Function for High-Frequency Pore Fluid Flow
$<h_r>$	Average Hydraulic Radius [cm]
k	Hamilton's Proportionality Factor
K	Dynamic Permeability
	[cm^2, m^2, mdarcy ,darcy, cm/sec, m/sec]
K_b	Frame Bulk Modulus (Real and Imaginary) [Pa]
K_f	Pore Fluid Bulk Modulus [Pa]
K_r	Grain Bulk Modulus (Real and Imaginary) [Pa]
$<K_i>$	i^{th} Dynamic Permeability of the i^{th} Thickness
	[cm^2, m^2, mdarcy, darcy, cm/sec, m/sec]
$<K_{geo}>$	Average Geometric Dynamic Permeability
	[cm^2, m^2, mdarcy, darcy, cm/sec, m/sec]
l	Complex Wavenumber (Real and Imaginary)
m	"m" Parameter
M	Biot's Complex Elastic Coefficient
Q^{-1}	Dissipation Factor
u	Pore Fluid Displacement Vector
U	Skeletal Frame Displacement Vector

v	Phase Velocity [m/sec]
z_i	i^{th} Core Depth Interval thickness

PREFACE

Acoustic waves in ocean sediments may be seen as a particular case in a more general category of mechanical waves in fluid-saturated porous media. The seabed and its acoustic properties are of interest to geologists, geophysicists, and ocean engineers in relation to marine construction, interpretation of sidescan sonar data, locating buried toxic waste materials and in naval military applications (Stoll, 1989; Richardson, 1986; Kibblewhite, 1989). The first significant study of the acoustic properties of the seabed arose from the application of high-frequency sonar to detect objects lying on the sea bottom, or buried in seabed sediments (Ogushwitz, 1985). The interest in such waves has been focused on different frequency and amplitude ranges over time, generally a function of the researcher's main interest.

In this work, we present the analysis and discussion of acoustic data in a frequency range between 20 and 100 kHz, collected in 1998 in different carbonate sediments at three different locations in Kaneohe Bay, Oahu, Hawai'i. New transducer materials allowed us to measure the dispersion of compressional wave velocity and attenuation parameters in the same location over an extended frequency range, rather than at a single discrete frequency. Core samples were collected in order to determine sediment properties. We observed wave velocity dispersion in the coarser of the investigated sediments, but not in the finer ones. The data have been used to test the existing theories on sediment geoacoustic properties (Hamilton and Biot-Stoll models), by implementing a mathematical model that uses measured sediment physical parameters, and attempts to reasonably match the measured wave velocities and attenuation.

By inputting the core data into the model, the wave velocity was fitted only qualitatively since the overall dispersion could not be matched. Good fits to the compressional wave velocity dispersion were obtained for porosity values close to those estimated or calculated from the cores, but for lower values of permeability. This effect may be controlled by sediment parameters like grain size, compaction and sorting that are hardly known a priori from acoustic data.

CHAPTER 1

GEOLOGICAL SETTINGS

1.1 Regional Geology of Oahu

The geologic history of the Hawaiian Islands and of the island of Oahu has been extensively discussed and presented in several works (Stearns and Vaksvik, 1935; Stearns, 1966; Macdonald and Abbott, 1970). It is proved that Oahu developed through the coalescence of the Waianae shield volcano from the western part of the island, and the younger Koolau shield volcano from the eastern part. The Waianae Range on the west and the Koolau Range on the east are the actual eroded remnants of the two volcanoes. Rocks from these volcanoes are named respectively the Waianae Volcanic Series and the Koolau Volcanic Series.

The initial stage of relief building ended in a period of volcanic quiet, probably spanning 2 million years. During this time, a thousand meters deep canyons were cut into the eastern part of the Koolau shield, alluvium was accumulated as the island sank for at least 360 meters. and streams carved out many deep amphitheater-headed valleys. This erosional stage persisted until only narrow divides remained between the valleys on both sides of the Koolau Range. After the quiescence period, volcanic activity returned with magmas of very different composition from the older Koolau rocks. Lava flows, cinder and tuff cones were formed and are actually known as the Honolulu Volcanic Series.

1.1.1 The Waianae Volcanic Series

Erosion has removed most of the western portion of the Waianae shield complex, exposing the internal structure of the volcano. The caldera of the Waianae volcano extended for about 14.5 kilometers, and the shield structure was built by eruptions that took place principally along three rift zones. The Waianae series is divided into three members (lower, middle, and upper): the lower and most of the middle members consist of rocks of tholeiitic groups, whereas alkalic basaltic rocks begin to appear at the top of the middle member. Hawaiite and lesser amounts of alkalic olivine basalt largely form the upper member.

1.1.2 The Koolau Volcanic Series

The Koolau volcano was built by eruptions along a northwest trending rift zone, thus resulting in an unusual elongated shield. Its caldera was about 13 kilometers in length and at least 6.5 kilometers in width, extending from beyond Kaneohe at the northwest, to Waimanalo at the southeast. Almost all the rocks forming the Koolau Volcanic Series are tholeiitic basalts and olivine basalts, with amounts of oceanite. In the original systematic study of the geology of Oahu, some caldera-filling weathered rocks were believed to belong to an older volcano, buried by the Koolau shield, and thus grouped under the Kailua Volcanic Series. Later studies have shown that these rock are unquestionably part of the Koolau volcano (Stearns, 1940).

Within the Kaneohe area, the heads of the valleys were eroded until they merged with a resequent fault-line scarp of the exhumed caldera, to form the Koolau Pali (Macdonald and Abbot, 1970). The Pali is a steep cliff that rims much of the Kaneohe watershed. Lavas from the Koolau volcano formed the sloping surface of the Schofield Plateau, while banking against the eroded slope of the Waianae volcano.

1.1.3 The Honolulu Volcanic Series

The end of the Koolau activity was followed by a period of erosion during which great part of the eastern flank of the shield was removed. Volcanic activity resumed on the southern end of the present Koolau Range with more than 30 separate eruptions, scattered over a period of hundreds of thousands of years (roughly between the mid-Pleistocene to recent).

The arrangement of these eruptions shows no relationship with the older Koolau volcano, although several vents lie along a parallel line to the minor south-southwest trending rift. Further, most of the vents appear to lie almost at right angles to the main rift zones of the Koolau volcano.

It is then doubtful that the Honolulu volcanism could be regarded as a renewal of the Koolau activity. Moreover, the lavas of this series include nephelinites, basanites, and alkalic olivine basalts: all are rich in iron and magnesium, and undersaturated with silica. The eruptions formed cinder, spatter, ash cones, and poured lava flows onto the deeply eroded topography and over the fringing reefs. Diamond Head, Hanauma Bay, Punchbowl, and Tantalus are between the forms resulting from this effusive activity. The volcanic foundation of the Mokapu peninsula, forming the southeast boundary of Kaneohe Bay, was formed by the Honolulu volcanism. (Stearns and Vaksvik; 1935; Stearns, 1966).

1.2 Geology and Evolution of Kaneohe Bay

Kaneohe Bay is located on the northeast coast of Oahu (figure 1.2) and is the largest estuary-lagoon system of the Hawaiian Islands, encompassing an area of approximately 18 squared miles (Bathen, 1968). The adjacent watershed, about 32 squared miles (Moberly, 1963), is drained by at least twelve perennial and intermittent streams. It occupies almost the center position of a deeply dissected volcanic shield, including the northern half of its ancient caldera. The geological history of Kaneohe Bay area is conveniently divided into three major episodes:

- The first is a period of volcanism formed the basement rock of Kaneohe Bay (Stearns, 1966), apparently in pre-Pleistocene. It must be noted that Holocenic volcanic rocks can be found along the shore of the bay, while no volcanic rocks are known to be exposed below the sea level in the bay itself. As exception, several islands present in the bay have visible volcanic cores.

- The second episode is a period of deposition that grossly shaped the region into the present topography. Over the past 50000 years the sea level rose and fell several times (Stearns, 1974), resulting in considerable rates of erosion in the form of valley streams (Roy, 1970), deposition of calcareous material that now is found as limestone (lithified sand dunes), and the apparent soil profile of the basement rock.

- The third episodes starts 12000 years ago, with a sea level probably 100 m lower than the present level (Stearns, 1974). In the subsequent 4000 years the sea level rose rapidly, then at a slower rate for other 4000. The position of the sea level in the remaining 4000 years to the present is object of debate, but most authors place within ± 2 m of the present level.

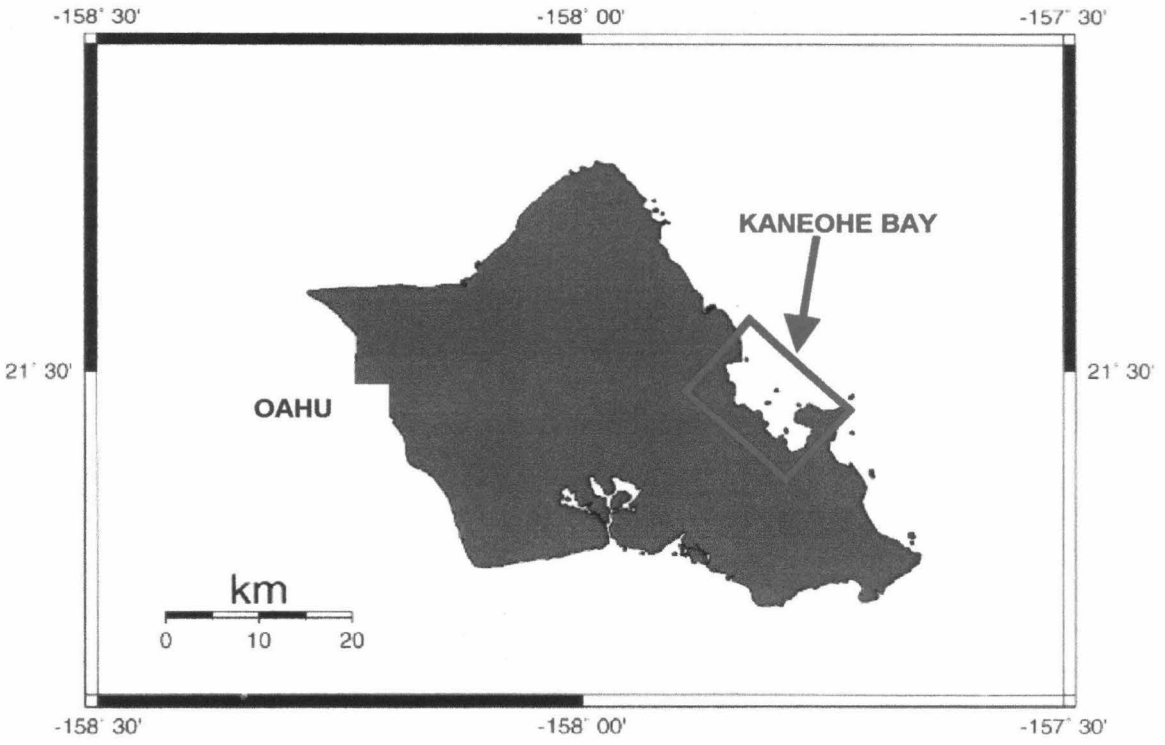

Figure 1.1

Location of Kaneohe Bay on the Northeast side of the island of Oahu

In these 12000 years, Kaneohe Bay went completely below sea level and underwent four major depositional processes and two erosional:

- The depositional processes include the formation of reefs where biogenic calcareous material was produced and then the discharge of terrigenous material in the shallow waters at the stream mouths. The development of the Kaneohe area into water estuarine began with the growth of a barrier and fringing reef across the embayement formed by the Mokapu peninsula and Kualoa Point. As the sea levels changed during the Quaternary, the coral kept its growing rate, maintaining a reef dam across the bay mouth. The third depositional process is the settling of both calcareous and terrigenous materials out of suspension onto a deep-water lagoon floor, in analogy with deep-sea pelagic environment (Roy, 1970). The fourth and final depositional stage consists in the stabilization of calcareous bedload sediment, as the energy of the environment becomes unsuitable for material transport.

- The first erosional process is largely mechanical, probably confined to the seaward portion of the bay. The stream channeling and fresh water discharge through the reef complex may have partly led to the separation of fringing and barrier reef, as well as to the formation of the sand channels that cut each reefs. The second erosional stage is biological and leads to the reef breakdown, as product of activity by mollusks, echinoderms, sponges and other organisms that bore through the rocks.

Ancient shorelines that have existed above the present sea level are marked by wave-cut terraces, nips, sea diffs and lithified sand dunes located as much as a mile inland (Macdonald and Abbott, 1970). Other shorelines, now below sea level, are marked by submerged benches and other wave-cut features, or buried below younger coral and alluvium.

CHAPTER 2

KANEOHE BAY SEDIMENTS

2.1 Physiography of Kaneohe Bay

Kaneohe Bay is generally divided into six physiographic provinces from the bathymetry (Figure 2.1): lagoon, fringing reef, patch reef, deep barrier reef, shallow barrier reef, and sand channels (Bathen, 1968; Roy, 1970). Large embayments in the fringing reef, at the mouths of all major streams, allow terrigenous sediments to be deposited directly into the lagoon area.

The lagoon floor is generally very smooth and slopes gently from the stream mouths to the toe of the barrier reef. Around the lagoon, there are numerous patch reefs, with vertical edges that commonly drop from a few feet below sea level to depths of 13 meters. Moats a few feet deep, but even 30 meters wide are present around the reefs. Deep areas in the lagoon exceed 20 meters of depth and since are found in narrow passes between reefs, their origin is likely to be related either to lower sedimentation rate or sediment scouring (Roy, 1970). Bottom current velocity patterns in the bay support this viewpoint (Bathen, 1968).

Geophysical profiles in the bay from previous works (Hollet, 1977) indicated that the reefs are supported on older buried reefal material, and that the moats could have been originated as a result of sediment scouring. The same profiles (reflection seismic) showed large areas of ponded sediment covering older reef structures, possible evidence of lower sea level stands. The maximum depth of the buried shorelines has been estimated to 40 meters, but based on the sound velocity in very fine and porous materials, where compressional velocities and attenuation show very little dispersion.

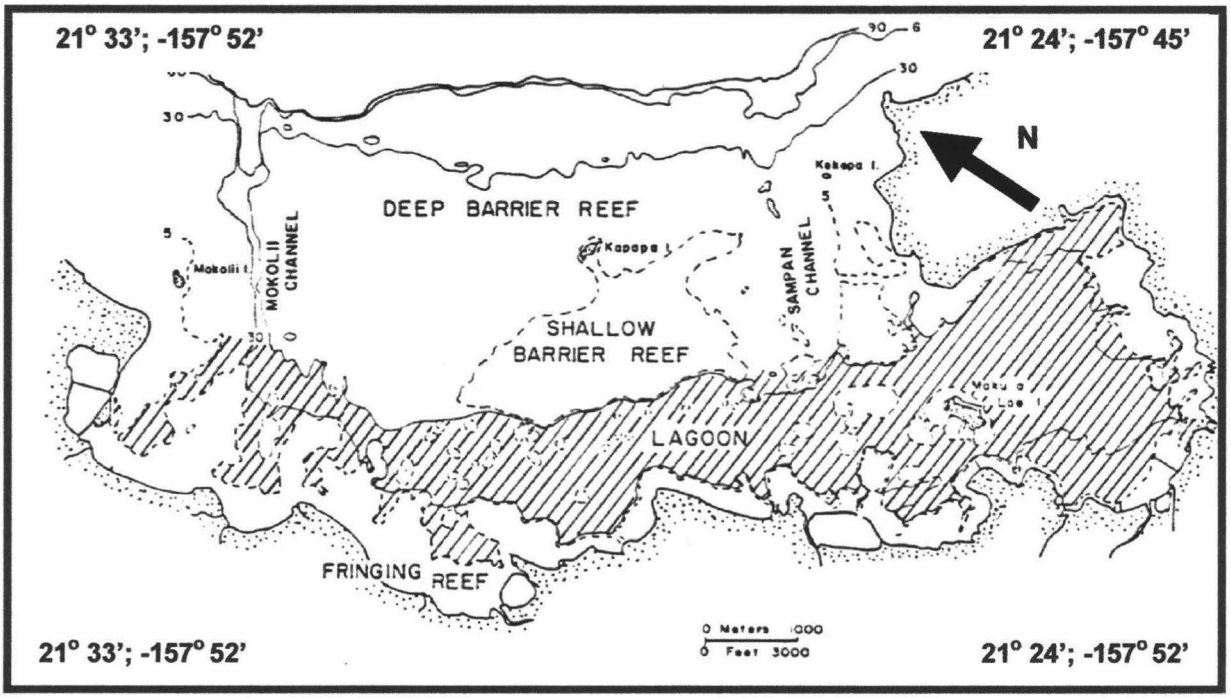

Figure 2.1

Physiographic provinces and general bathymetry

of Kaneohe Bay in feet (after Hollet, 1977).

2.2 Kaneohe Bay Sediment Mineralogy

Various investigators have studied and described the sediments of Kaneohe Bay (Moberly, 1963; Moberly and Campbell, 1969; Roy, 1970; Fan, 1975; Hollet, 1977). In general, the major part of the sediments in Kaneohe Bay consists of $CaCO_3$ (calcareous muds composed of fine-grained calcite or aragonite), while terrigenous rich-clay sediments compose the rest. Aragonite is the predominant mineral derived from coral and framework of the reefs, with a seaward-decreasing pattern. Calcite is the next most abundant mineral, derived from skeletal sands, most of which consist of foraminifera.

High proportions of the lagoon sediments are reef derived, as indicated by the sediment mineralogy (Fan, 1975): patch and fringing reefs are high in aragonite, whereas the lagoon and barrier reef have a low aragonite content. The detrital grains derive from the land and contain no carbonate minerals. Clay mineral distribution in the bay sediments is mostly kaolinite, from the weathering of the watershed volcanic rocks (Fan, 1975). Some land-derived silts and clays are carried onto the fringing reefs. Terrigenous infilling is evident in the southern part of the lagoon, where sediments are characteristically dark brown, as opposite to the gray carbonate material found elsewhere in the bay. Studies of the terrigenous mineral distribution suggest that three basic mineralogical suites can be found in Kaneohe Bay sediments. A primary suite of magnetite, ilmenite, plagioclase, and augite. A secondary suite or weathering products, of hematite, gibbsite, goethite, anatase, montmorillonite, and kaolinite group clays. A third suit, hydrotermal and eolian suite, of quartz, mica, and christobalite.

Mixed opinions exist concerning the origin of the quartz found in the soils and sediments of the Hawaiian Islands: one opinion has it that quartz may be pedogenic (Rex et al., 1969), and another that much of it is of eolian origin (Jackson et al., 1971). Local hydrotermal activity in the southeastern Oahu and in the rocks of the Koolau Range in the Kaneohe Bay region may also be responsible for the quartz found in the bay (Stearns and Vaksvik, 1935).

2.3 Grain Size Distribution and Sedimentation Patterns

Very coarse to fine sand is concentrated on the reef flats. Finer sediments have a size ranging to fine silt and clays. A previous analysis indicates for the finer materials grain size ranging from 2.36 phi to 8.81 phi, whereas for the coarser material the grain size variation is between –0.86 phi to 2.65 phi (Fan, 1975; Hollet, 1977). This size distribution is a direct result of the bay morphology, which controls patterns of currents, waves and stream discharge. Sand transport is accomplished mainly by ripple migration: during this process, the coarse material (entirely calcareous, composed of the skeletal parts of shallow-water marine invertebrates and algae) is reduced in size by mechanical processes (grinding as a result of grain-to-grain friction). Silts and clays are then selectively removed by wave-generated currents and carried lagoonward, to a calmer environment where they settle and mix with the terrigenous material brought by the streams. The coarser sediments, primarily sand-size materials, continue their migration towards the reef edges, settling onto the reefs and sand channels (Moberly and Campbell, 1969).

CHAPTER 3

SEDIMENT LABORATORY ANALYSES

3.1 Sediment characteristics and classification

Short diver push-cores were taken at each experimental site (Figures 3.1 and 3.2), and measurements of porosity, bulk density, and grain size (Figure 3.2) were carried out shortly after core retrieval. Plastic cylinders were pushed into the sediment and sealed from below. Since site H2 processing was not carried on, we decided not to include its pertinent data from now on.

3.1.1 Site H1 Sediments

The sediment found at site H1 is the typical calcareous mud of the lagoonal floor in Kaneohe Bay, with a general fining-upward trend. Clays represent the highest volumetric fraction (between 52% and 72%), then silts (between 29% and 46%): gravel is absent, and sand is present only in traces. Shells fragments are occasionally present at various depths in the cores. Variations of clay and silt fractions lead to classification of this sediment as both clay and mud (Table 3.1). The material is very poorly sorted, coarse skewed, and mesokurtic (Lewis, 1984). There is a noticeable variation in the clay and silt content in the sample between 2 and 12 cmbsf. Porosity averages 0.84 over a 30-cm depth, decreasing downward with increasing sand fraction (Figure 3.3).

3.1.2 Site H3 Sediments

The gravelly sand found at site H3 is poorly sorted, very fine skewed and leptokurtic, with no remarkable variation in classification over the whole core length (Table 3.1). The sand fraction represents over 80% of the total volume, while silts and clays appear only in very low percentage (Figure 3.4). Gravel is primarily represented by mollusk and gastropoda shells, shells or reef fragments, and accounts for an average 10% of the sample. Porosity is almost constant around 0.47, with a spike of 0.63 at 5 cmbsf, most likely due to the presence of finer interbedding, or a shell fragment. Without this value, average porosity would decrease to about 0.44.

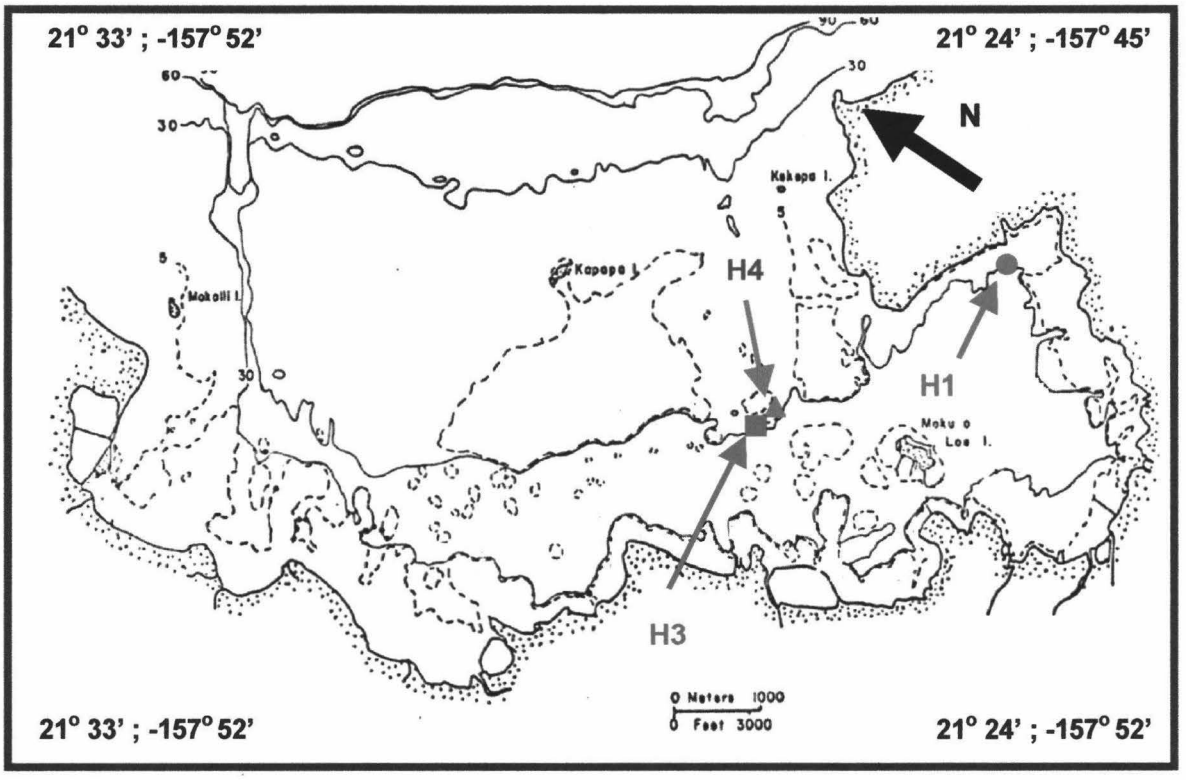

Figure 3.1

In-situ cores sampling and acoustic experimental sites

with Kaneohe Bay bathymetry in feet (after Hollet, 1977).

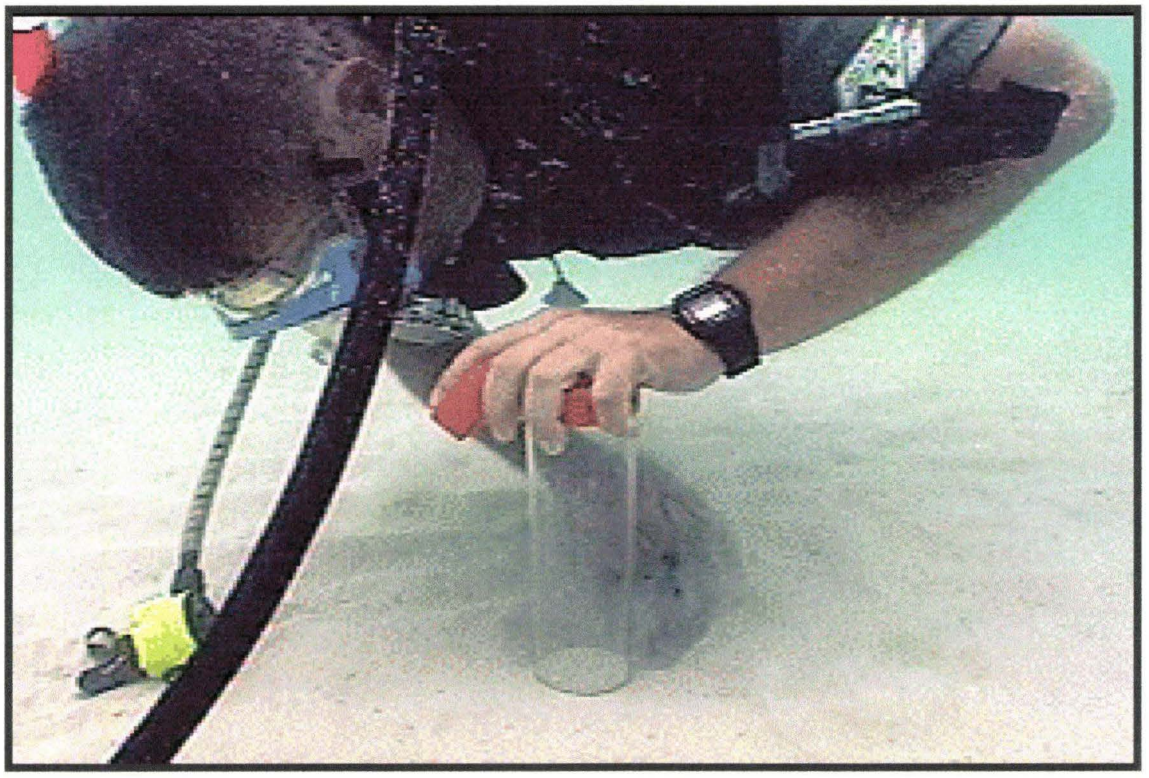

Figure 3.2

Diver scooping sediment below push-core sampler

in Kaneohe Bay sediments at site H1.

3.1.3 Site H4 Sediments

Site H4 is represented by a poorly sorted and leptokurtic sediment, whose classification shows the highest variation, changing from silty to muddy sand, to slightly gravelly sand at some depth intervals. Gravel size is present in traces, sand is around the 75% of the volumetric fraction, silt is 18%, and the clay fraction is around 5% (figure 3.5).

Table 3.1.

Classification of sediments from core samples.

Depth (cmbsf)	Core H1-3	Core H3-2	Core H4-2
1	Mud	Gravelly Sand	Silty Sand
3	Clay	Gravelly Sand	Silty Sand
5	Clay	Gravelly Sand	Silty Sand
7	Clay	Gravelly Sand	Silty Sand
9	Clay	Gravelly Sand	Slightly Gravelly Muddy Sand
11	Clay	Gravelly Sand	Silty Sand
13	Mud	Gravelly Sand	Silty Sand
15	Mud	Gravelly Sand	Silty Sand
17	Mud	-	Slightly Gravelly Muddy Sand
19	Mud	-	Muddy Sand
21	Mud	-	Silty Sand
23	Mud	-	Slightly Gravelly Muddy Sand
25	Mud	-	Silty Sand
27	Mud	-	Silty Sand
29	Mud	-	-
31	-	-	-

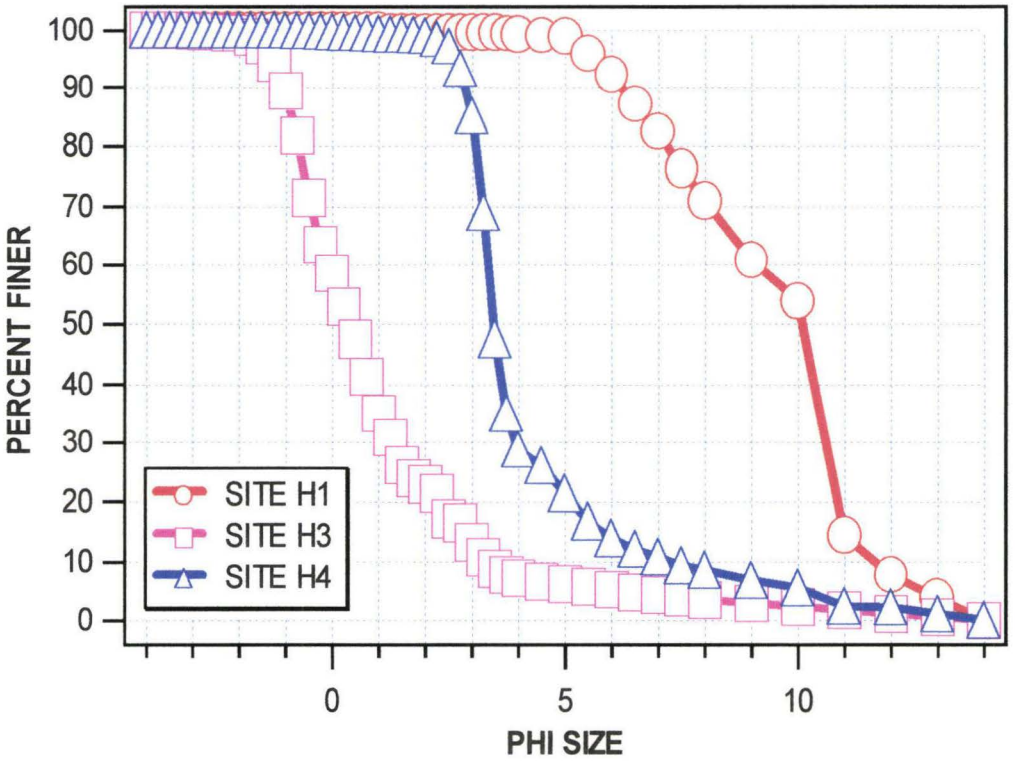

Figure 3.3

Grain size distribution curves for three cores at depth 10 ± 2 cmbsf.

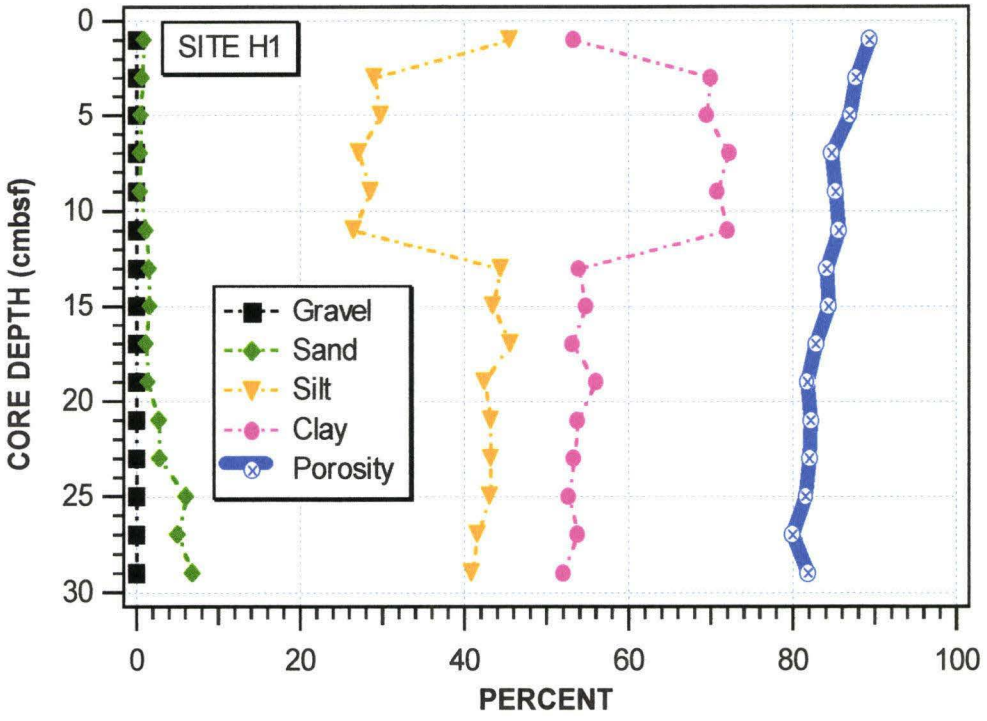

Figure 3.4

Weight fraction variations versus depth for core H1-3.

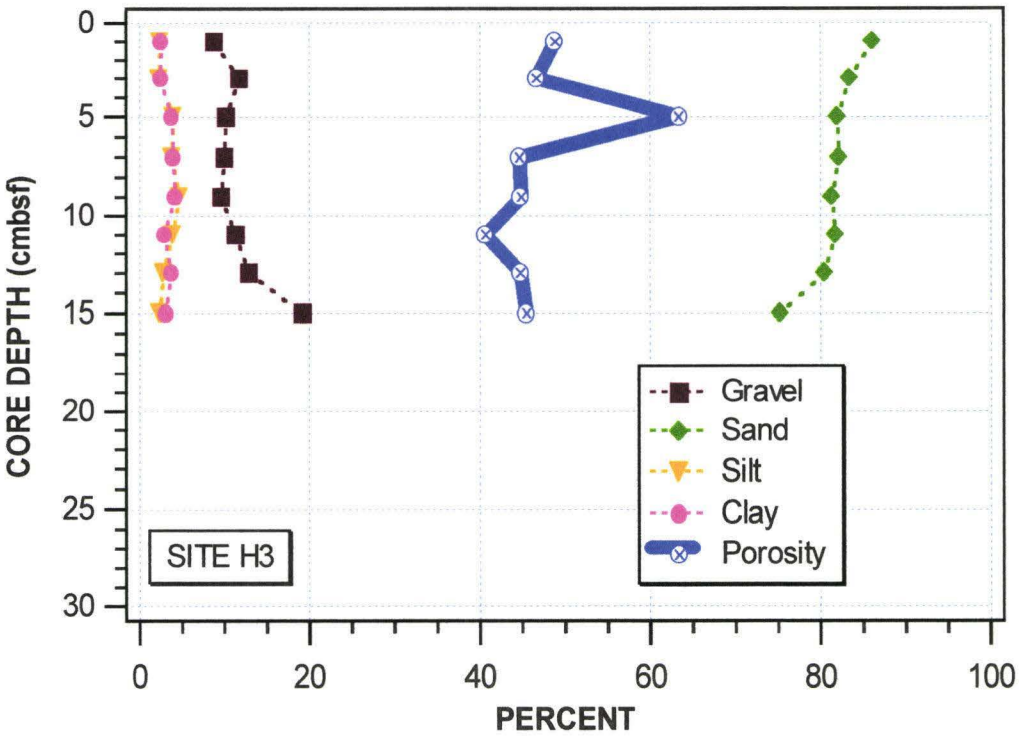

Figure 3.5

Weight fraction variations versus depth for core H3-2.

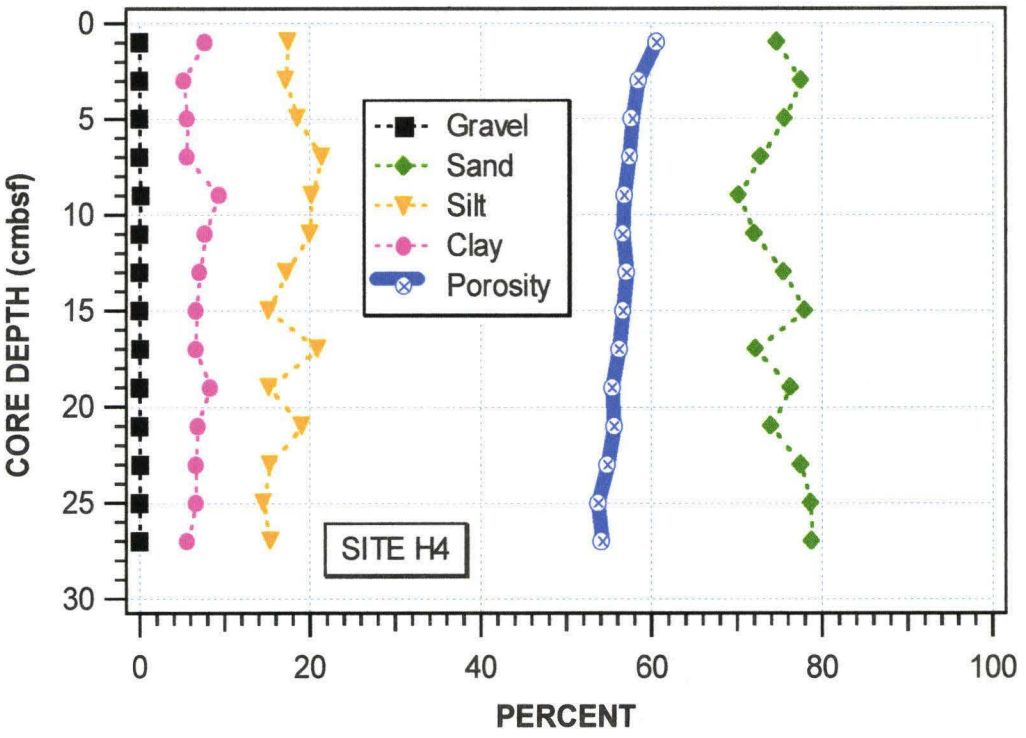

Figure 3.6

Weight fraction variations versus depth for core H4-2.

3.2 Sediment Dynamic Permeability Estimation

We estimated the possible range of sediment permeability for three core samples by using standard and well-known relationships that relate porosity to void ratio and grain size parameters. First, an average hydraulic radius ($<h_r>$) was calculated as a function of the grain size distribution median (D_m) and of the porosity (ϕ) every two centimeters over the core length for three samples (Hovem et al., 1984):

$$< h_r >= \frac{D_m}{6}\left(\frac{\phi}{1-\phi}\right) \qquad (1)$$

The corresponding average permeability was derived by using the Carman-Kozeny equation:

$$< K_i >= 5\frac{< h_r >^2}{\phi} \qquad (2)$$

The geometric average permeability (Donaldson et al., 1996) was finally calculated for the whole core length: it is a reliable measure of media permeability, since it falls between the average arithmetic permeability (which gives more weight to high permeability zones), and the reciprocal average permeability (which, in turn, gives more importance to low permeability zones).

$$< K_{geom} >= \frac{\left(\sum_{i=1}^{n} z_i * \log < K_i >\right)}{\sum_{i=1}^{n} z_i} \qquad (3)$$

In equation (3), z_i is the considered interval thickness.

To account for the influence of the finer sizes on the sediment permeability (a lower permeability may result from a fine matrix), the average permeability was calculated again with the Allen-Hazen equation, by using the effective grain size D_{10}, barely at 10% on the finer grain size distribution curves:

$$< K >= 100 \cdot (D_{10})^2 \qquad (4)$$

The values resulting from the use of the above relationships are shown in Table 3.2. Compressional wave velocity gradients in the cores from sites H3 and H4 tend to be positive with almost constant porosity, suggesting increasing compaction of the sediment (Richardson, 1986).

Table 3.2.

Average permeability and estimated dynamic permeability from the examined cores.

Parameter	Core H1-3	Core H3-2	Core H4-2
Average Porosity	0.84	0.47 (0.44)*	0.56
Median (phi)	10.10	0.37	3.88
Vertical Permeability (m^2)	3.62E-13	1.17E-09	2.45E-11
Horizontal Permeability (m^2)	9.97E-13	1.61E-09	2.56E-11
Average Geometric Permeability (m^2)	6.23E-13	1.30E-09	2.50E-11
Effective Grain Size (phi)	11.71	3.28	7.28
Average Permeability (m^2)	1.48E-14	1.14E-11	2.26E-13

* – if 0.63 at 5-cmbsf subtracted

3.3 Sediment Grain Density Estimations

Grain density ρ_g was calculated from the known core bulk density and porosity (Figures 3.6 and 3.7), resulting in an average of 2740 kg/m^3, with standard deviation 0.02 for all the samples. We used the inversion of the following equation (Donaldson et al., 1996):

$$\rho_b = \phi \cdot \rho_f + (1-\phi)\rho_g \qquad (5)$$

Here, ρ_b is the sediment density, ρ_f is the seawater density corrected for 23 °C, and ϕ the porosity.

Table 3.3.

Calculated grain density for each of the examined cores

Depth (cmbsf)	H1-3 Grain Density ρ_g (g/cm^3)	H3-2 Grain Density ρ_g (g/cm^3)	H4-2 Grain Density ρ_g (g/cm^3)
1	2.70	2.74	2.74
3	2.73	2.74	2.73
5	2.84	2.76	2.72
7	2.71	2.73	2.73
9	2.70	2.72	2.73
11	2.73	2.72	2.75
13	2.71	2.74	2.74
15	2.75	2.72	2.75
17	2.70	-	2.73
19	2.71	-	2.74
21	2.75	-	2.73
23	2.73	-	2.77
25	2.74	-	2.75
27	2.71	-	2.74
29	2.71	-	-
31	-	-	-

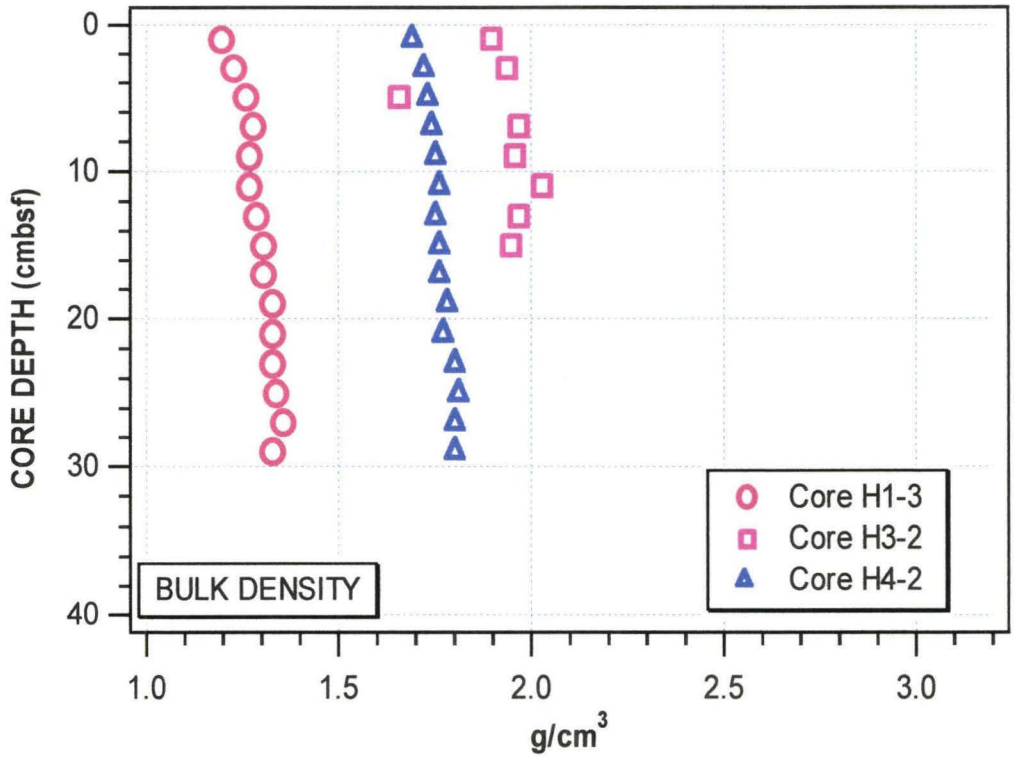

Figure 3.7

Plot of estimated bulk density versus depth for the examined cores.

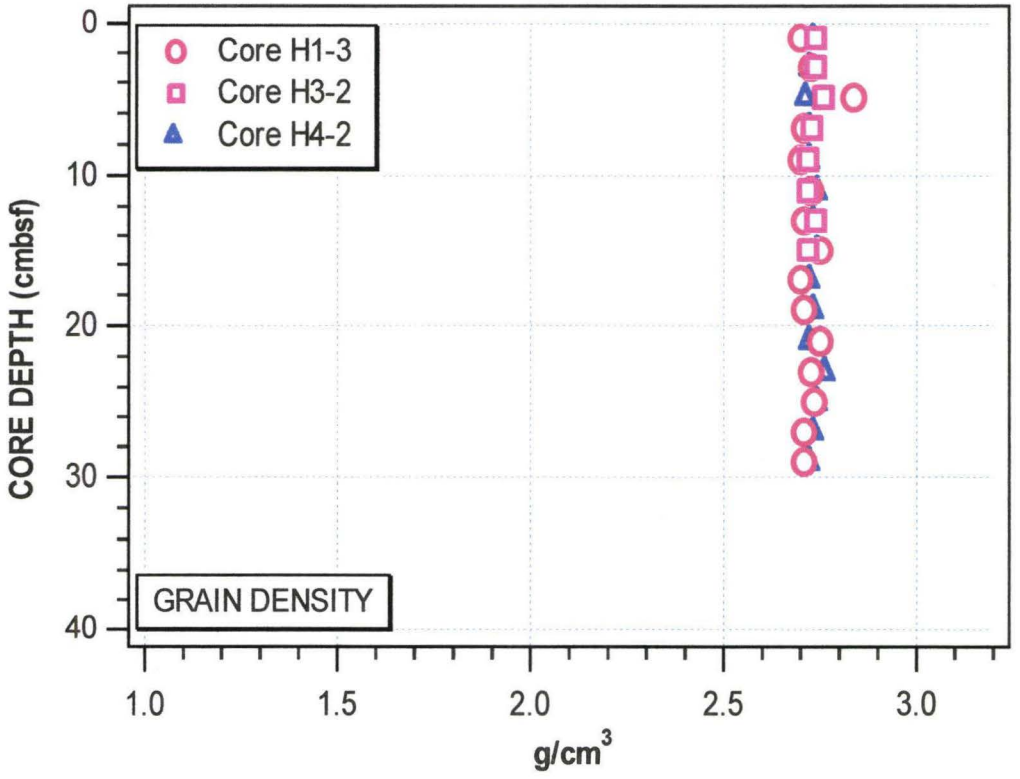

Figure 3.8

Plot of calculated grain density versus depth for the examined cores.

Standard deviation is less than 0.02 for all samples.

CHAPTER 4

LITERATURE REVIEW

4.1 Attenuation Definition and Related Parameters

The term "attenuation" defines very generally the amplitude decrease of a seismic, acoustic, or ultrasonic wave travelling through a medium, or different media (Stoll, 1977). The nature and source of attenuation is rather complex, thus there are various theories and models to explain the attenuation effects and the various dependencies. Attenuation is usually defined with two coefficients (Toskoz et al., 1981):

- Attenuation Coefficient α [dB/m or Nepers/m].
- Dissipation Factor Q^{-1} [dimensionless].

The most used relationship between these two factors is:

$$Q^{-1} = \frac{\alpha \cdot v}{\pi \cdot f} \qquad (6)$$

where v is the phase velocity at a frequency f. The commonly accepted relationship that relates the attenuation factor α to frequency is (Ogushwitz, 1985):

$$\alpha = k \cdot f^{n} \qquad (7)$$

k is a proportionality constant, and value of the exponent (n) is still debated and poorly understood.

For Hamilton (1972), the same relationship can be expressed as function of an attenuation factor α_{ref} extrapolated for a reference frequency f_{ref} (kHz):

$$\alpha = \alpha_{ref} \cdot \left(\frac{f}{f_{ref}} \right)^n \qquad (8)$$

Attenuation of waves in porous sedimentary media are mainly influenced by (Stoll, 1985; Schon, 1996):

- Properties of the skeletal frame (particle bonding, cementation, and porosity).
- Properties of the pore fluid.
- Interactions between solid and fluid components.
- Pressure and temperature.

Attenuation is caused by two mechanisms:

- *Intrinsic Attenuation* is caused by the skeletal frame inelasticity and relative displacement between skeletal frame and pore fluid.
- "*Scattering*", the energy loss due to inhomogeneities of the sediment (gas bubbles, shells) or wave conversion.

The total of all losses is the *Effective Attenuation*. Unconsolidated sediments generally show the highest attenuation among all types of rocks. Increasing pressure results in decreasing

attenuation as a result of the sediment compaction, improvement of grain-to-grain contacts (and energy transfer), and porosity (Ogushwitz, 1985).

4.2 Examined Attenuation Models

There are two lines of the mathematical and physical description for attenuation. The first tends to explain attenuation in terms of generalized equation of linear elasticity, or by modified equations in order to allow certain non-linearities. In most of the cases, these equations describe rheological models and represent macroscopic deformation behaviors as combinations of elastic and viscous parts of an element. The second approach is more concerned about the medium behavior during elastic wave propagation (Schon, 1996).

The Hamilton Viscoelastic model (Hamilton, 1980), assumes that sediment is an isotropic two-phase system (grains and water) for which wave velocity and attenuation are independent of frequency and energy dissipation is proportional to frequency due to grain-to-grain friction. In this model both velocity and energy loss per cycle is constant, meaning that the total energy loss varies as the first power of the frequency. Other developments (Gassmann, 1951) led to models dealing with a closed system with no pore fluid motion, which allow the computation of wave velocities (with known sediment elastic moduli). Wood's equation (Wood et al., 1964), is a particular case of this model with no frame rigidity in the sediment.

The Biot-Stoll model (Biot, 1956; Stoll, 1977; Brunson et al., 1980; Brunson, 1983) introduces viscous losses due to the relative motion between pore fluids and the skeletal frame. The sediment dynamic response to acoustic propagation is dependent on intergranular friction at the contact area between the frame components, as well as the viscosity of the pore fluid. The overall motion of the pore fluid relative to the skeletal frame results in a frequency-dependent damping, and is a function of the material permeability. High-permeability materials (e.g., sands) will follow this relation at lower frequencies than low-permeability materials (e.g., silt).

4.3 Review of Experimental Data

Many experiments over the past 30 years reinforce the conclusion of a first-power dependence between frequency and attenuation. Early measurements in tidal mud demonstrated a convincing linear relationship (i.e., $\alpha = kf^1$), in the frequency range 4-50 kHz (Wood et al., 1964), as well as a terrestrial study of layered sediments in the frequency range 50-400 Hz (Cole, 1965). All other available data for unconsolidated sediments over the frequency range $1\text{-}10^6$ kHz suggested an overall linear relationship and lack of velocity dispersion. Departures from such a relation were attributed to the use of different measurement techniques at different frequencies.

Stoll (1989) demonstrated with laboratory shear wave experiments the validity of viscous losses as a contribution to overall attenuation in silts and sands, under both saturated and unsaturated conditions. Published studies showed non-linear relationships: $\alpha = kf^{1.26}$ in sand over the range 5-500 kHz (Hampton, 1967), $kf^{1.37}$ for clays in the range 4-600 kHz (Tullos et al., 1969), and kf^4 or higher in other sediments (Hampton, 1985). Hamilton (1987) analyzed existing data sets that confirmed a linear dependence at low frequencies, assuming differences in sediments and compaction as the cause of reported variations of attenuation with depth.

As reported by Hamilton (1987), only a small number of investigations have measured compressional and shear waves velocities, both in situ and in laboratory conditions. All concluded that velocity dispersion is negligible or not measurable from seismic frequencies into the MHz range (Birch et al., 1960; White, 1975; Richardson, 1986). Velocity dispersion in high porosity silts and clays has been reported as negligible by many authors both in situ and under laboratory conditions (Urik, 1947; Shumway, 1970; Hamilton, 1970). On the other hand, tests on different sandstones showed velocity dispersion between 0 and 500 kHz, in good accordance with Biot's theory (Winkler et al., 1981). Other tests in silt-clays (Hampton, 1967) over the range 3-200 kHz showed velocity dispersion around of 5%, but further experiments under the same conditions and within the same frequency range did not support the experiment and its results.

Hamilton proposed the possibility that the sediments used in the experiment were not fully saturated. Stoll (1985) shows in situ and laboratory compressional and shear wave velocity dispersion as predicted by Biot's theory: decreasing permeability in the medium increases the dispersion frequency (i.e., dispersion begins at higher frequencies as permeability decreases). In Stoll's model, pore fluid viscosity is considered a function of the frequency and mathematically corrected. Recent experimental marine data in surficial sediments from the Yellow Sea (Zhou et al., 1987), over the frequency range 100-500 Hz show propagation patterns that are explainable with dispersion in both attenuation and velocity.

More recent experimental data from the Baltic Sea, Adriatic Sea, and from the Gulf of Mexico reported the influence of spatial and temporal sediment variability on geoacoustic properties, with subsequent scattering and propagation of high-frequency energy (Richardson, 1983). Other studies on Hawaiian carbonate sediments reported the influence of the acoustic response of microporosity and interbedding (Frazer et al., 1997; Fu et al., 1998).

CHAPTER 5

IN-SITU ACOUSTIC DATA

5.1 Acoustic Data Collection

Acoustic signals (Figure 5.7 shows two waveform examples) were collected at four experimental locations in Kaneohe Bay by using a modified *In Situ Sediment Acoustic Measurement System* (Barbagelata et al., 1991; Richardson, 1993), as well as several short diver cores. Insertion depth in the sediments was 10 cmbsf, while the water depth less than 9 meters. The equipment is designed for measurement of near surface compressional and shear wave velocities. Modifications to the original system design consisted of a linear assemblage of four transducers rather than the original triangular pattern (Figure 5.1 and Figure 5.2) and new transducer materials. Insonification of the sediments at four sites (H1 through H4) was coupled with corresponding measurements in seawater for calibration and eventual determination of the attenuation coefficients α and k. We constructed the transducers of a PZT-polymer composite material that can be used over a wide frequency range, both as source and receiver (Gentilman et al., 1994). The piezocomposite elements consist of 1 cm X 3 cm (6 mm thick) tiles containing a 7 X 24 array of 1 mm diameter PZT rods embedded in a polymer matrix. Their acoustic impedance is close to that of water, electric impedance is high, and the elements exhibit good sensitivity and low noise as receivers. Used as sources, piezocomposites have very efficient transmitting response, and their signal is highly directional. Compressional waves were initially captured in recording oscilloscope, a frequency range between 5 kHz and 150 kHz, with variable steps of 5 kHz or 10 kHz and 1 μsec sampling rate. At site H1 four shear wave signals at low frequency (70 Hz and 100 Hz) were also recorded.

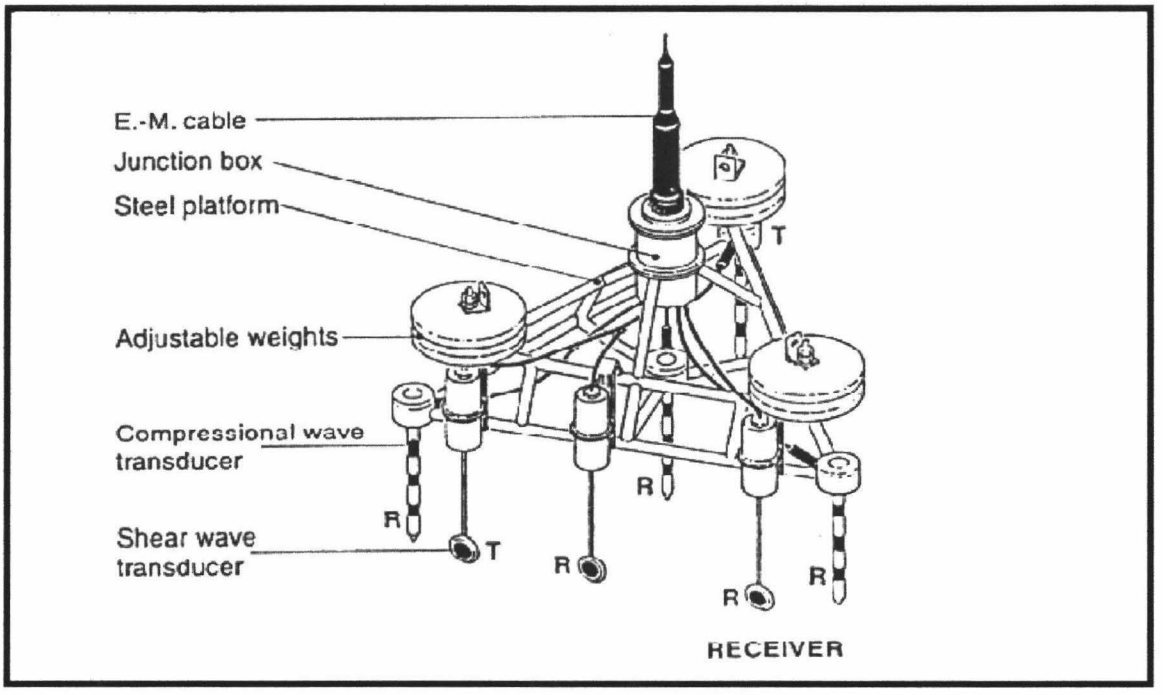

Figure 5.1

Original configuration of the *In-Situ Sediment Measurement System*.

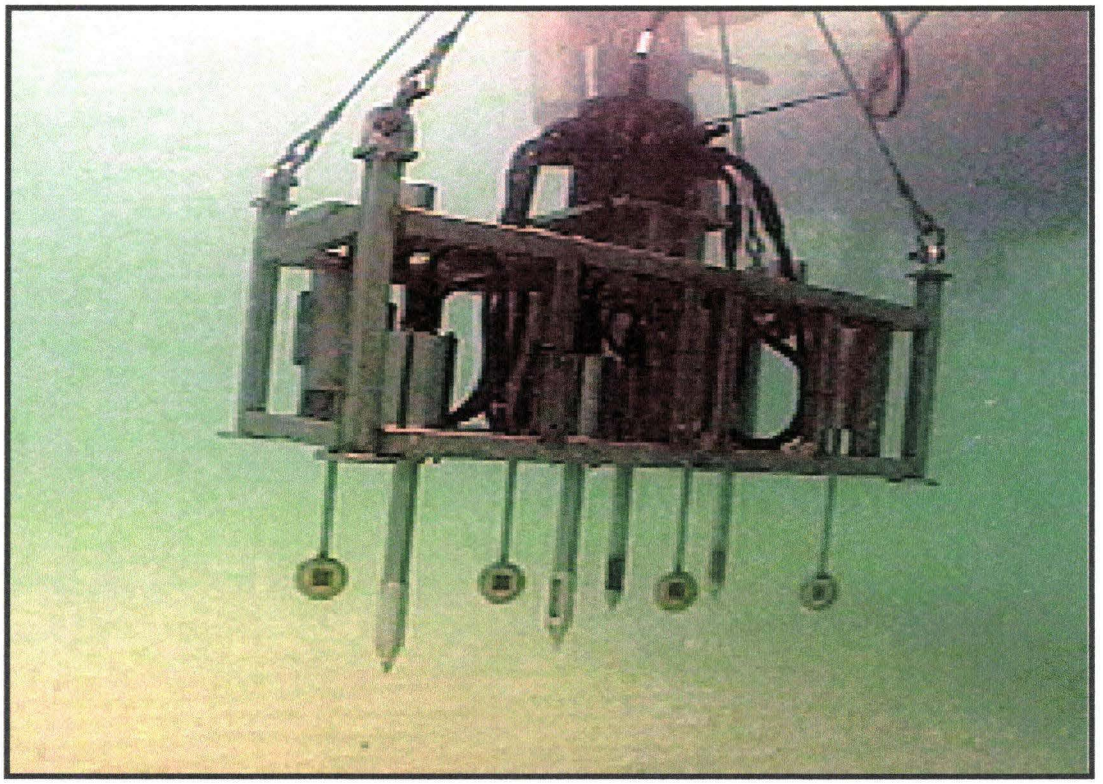

Figure 5.2

Picture of the modified *In-Situ Sediment Measurement System*

during insertion into Kaneohe Bay sediments.

5.2 Acoustic Data Processing: Compressional Wave Velocity

Spectral analysis was performed for each signal, and in practice, we were able to get clean arrivals between 20 and 130 kHz, and essentially monotonic spectra from 20 to 100 kHz (Figure 5.3). For frequencies less than 20 kHz and greater than 100 kHz, marked noise was present, likely caused by resonance phenomena in the transducer materials. Data analysis in this study considers signals between these frequencies. Site H2 data were not used since seawater leaked into the equipment and significantly affected the data.

In-situ compressional wave velocities (Table 5.1 and Figure 5.4) have been calculated by picking first-arrival time difference ($\Delta t_{arrivals}$) for two different transmitter-receiver sets over known and fixed horizontal transducer spacing, and using the following equation:

$$V_p = \frac{spacing}{\Delta t_{arrivals}} \qquad (9)$$

Table 5.1

In-situ compressional wave velocity

Frequency (kHz)	Site H1 Vp (m/sec)	Site H3 Vp (m/sec)	Site H4 Vp (m/sec)
20	1479.78	1687.67	1571.99
30	1479.78	1690.63	1571.99
40	1476.75	1692.62	1576.26
50	1476.38	1697.09	1574.55
60	1477.13	1692.62	1578.85
70	1477.13	1697.65	1577.98
80	1477.13	1700.56	1578.83
90	1476.38	1699.60	1581.43
100	1478.64	1699.60	1580.56

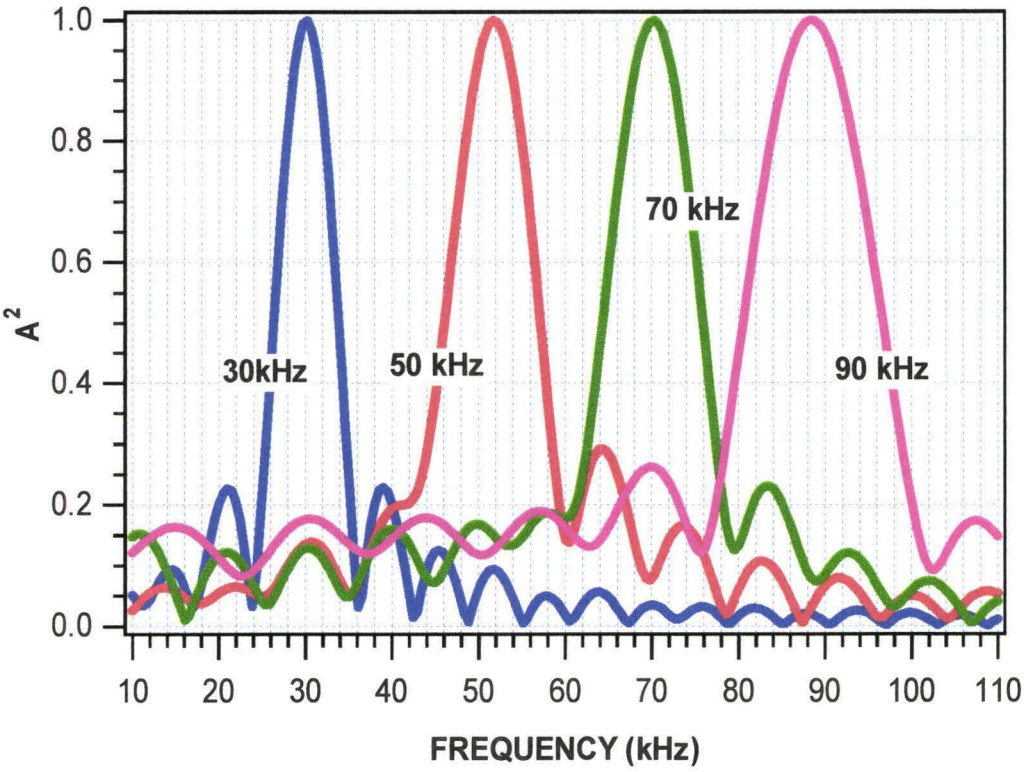

Figure 5.3

Example of monotonic spectra from in-situ compressional signals.

At site H1, we have almost constant compressional wave velocities, between 1476 and 1480 m/sec. Shear wave velocities for the same site, not plotted, average 11.24 m/sec. For this very fine material, ultrasonic compressional wave velocity (at 400 kHz) averaged 1496 m/sec over three cores (standard deviation 7.5 m/sec), and 1496 m/sec at 10 cmbsf, our test depth (standard deviation 0.60 m/sec) as shown in Figure 5.5. The corresponding Poisson's ratio was calculated at 0.50 by considering the average shear wave velocity and the estimated density of 2.74 g/m^3.

At sites H3 and H4 velocities vary: between 1688 and 1701 m/sec for the former and from 1572 to 1581 m/sec for the latter. For site H3 cores, the average ultrasonic compressional wave velocity is around 1535 m/sec (standard deviation 16 m/sec), 1495 m/sec at investigation depth (standard deviation 0.80 m/sec). Ultrasonic compressional wave velocity for site H4 cores at 10 cmbsf is measured at 1605 m/sec (standard deviation 12 m/sec), with an overall average of 1606 m/sec (standard deviation 2.23 m/sec).

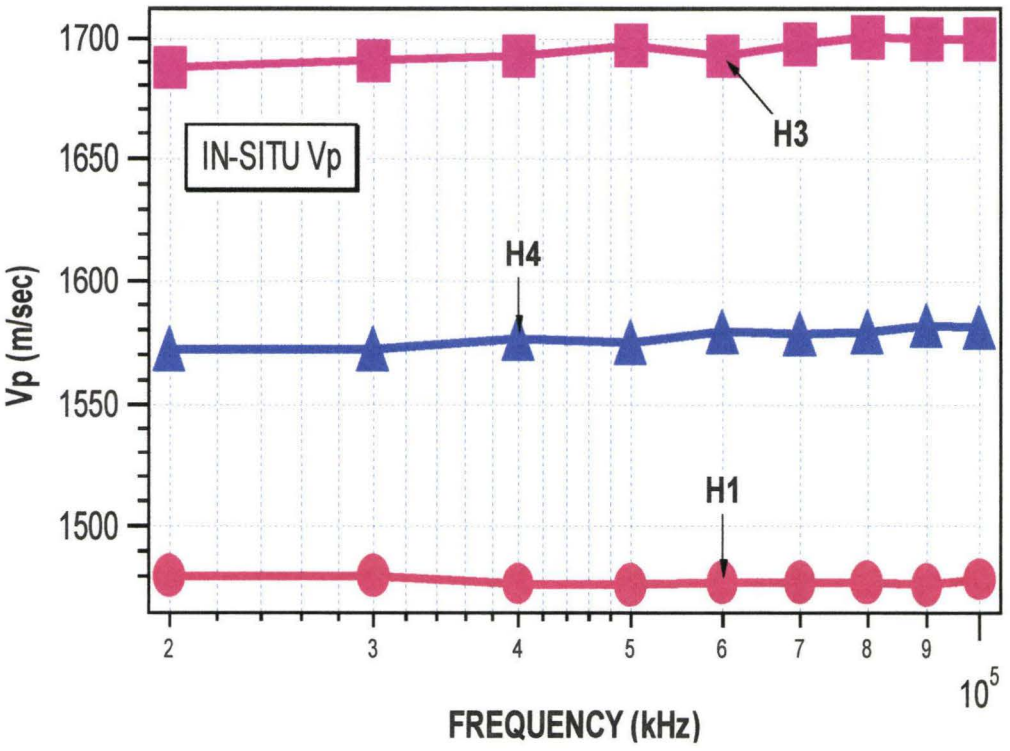

Figure 5.4

In-situ compressional velocity for each test location.

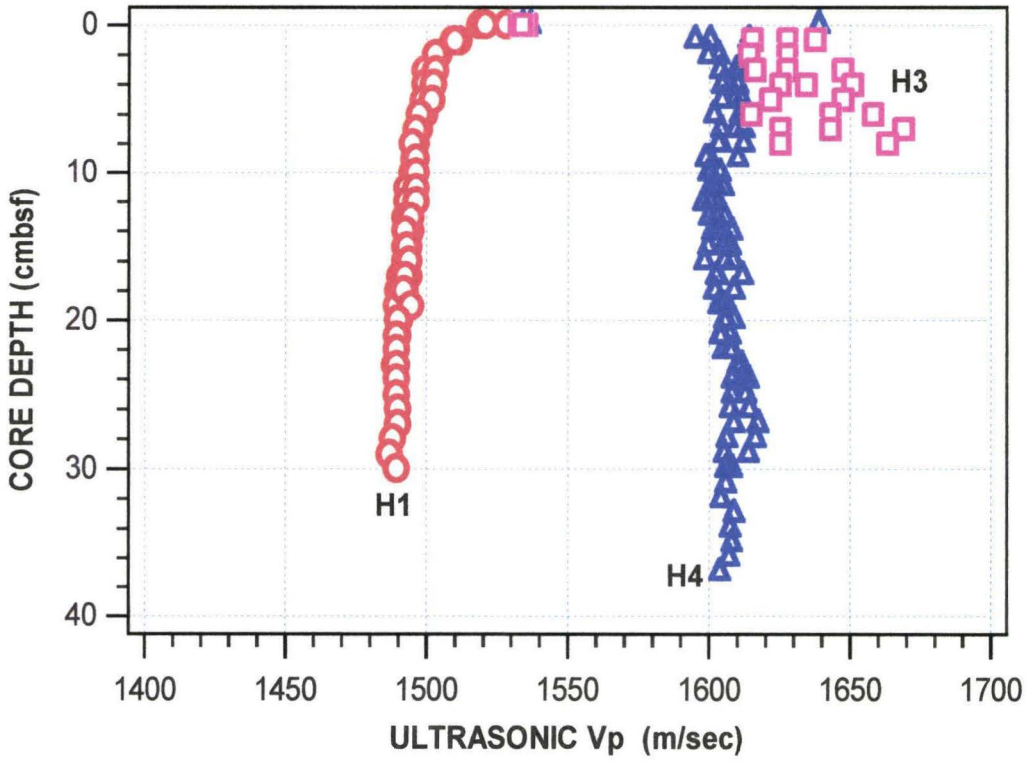

Figure 5.5

Compressional wave velocity in cores

H1-3, H3-2, and H4-2.

5.3 Acoustic Data Processing: Compressional Wave Velocity Dispersion

The average compressional wave velocities have been normalized to the corresponding wave velocities in seawater (Table 5.2, Figure 5.6). Site H1 muds show, as expected from the theory, negligible wave velocity dispersion with a dispersion gradient of 0.04m/sec-kHz and a constant wave velocity ratio of 0.97. Velocity dispersion at the two other sites is more evident: 0.14 m/sec-kHz for the dispersion gradient (velocity ratio of 1.01) for H3, while at site H4 we find a velocity ratio of 1.03 and a dispersion gradient of 0.09 m/sec-kHz.

Table 5.2.

Calculated compressional wave ratios at each experimental site.

Frequency (kHz)	Site H1 Vp(sediment)/Vp(water)	Site H3 Vp(sediment)/Vp(water)	Site H4 Vp(sediment)/Vp(water)
20	0.9718	1.1081	1.0321
30	0.9731	1.1100	1.0321
40	0.9706	1.1113	1.0349
50	0.9704	1.1113	1.0311
60	0.9703	1.1090	1.0344
70	0.9703	1.1123	1.0339
80	0.9703	1.1148	1.0350
90	0.9704	1.1147	1.0372
100	0.9718	1.1130	1.0350

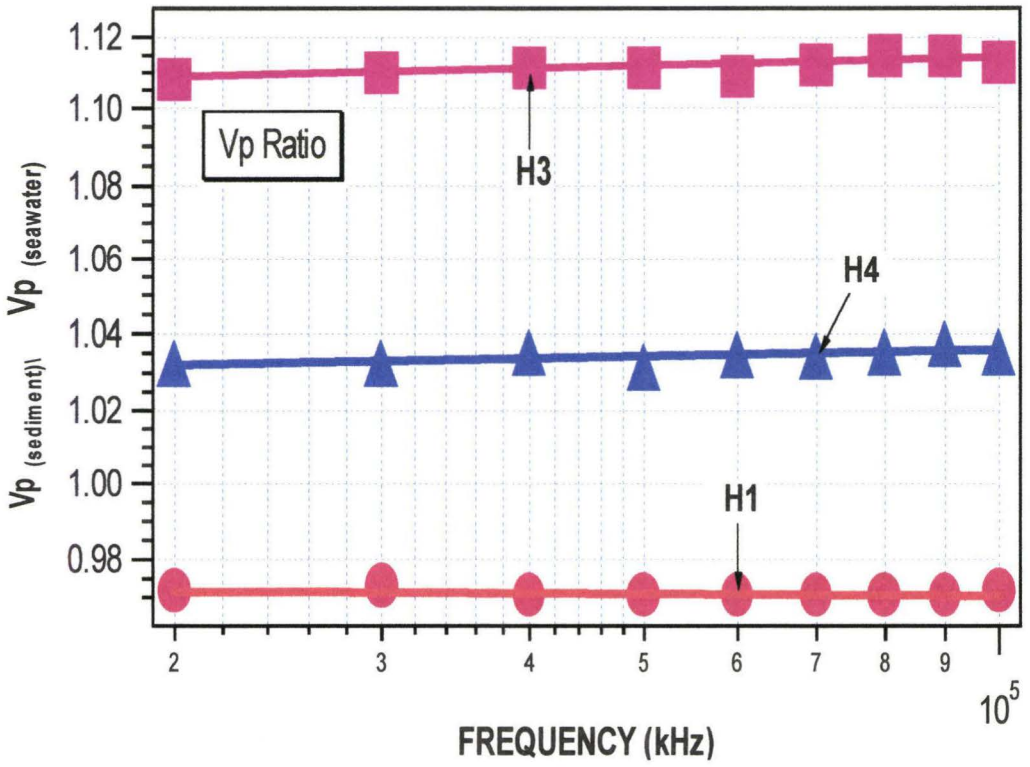

Figure 5.6

Ratio of compressional wave velocity in sediment

to wave velocity in seawater versus frequency.

5.4 Acoustic Data Processing: Effective Attenuation

In-situ effective attenuation (Table 5.3 and Figure 5.8) was calculated using equation (Richardson, 1993):

$$\alpha = \frac{1}{spacing} 20 \cdot \log\left(\frac{A_w}{A_s}\right) \qquad (10)$$

where A_w is the average amplitude of the first three peaks (and troughs) of a signal in seawater, and A_s is the same average for the same frequency signal in the sediment, as shown in Figure 5.6. The effective attenuation factor (α) is expressed in dB/m. The corresponding Hamilton's parameter (k) is α normalized by the frequency f, thus expressed in dB/m-kHz:

$$k = \frac{\alpha}{f} \qquad (11)$$

Table 5.3.

Calculated effective attenuation factors at each experimental location.

Frequency (kHz)	Site H1 Attenuation Factor (dB/m)	Site H3 Attenuation Factor (dB/m)	Site H4 Attenuation Factor (dB/m)
20	18.39	41.86	47.43
30	11.28	55.70	45.00
40	11.99	55.20	42.94
50	10.95	66.67	53.66
60	14.92	77.61	63.59
70	12.03	80.35	65.06
80	13.75	90.94	73.58
90	14.48	99.46	81.29
100	18.35	104.44	85.54

Measuring attenuation is generally a difficult task, especially when there is energy backscattering in the sediment and unknown material phenomena are affecting low and high frequency responses. Therefore, we decided to use a relatively simple estimation of the attenuation parameters, that is consistent with previous ISSMAS experiments.

In-situ values of α at site H1 range between 11 and 18 dB/m. Globally, the power best fits of the data show very low reliability (R^2=0.59), probably due to the very small variation of attenuation of this very fine sediment over the frequency range. The exponent in the attenuation-frequency relationship is about 0.32, with a proportionality parameter equal to 0.40 (Table 5.4). The core effective attenuation factors (Figure 5.9) calculated at 400 kHz average 65 dB/m (standard deviation 8.46 dB/m): with the same average value recorded at 10 cmbsf (with standard deviation 1.9 dB/m). At site H3, in-situ α ranges between 42 and 104 dB/m (R^2=0.97). The exponent (n) is equal to 0.56 and the proportionality parameter is equal to 0.16 (R^2=1). Core attenuation for this site averages 739 dB/m (standard deviation 301 dB/m), while no measurements were made at 10 cmbsf. Sampling disturbance may be the cause of the remarkable attenuation variation over the core sample. For site H4, effective attenuation factors vary from 41 to 85 dB/m. The k parameter is equal to 0.55 (R^2=0.80), while the relationship exponent is about 0.43. Ultrasonic attenuation factors very between 235 and 238 dB/m (standard deviation 28.47 dB/m), with a 10-cmbsf average of 235 dB/m (standard deviation 2.3 dB/m).

Table 5.4.

Calculated effective attenuation power exponent at each experimental location.

Site	Calculated n	Calculated k (dB/m-kHz)
H1	0.32	0.40
H2	0.56	0.02
H3	0.43	0.55

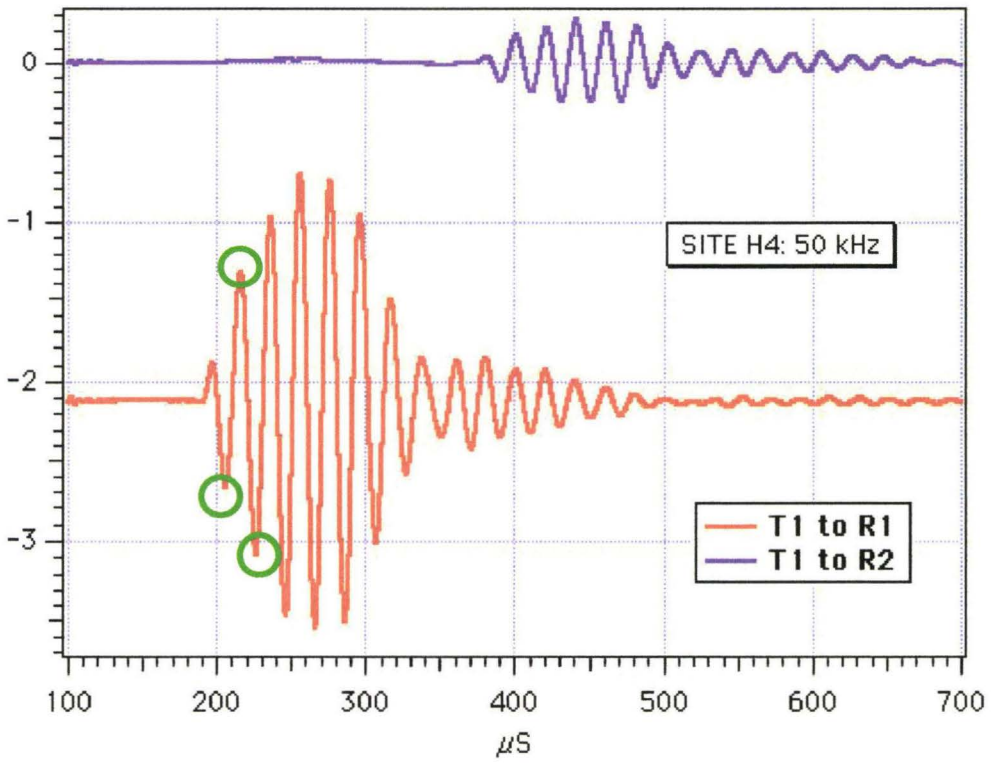

Figure 5.7

Waveforms in site H4 fine sands, frequency 50kHz. The green circles indicate the amplitudes averaged in the attenuation calculation.

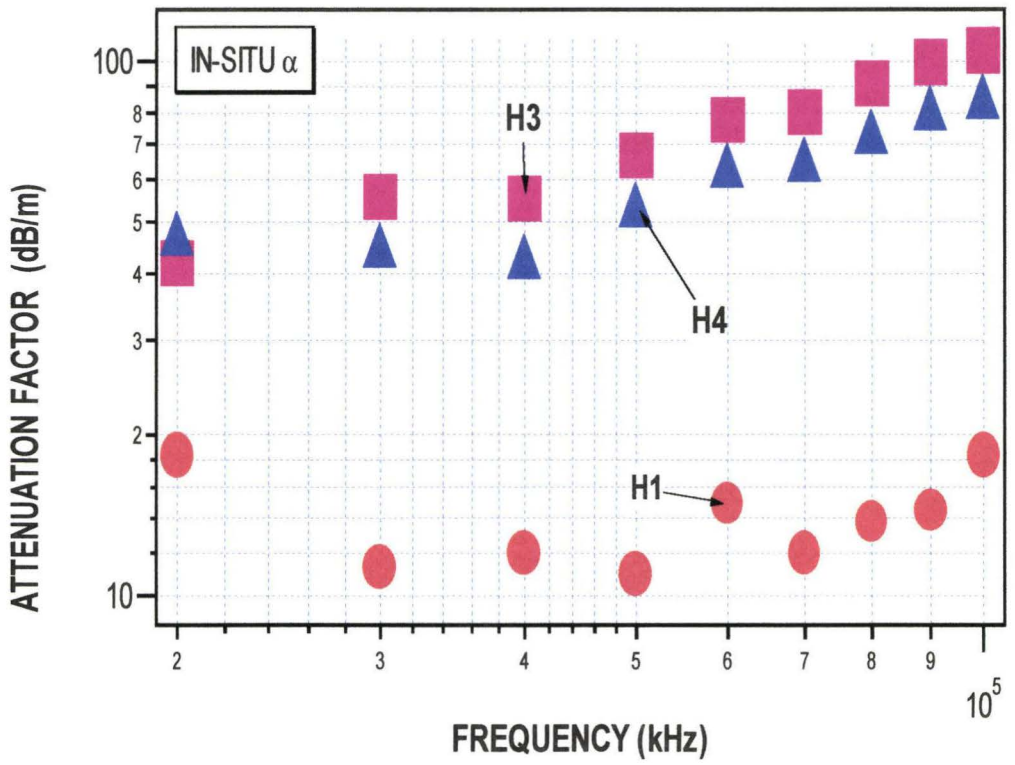

Figure 5.8

Calculated effective attenuation factors versus frequency.

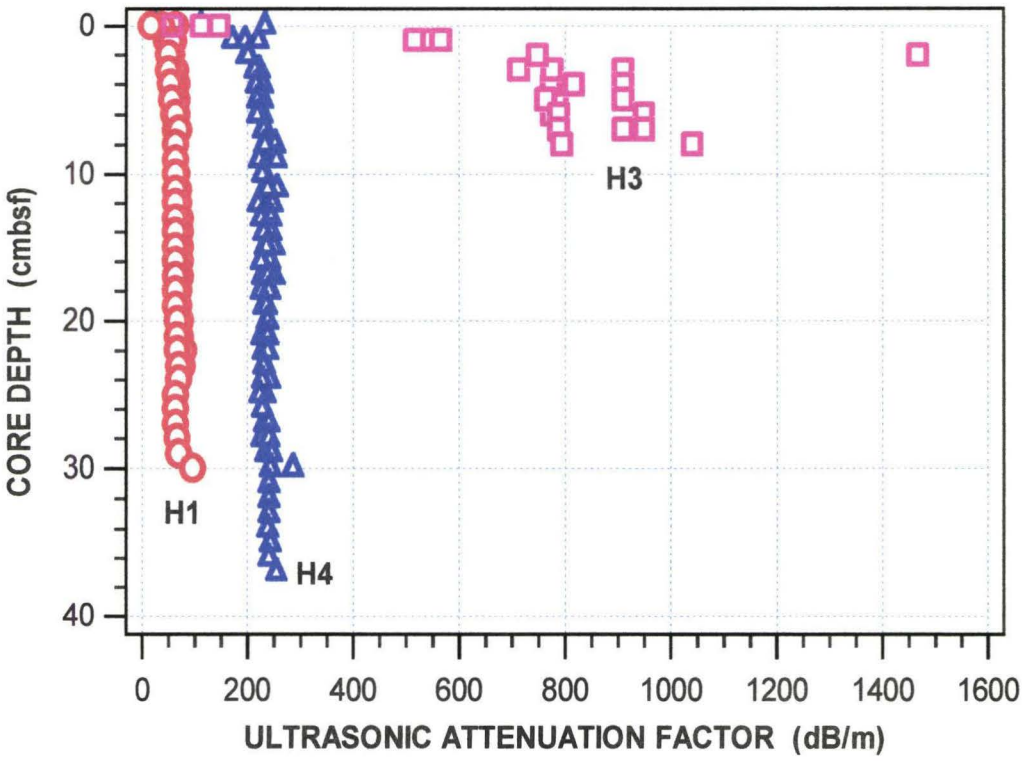

Figure 5.9

Ultrasonic effective attenuation for cores

H1-3, H3-2, and H4-2.

CHAPTER 6

MATHEMATICAL BACKGROUND

6.1 Biot's Fundamental Equations

Biot (1941) developed a comprehensive theory for the static and dynamic response of porous, saturated material. He considered both low and high frequency behaviors, including the possibility of viscoelastic or viscodynamic response in his model components. Biot's theory predicts that three kinds of body waves may exist in a porous, fluid-saturated medium: a "first kind" compressional wave and a shear wave, (similar to waves found in ordinary elastic media), and a "second kind" compressional wave, highly attenuated (Stoll, 1989).

In the case of first kind compressional and shear waves, the motion of the skeletal frame and of the pore fluids are nearly in phase, and attenuation owing to viscous losses is relatively low. Conversely, for compressional waves of the second kind the frame and pore fluids are moving largely out of phase (Biot, 1956). Energy loss is seen to be caused by the frame inelasticity and by the pore fluid viscosity, as it moves relatively to the frame.

Biot's model predicts that sound velocity and consequent attenuation will depend on frequency, on the elastic properties of the frame and of the pore fluids, mean grain size, permeability, and effective stress. The mathematical formulation we used to design our model follows that of Biot (1956) and Stoll (1989). Sediment porosity was assumed constant under small magnitude strains typical of acoustic waves. Biot (1956) derived wave equations both for compressional and shear waves from the constitutive equations, the equations of motions and Darcy's law of flow through porous media.

6.2 Model Governing Equations

The compressional wave equations are conveniently expressed as:

$$\nabla^2(He - C\zeta) = \frac{d^2}{dt^2}(\rho e - \rho_f \zeta) \tag{12}$$

$$\nabla^2(Ce - M\zeta) = \frac{d^2}{dt^2}(\rho_f - m\zeta) - \frac{\eta F}{k}\frac{d\zeta}{dt} \tag{13}$$

where ρ_f is the fluid density, η is the fluid viscosity, k is the dynamic permeability of the frame, ρ_r indicates the sediment grains density. e is the vector describing the pore fluid displacement relative to the skeletal frame, ζ is the divergence of the fluid-frame vectors difference times e, and ρ is the sediment saturated density (Stoll, 1977). D, H, C, and M are the Biots' elastic coefficients:

$$D = K_r\left[1 + \left(\frac{K_r}{K_f}\right)\phi\right] \tag{14}$$

$$C = K_r\frac{(K_r - K_b)}{(D - K_b)} \tag{15}$$

$$H = \frac{(K_r - K_b)^2}{(D - K_b)} + K_b - \frac{4}{3}\mu_b \tag{16}$$

$$M = \frac{K_r^{\,2}}{(D - K_b)} \tag{17}$$

Here K_r is the grain bulk modulus, K_f the pore fluid bulk modulus, ϕ the porosity, K_b is the bulk modulus of the skeletal frame, while μ_b is the frame shear modulus. Stoll (1977) showed that

these constants could be identified with measurable physical parameters and set to be complex in order to incorporate the frame inelasticity.

The parameter "*m" is* given by the equation:

$$m = a'\left(\frac{\rho_f}{\phi}\right) \qquad (18) \quad [a' > 1]$$

The "structure factor a' " accounts for the apparent increase in fluid inertia caused by the tortuosity of pores. Viscous resistance to the fluid flow must be made frequency-dependent to correct the deviations from Poiseuille flow occurring at all but very high frequencies. Further, the inelastic nature of the skeletal frame (owing to frictional losses and relaxation of intergranular bonds) and the local viscous losses (local motion in the fluid at the intergranular contacts) must be accounted for. This local fluid motion is similar to "squeeze film motion" that is well known in the lubrication theory: Biot (1956) suggested it as an additional mechanism of energy dissipation.

In order to incorporate the frequency dependency of viscous flow, Biot derived a complex correction factor to be applied to the fluid viscosity by considering the microvelocity field in the pore channels of an ideal porous media. Biot's solution gives the ratio of the friction force exerted by the fluid on the frame to the average relative velocity. The frequency dependence of the viscous resistance to fluid flow is expressed by the ratio η/k and is replaced by a complex factor $F=F(\eta/\kappa)$ in the frequency domain:

$$F(\kappa) = \frac{\kappa T(\kappa)}{4\left[1 + 2i\dfrac{T(\kappa)}{\kappa}\right]} \qquad (19)$$

T (κ) is given by the complex Kelvin function, while κ is function of angular frequency ω and of the pore size a:

$$T(\kappa) = \frac{ber'(\kappa) + ibei'(\kappa)}{ber(\kappa) + ibei(\kappa)} \qquad (20)$$

$$\kappa = a\left(\frac{\omega\rho_f}{\eta}\right)^{\frac{1}{2}} \qquad (21)$$

Solutions of equation (12) and (13) are assumed of the form:

$$e = A_1 \exp[i(\omega t - lx)] \qquad (22)$$

$$\zeta = A_2 \exp[i(\omega t - lx)] \qquad (23)$$

Direct substitution back in equation (12) and (13) yields to the dispersion relations:

$$\begin{vmatrix} Hl^2 - \rho\omega^2 & \rho_f\omega^2 - Cl^2 \\ Cl^2 - \rho_f\omega^2 & m\omega^2 - Ml^2 - i\dfrac{\omega F\eta}{k} \end{vmatrix} = 0 \qquad (24) \quad \text{[compressional waves]}$$

$$\begin{vmatrix} \rho\omega^2 - \mu l^2 & \rho_f\omega^2 \\ \rho_f\omega^2 & m\omega^2 - i\dfrac{\omega F\eta}{k} \end{vmatrix} = 0 \qquad (25) \quad \text{[shear waves]}$$

The Biot's elastic coefficients are now are complex functions of frequency, derivable by Laplace transformation in the case of viscoelastic operators.

The solutions of the respective determinants lead to the roots:

$$l = l_r + il_i \tag{26}$$

Each root of these equations corresponds to a wave with wavenumber l_r and attenuation l_i. Equation (24) yields two roots: the first corresponds to the "compressional wave of the first kind" (the usual high-phase velocity compressional wave), and the other root corresponds to the compressional wave of the "second kind" (with very low phase velocity and high attenuation). Equation (25) has only one solution, corresponding to a unique shear wave (Berryman, 1980; Stoll, 1989).

CHAPTER 7

MODEL SENSITIVITY TESTS

7.1 Model Testing

After processing of the data, we realized that both sites H3 and H4 exhibited slight but regular velocity dispersion. We decided to use the in-situ data to test the Biot-Stoll model with inputs reasonably reflecting both measured and estimated properties of the investigated sediments. The mathematical background of the Biot-Stoll theory was examined in the previous chapter, while a flow chart and the code are examined in Appendices A and B. In general, a Biot-Stoll model requires an input of at least 13 parameters (Table 7.1): many of them are directly measured, others are found in the existing literature or can be determined by empirical relationships (4), by using properties determined from core and log data. Here, we discuss these parameters and their general influence on the model, tested by varying a single input, even if some of the resulting combinations are not the most probable for naturally occurring sediments (Dutta et al., 1979; Hovem, 1979; Ogushwitz, 1985; Stoll 1989).

7.1.1 Grain and Pore Fluid Properties

Sediment grains may be assigned values of density and bulk modulus (Ogushwitz, 1985). In this case, such values can be considered constant over the range of hydrostatic pressures that are representative of sea bottom conditions. We simulated two different predominant mineralogical assemblages (carbonate and silicate clays) by varying the grain bulk modulus between 47 and 74 GPa and respective grain densities from 2700 to 2800 kg/m^3.

The resulting compressional wave velocity is shown in Figure 7.1, and is generally higher with the increasing bulk moduli (2 m/sec at 50 kHz), while the corresponding attenuation factor shows a low sensitivity (Figure 7.2). Fluid properties are also considered constant and not significantly varying. These properties may be calculated as functions of hydrostatic. We chose to assign a pore fluid density of 1000.0020 kg/m^3, with a bulk modulus of 2.0 GPa.

7.1.2 Porosity

Porosity exhibits a clear control on wave velocity: increasing porosity leads to lower compressional wave velocities. We simulated a modeled porosity increase between 0.40 and 0.55 for coarse and very permeable carbonate sand (Figures 7.3 and 7.4). Since sampling tends to disrupt the natural packing, in-situ porosity for unconsolidated media estimation is considered good to 1 or 2%. Useful but general empirical relations derived from laboratory analysis (of core samples) are given by Hamilton (Hamilton, 1975). These equations estimate porosity as function of depth and sediment type. Void index is generally calculated as a function of the porosity.

7.1.3 Dynamic Permeability

The sediment dynamic permeability can be calculated by empirical relationship (Bryiant et al., 1975; Lambe and Whitman, 1970), or calculated from porosity and grain size parameters as shown in Chapter 3. Since viscous losses in the fluid dominate the overall energy dispersion and attenuation, variations in dynamic permeability with fixed porosity lead to a frequency increase in the main velocity dispersion shift (Figures 7.5 and 7.6). In coarse permeable sediments, this effect begins at relatively low frequencies. Velocity, with fixed porosity, varies little with changes in permeability.

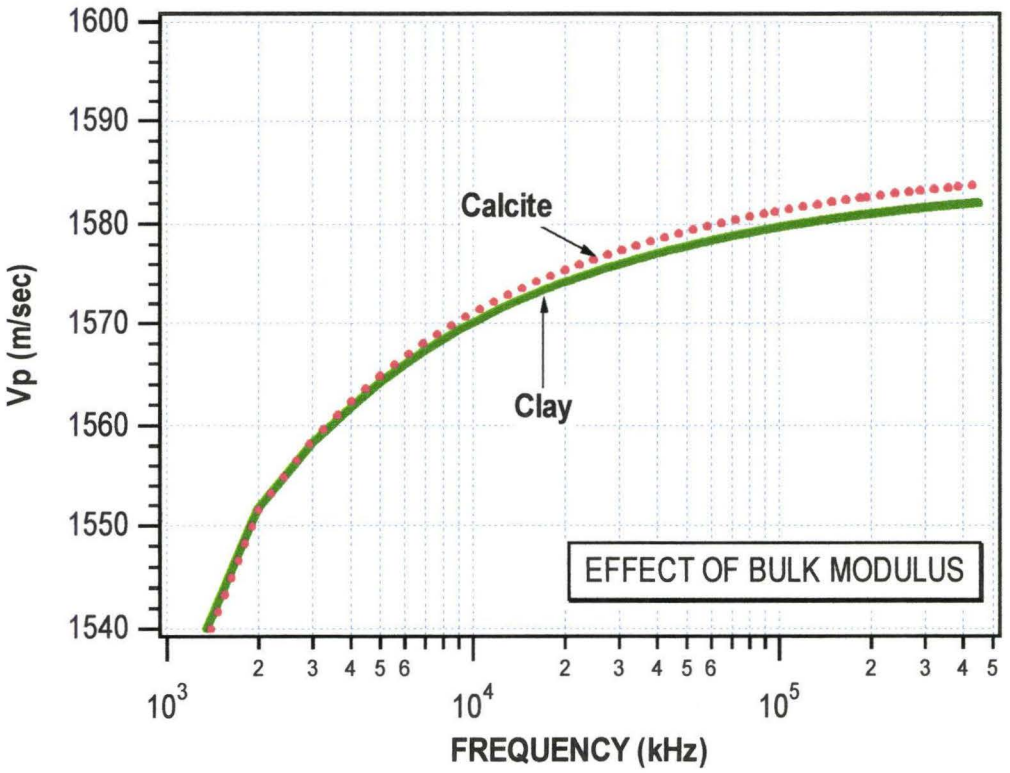

Figure 7.1

Effect of density and bulk modulus variation on compressional wave velocity.

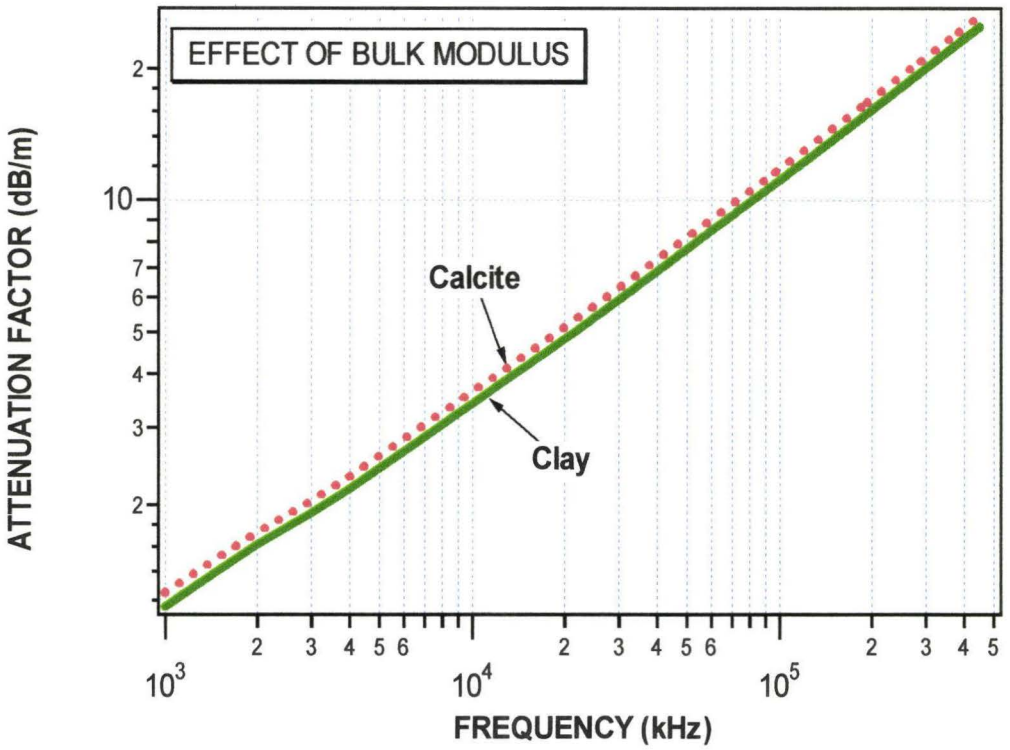

Figure 7.2

Effect of density and bulk modulus variation on

intrinsic attenuation factor α.

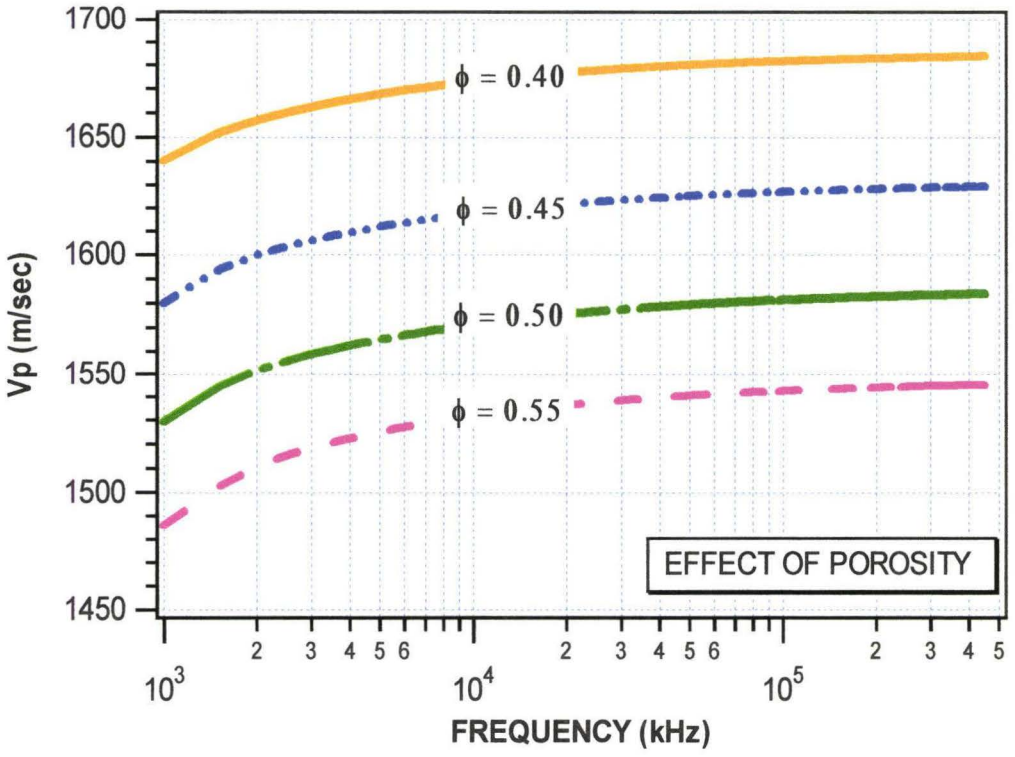

Figure 7.3

Effect of porosity increasing on compressional wave velocity.

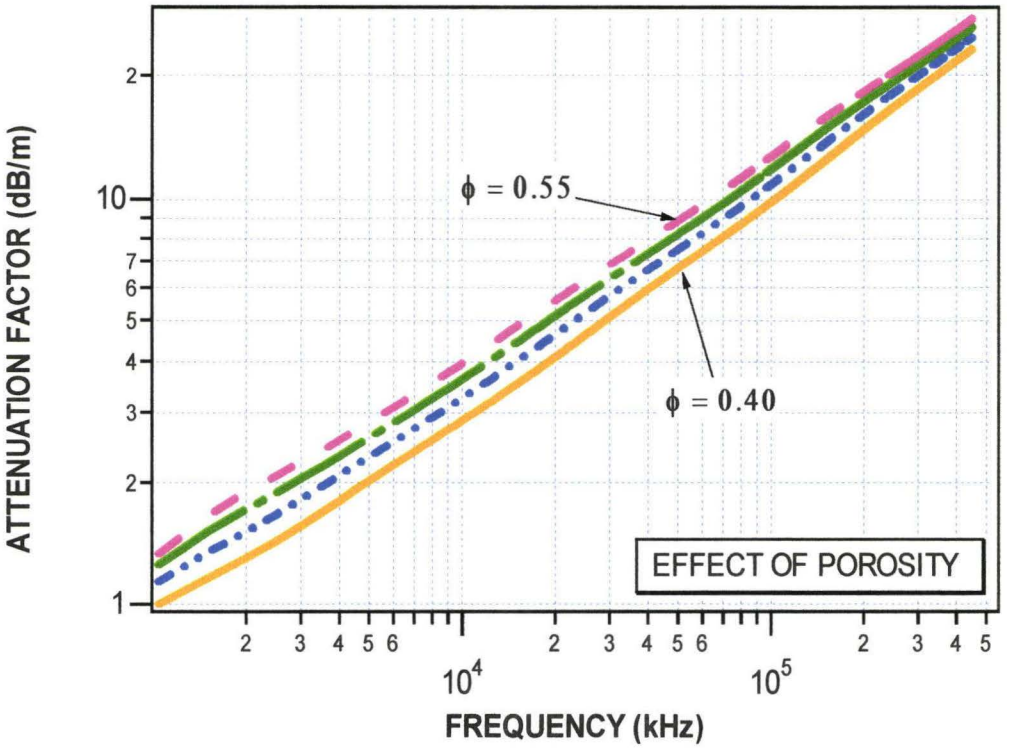

Figure 7.4

Effect of porosity increasing on intrinsic attenuation factor α.

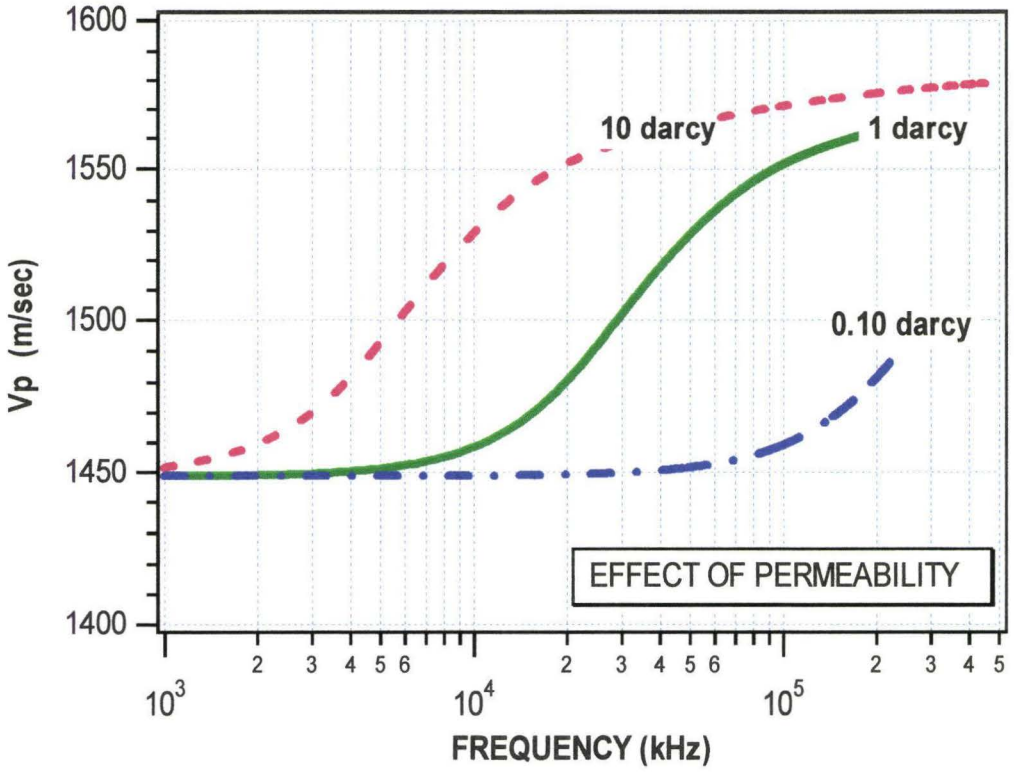

Figure 7.5

Effect of dynamic permeability decreasing on

compressional wave velocity.

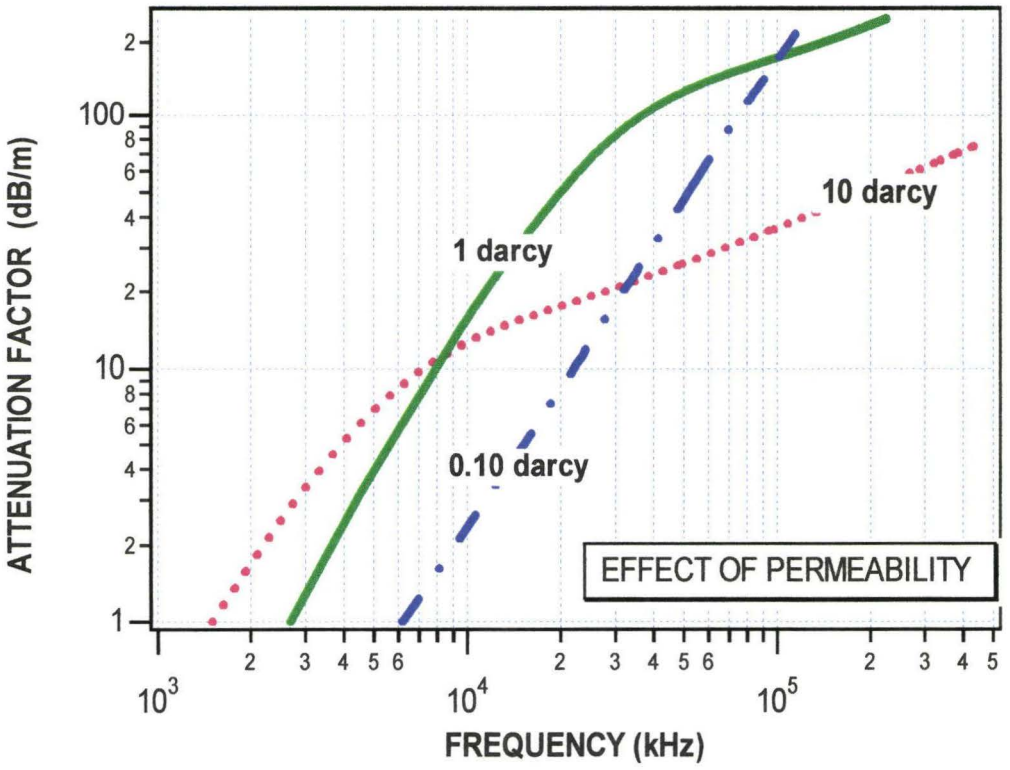

Figure 7.6

Effect of dynamic permeability decreasing on

intrinsic attenuation factor α.

7.1.4 Pore-size Parameter

The pore-size parameter is a scaling factor in the argument of Biot's flow correction [F=F (κ)]. Stoll suggests that this parameter cannot be measured, but only estimated (Stoll et al., 1970). In our sensitivity tests, we assumed spherical pores and calculated a pore-size parameter equal both to the hydraulic diameter (Hovem et al, 1979) and to the hydraulic radius (Stoll, 1977), without remarkable effect on the output. We observed a wave velocity increase of less than 0.5 m/sec, with a corresponding intrinsic attenuation variation of less than 0.10 dB/m.

7.1.5 Structure Factor

The structure factor parameter accounts for an apparent increase in fluid inertia caused by pore tortuosity. Stoll considers that this factor must be estimated empirically. Values range from 1.00 for uniform pores with axes parallel to the pressure gradient to 3.00 for randomly distributed uniform pores (though Stoll determined an acceptable value of 4.30 from experimental data in his early works). The typical inputs for this parameter range from 1.25 for sands to 3.00 for clays. The structure factor is not constant with frequency: a critical frequency can be calculated (Stoll, 1984; Hovem et al, 1979), and applied to the model, as a function of viscosity, frequency and porosity. In both our sensitivity and simulation tests, the structure factor is not considered frequency dependent over the 1 kHz to 450 kHz interval, but varied between 1.00 and 3.00, low values for sandy sediments, highest values for the muds. As shown in Figures 7.9 and 7.10, compressional wave velocities and attenuation factors increase with values for the structure factor closer to one. We used this effect, and the fact that porosity controls primarily wave velocity, to obtain better model fits to the in-situ compressional wave velocity and effective attenuation.

7.1.6 Frame Poisson's Ratio

The frame Poisson's ratio of unconsolidated and consolidated sands is difficult to calculate without core or log analysis. Poisson's ratio variations have a slight influence on the slope of the velocity curve at frequencies above the major dispersion shift. We used an empirical equation that calculates this parameter as a function of the predominant mineralogy (Spencer et al., 1994):

$$\sigma_{frame} = 0.647 * \sigma_{\min eral} + 0.049 \qquad (27)$$

The value obtained (0.253) for carbonate sands is in agreement with the value of 0.25 used by Stoll and other investigators, though in the simulation tests we decided to increase its value for the sediments at each site.

7.1.7 Frame Bulk and Shear Moduli

Stoll's model requires knowledge of the real part of the frame elastic moduli, in order to calculate the other elastic properties and Biot's coefficients. We use empirical equations (Hardin, 1963: Hardin et al., 1968; Stoll, 1977), which relate the frame shear modulus to sediment type, void index, and the mean effective stress acting on the sediment. The vertical stress acting at z feet of depth in the sediment is (Stoll, 1984):

$$\tau_{vert} = \int (1-\phi) \cdot \Delta G \cdot \gamma \cdot dz \qquad (28)$$

Where ΔG is the difference between sediment and seawater specific gravities, and γ is the seawater specific weight. Empirical relationships are given to calculate the effective stress and

the real part of the frame shear modulus, as functions of sediment size and void ratio (Hardin et al., 1968; Ogushwitz, 1985; Stoll, 1989).

Since the effective stress is related to the depth in the model, we simulated the control of the frame shear modulus on compressional wave velocity and attenuation by increasing the depth below the seafloor. In the depth range that we simulated (between 0.10 and 1.00 mbsf), the compressional wave velocity exhibits a 7 m/sec increase at 100 kHz, while the intrinsic attenuation shows little sensitivity (Figures 7.7 and 7.8). Attenuation is regulated by the complex parts of the frame elastic moduli, which in turn are dependent on the logarithmic decrements: the logarithmic decrement for compressional and shear waves is a measure of frictional losses due to motion. It is determined as a function of the frame shear modulus ratio, as the frequency approaches zero. With increasing frequency, its value reaches a peak and then follows a decay pattern similar to a typical viscoelastic relaxation curve. Typical values (Stoll, 1989) are between 0.005 (sands) and 0.050 (finer materials). Our simulation between these values showed negligible influence on the attenuation and wave velocity outputs.

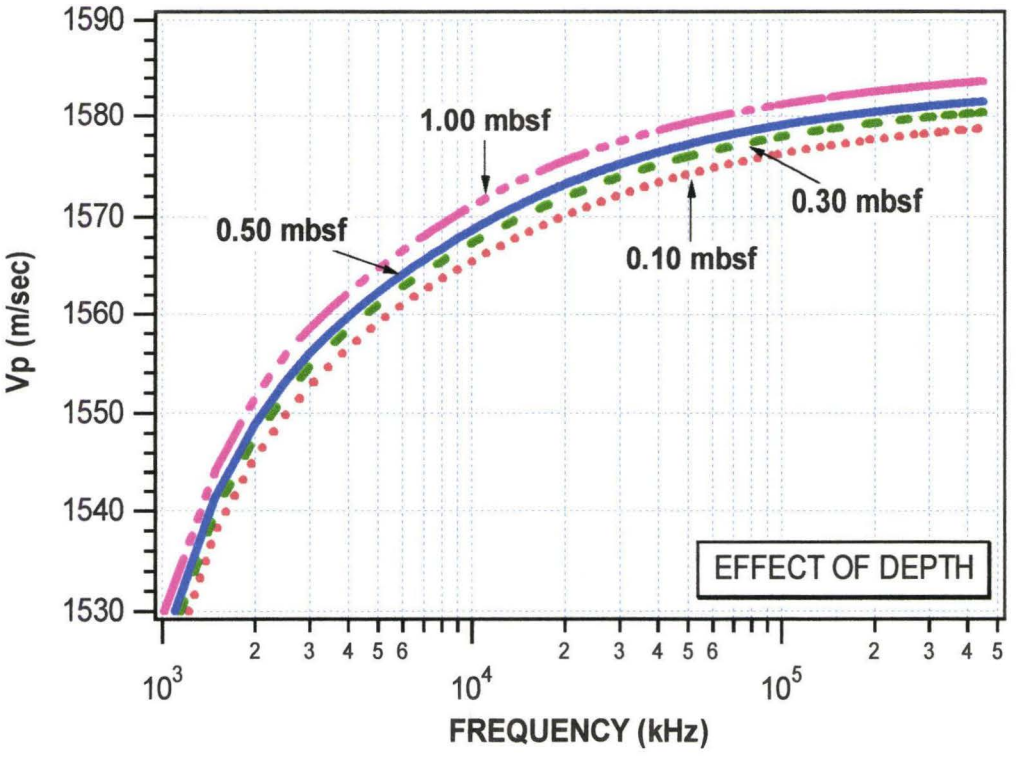

Figure 7.7

Effect of depth increasing on compressional wave velocity.

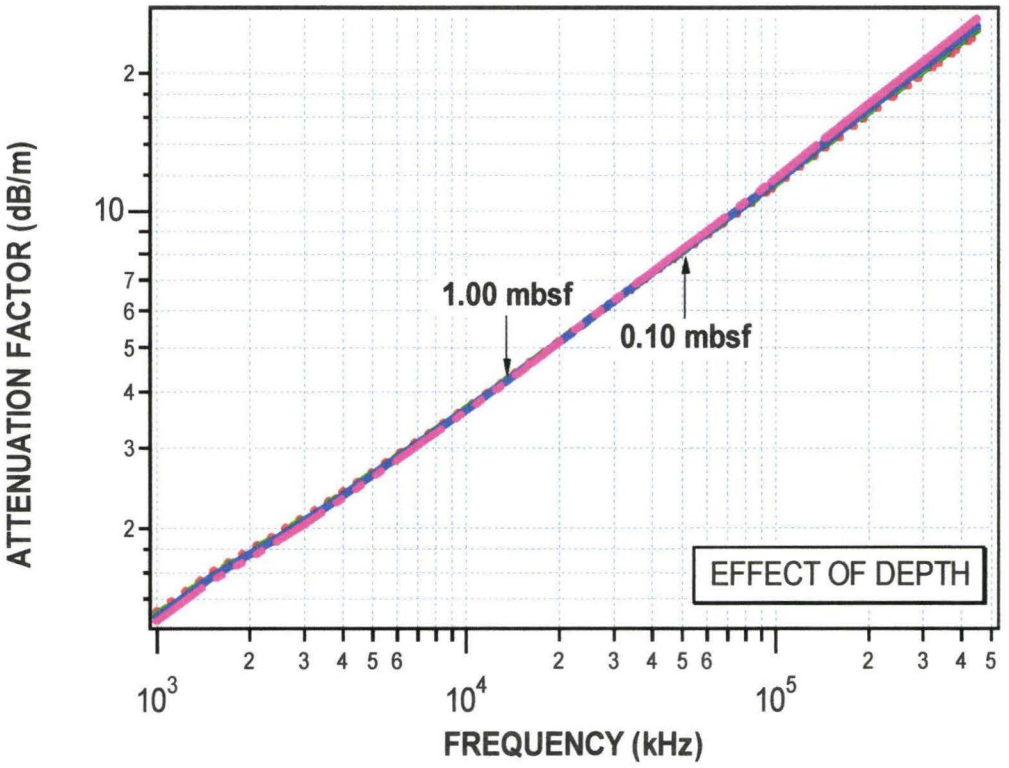

Figure 7.8

Effect of depth increasing on

intrinsic attenuation factor α.

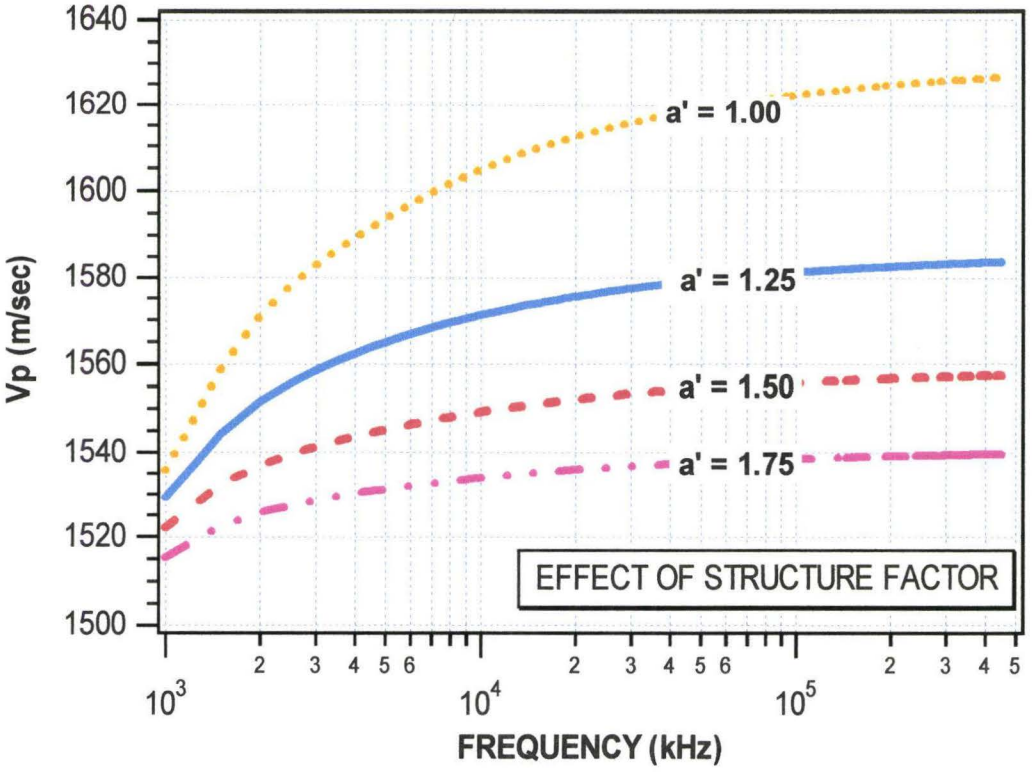

Figure 7.9

Effect of structure factor increasing on

compressional wave velocity.

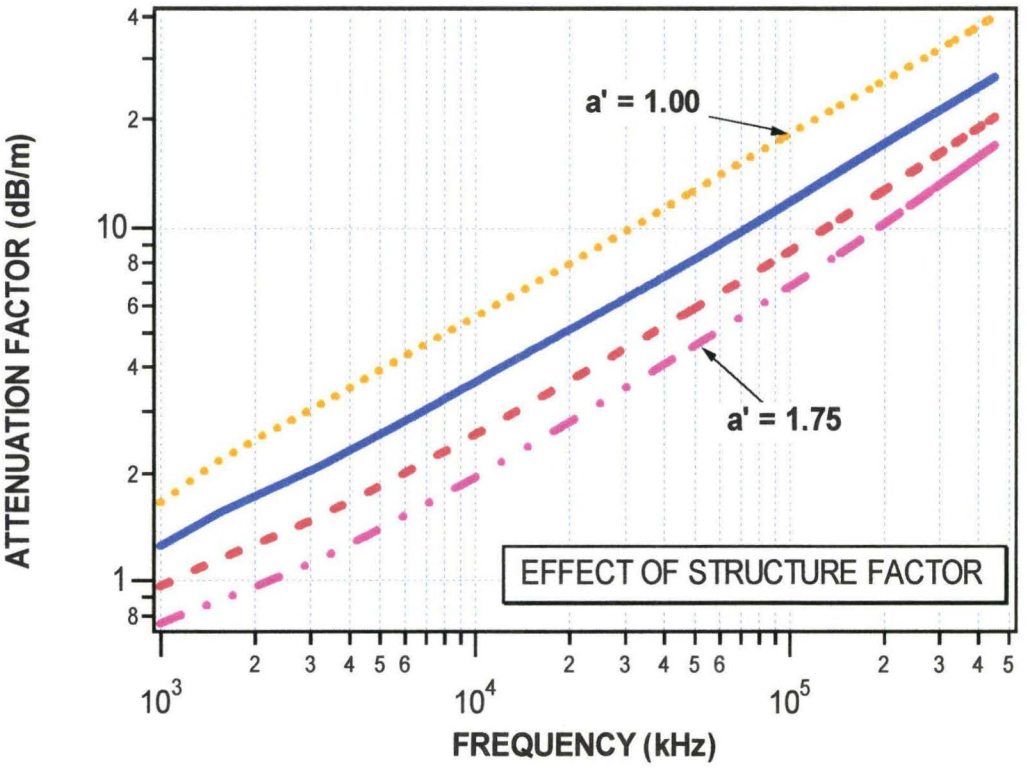

Figure 7.10

Effect of structure factor increasing on

intrinsic attenuation factor α.

Table 7.1.

List of parameters (or sediment properties) needed in the model and their source.

Parameter or Property	Calculated by model	From in-situ data	From core analysis	From literature
Porosity			X	
Permeability			X	
Grain Density			X	X
Grain Bulk Modulus				X
Pore Fluid Density			X	X
Pore Fluid Bulk Modulus				X
Structure Factor				X
Frame Poisson's Ratio	X	X		X
Shear Logarithmic Decrement				X
Logarithmic Decrements Ratio				X
Frame Elastic Moduli	X			
Investigation Depth		X		
Pore-Size Parameter	X			X

CHAPTER 8

MODEL SIMULATION TESTS

8.1 Model Simulations

In a very specific way, the purpose of this research is the attempt to answer three questions:

1. Will a model fit yield reasonable attenuation and sediment properties as inputs?
2. Conversely, will inputs derived from core analysis and literature correctly predict wave velocity dispersion and corresponding attenuation?
3. Finally, what will be the value of the exponent "n" in the attenuation-frequency relationship, within the investigated frequency range?

The model calculates wave velocities and intrinsic attenuation parameters relative to shear and compressional waves of the first and second kind (Stoll, 1989): Table 8.1 reports all the values estimated from the cores as well as those used in our simulations. A grain bulk modulus of 74 GPa was used, since the sediments are primarily carbonates, and it was kept constant in all the simulations because terrigenous fractions in the test location sediment are generally rather low (Fan, 1975; Hollet, 1977). Grain density was simulated between the estimated value of 2740 kg/m^3 and the literature value of 2800 kg/m^3. We thus considered low or negligible the influence of quartz, though it is present in Kaneohe Bay sediments mainly from hydrothermal sources.

8.1.1 Site H4

Since the sandy sediments at sites H3 and H4 show different wave velocities but similar attenuation, we simulated comparable values for permeability, but used porosity from average core data. The velocity model results for the fine sands at site H4 are shown Figure 8.1: a very good fit for velocities was obtained for a porosity of 0.52, structure factor equal to 1.10, and a value of 1.10E-10 m^2 for the permeability ("V_p Model" curve). Other good fits to the data, have porosity ranging from 0.50 to 0.54, permeability varying between 1.0E-11 to 2.40E-11 m^2, and structure factor varying between 1.00 and 1.25. The input frame Poisson's ratio is equal to 0.30 in all the simulations. The "Core Model" curve represents a simulation involving the estimated and calculated values from Table 8.2: porosity is set to 0.54 and permeability to 2.40E-11 m^2. Ultrasonic core values are plotted with the simulations, showing in general acceptable difference with respect to the in-situ data (around 1 or 2%).

Intragrain porosity may account for the higher difference between measured and modeled porosity (0.05, 9% of the total). Carbonate grains contain internal porosity, yet behave as solid particles in terms of wave velocity and attenuation. Data from other Hawaiian carbonate sands confirm this effect, especially in reef-derived materials (Fu et al., 1998). It can be inferred that as long as we reason in terms of porosity, permeability, and structure factor (and thus in terms of pore size and related geometry), when the porosity is increased towards its average value another parameter must be changed in order to increase the compressional velocity.

Table 8.1.

Comparison between estimated and used model parameters.

Parameter	H1 Estimated	H1 Simulated	H3 Estimated	H3 Simulated	H4 Estimated	H4 Simulated
Porosity	0.84	0.84	0.47 (0.44)	0.40-0.43	0.56	0.52-0.56
Permeability (m^2)	3.62E-13 1.48E-14	6.23E-13	1.17E-09 1.14E-11	1.00E-10 9.00E-11	2.45E-11 2.26E-13	1.00E-10 9.00E-11
Grain Size (phi)	8.15-11.71	17.80	0.17-3.28	0.032-3.37	3.65-7.28	2.87-4.20
Frame Poisson's Ratio	0.49	0.49	0.30	0.30	0.30	0.30
Structure Factor	-	3	-	1.00	-	1.00-1.10
Shear Logarithmic Decrement	0.50	0.50	0.05	0.05	0.05	0.05
Logarithmic Decrements Ratio	1.25	1.25	1.25	1.25	1.25	1.25
Pore-Size Parameter	3.52E-06 8.95E-07	3.85E-06	6.50E-04 8.89E-04	2.46E-04 6.46E-05	5,75E-05 7.96E-05	6.02E-05 1.96E-05
Investigation Depth (mbsf)	0.10	0.40-0.20	0.10	0.10	0.10	0.10

The "α Model" curve in Figure 8.2 shows our tentative, not particularly successful attempt, to reduce the attenuation gap between in-situ and simulated attenuation while keeping at the same time a good agreement with the compressional wave velocities. The input porosity is equal to 0.56 and permeability is equal to the lower estimation of permeability (2.00E-13 m^2), from the Allen-Hazen equation. We notice that decreasing permeability towards the Core Model value produces a corresponding intrinsic attenuation increase.

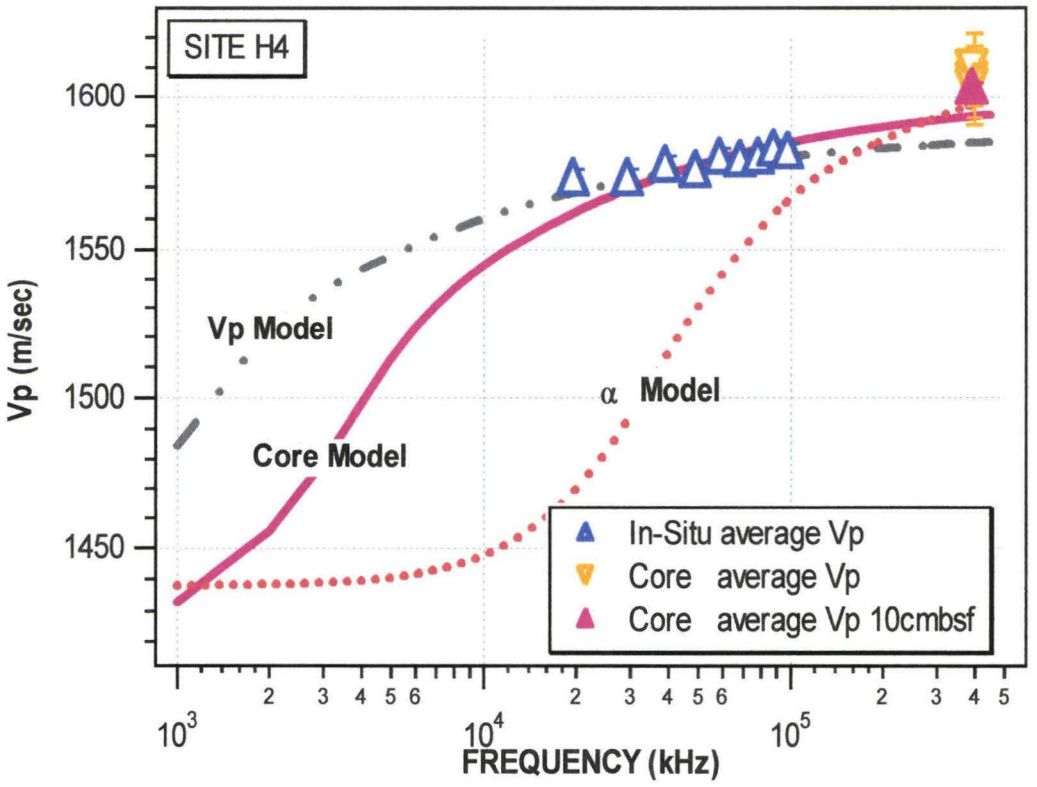

Figure 8.1

Model simulations for site H4 compressional wave velocity.

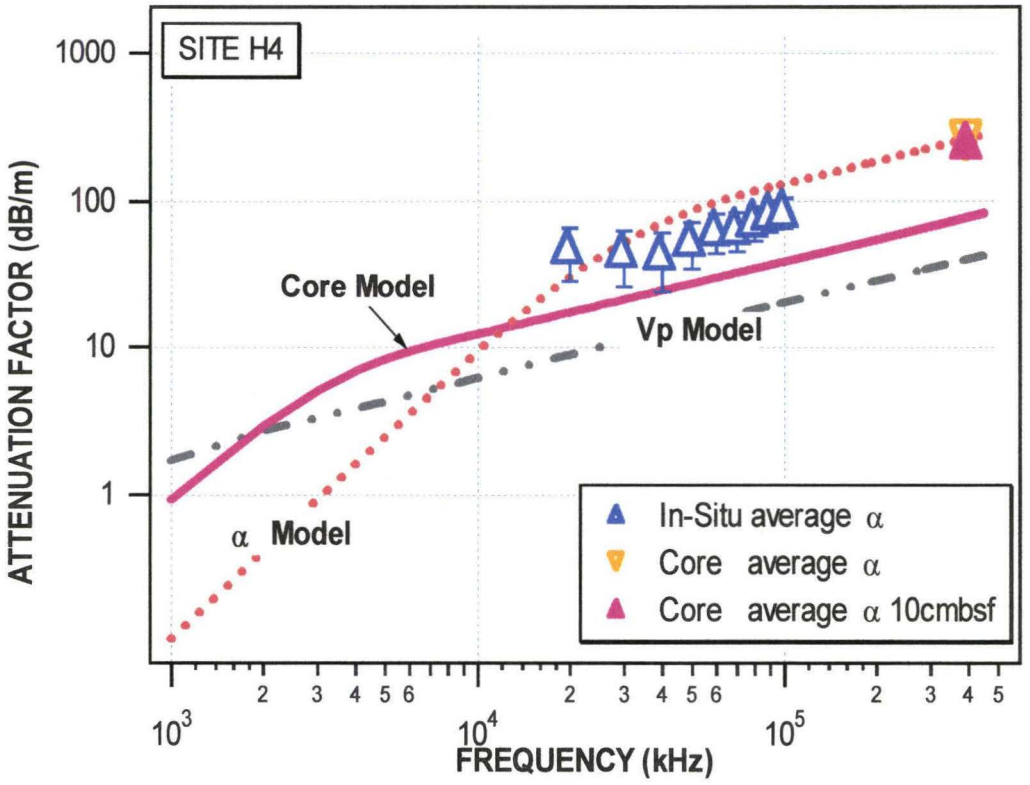

Figure 8.2

Model simulations for site H4 effective attenuation factor.

8.1.2 Site H3

Modeling site H3 sands yielded results similar to those for site H4 (Figure 8.3). Good agreement with compressional wave velocities could be obtained for porosity between 0.40 and 0.44, with permeability ranging from 1.00E-10 to 1.14E-11 m^2 (Vp Model and Core Model respectively). A Poisson's ratio equal to 0.30 still simulates satisfactorily the data, and the structure factor is held at 1.00. Both these values are lower than the core data estimations. The porosity reduction is still large, even considering intergrain effects. However, without the 0.63 porosity spike at 5 cmbsf that we observed in the core analysis (Figure 3.4), the average porosity would be approximately 0.44: thus, the microporosity reduction would account for a more reasonable 4.5% or less of the total porosity. The lower permeability, in this case closer to the Allen-Hazen equation estimation, can be explained by considering the sorting of this coarse sand (Figure 3.2). Finer materials between the larger grains actually control the sediment permeability.

A remarkable reduction of the H3 sands effective-intrinsic attenuation gap (α Model curve) is obtained for a porosity equal to 0.42 and a permeability input of 3.00E-12 m^2, values that again do not produce a match for the in-situ compressional wave velocities. As for site H4 simulations, values of porosity and permeability between the Vp and Core Models produce higher intrinsic attenuation.

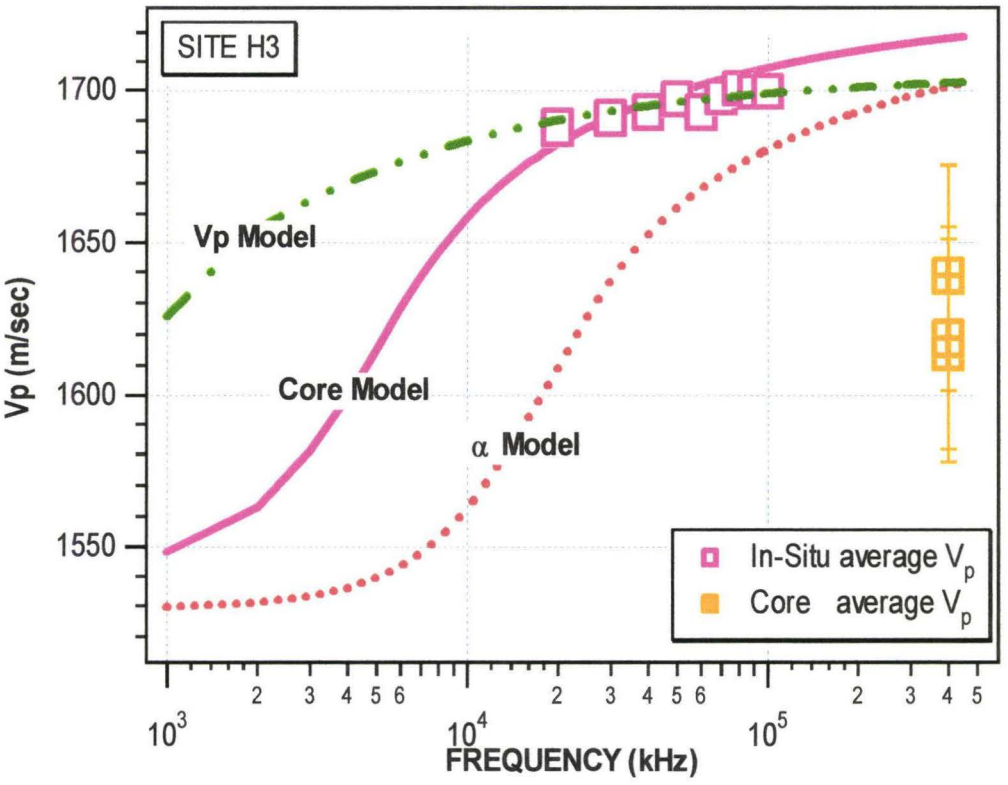

Figure 8.3

Model simulations for site H3 compressional wave velocity.

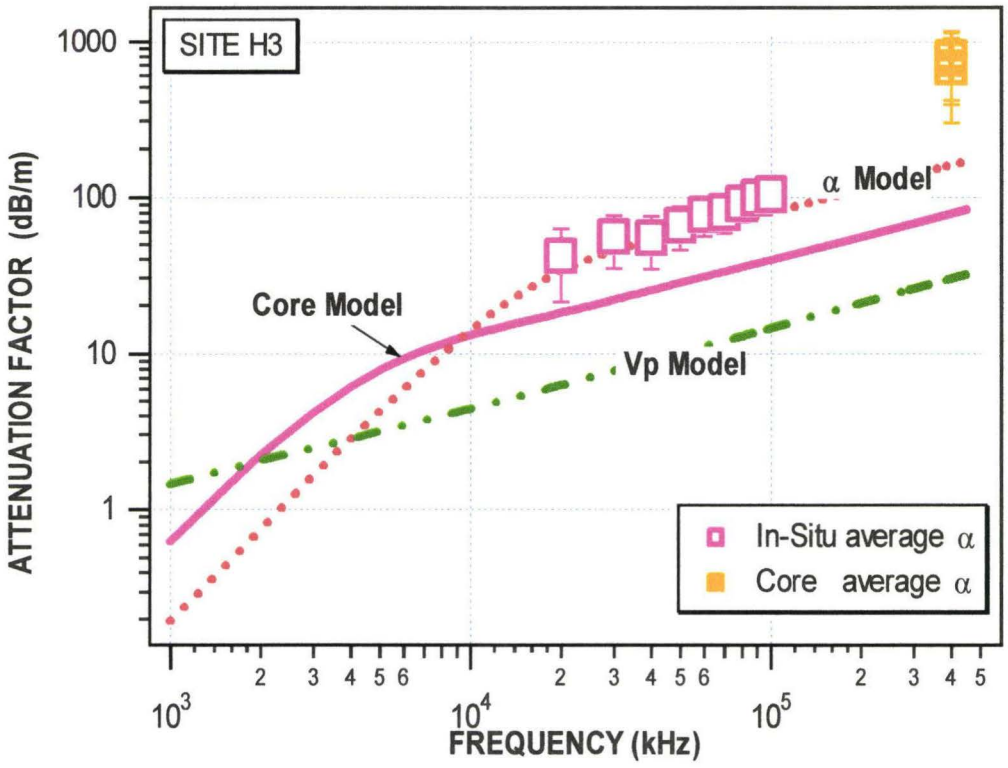

Figure 8.4

Model simulations for site H3 intrinsic attenuation factor.

8.1.3 Site H1

Simulation of the data at site H1 (Figures 8.5 and 8.6) required different assumptions than those of Stoll's previous work with fine-grained material. By using the calculated physical properties, we obtained good agreement for attenuation, but too low compressional wave velocity at a 10 cmbsf depth. This could be due to an increased frame loss, since the material is looser than the sands at site H4. Increasing the frame moduli values may seem a reasonable solution (Stoll et al., 1970), but such a decision would lead to higher compressional wave velocities. At this site we registered four sets of shear wave signals at 20 and 100 Hz.

Assuming a constant density of 2800 kg/m^3 and grain bulk modulus of 74 GPa, a total bulk modulus of 6.11 GPa and shear modulus of 3.54E5 Pa were determined from the in-situ shear and average compressional wave velocity. The Poisson's ratio calculated from these moduli is very close to 0.50, indication that this muddy sediment is very loose. Eventual application of the Gassmann's equation (Gassmann, 1951; Hamilton, 1972) with an assumed frame Poisson's ratio very close to 0.50 leads to slightly shallower input depth (from 4.6 to 3.2 cmbsf) to obtain the needed frame shear modulus of 7.98E5 Pa (and a frame bulk modulus of 3.99 GPa).

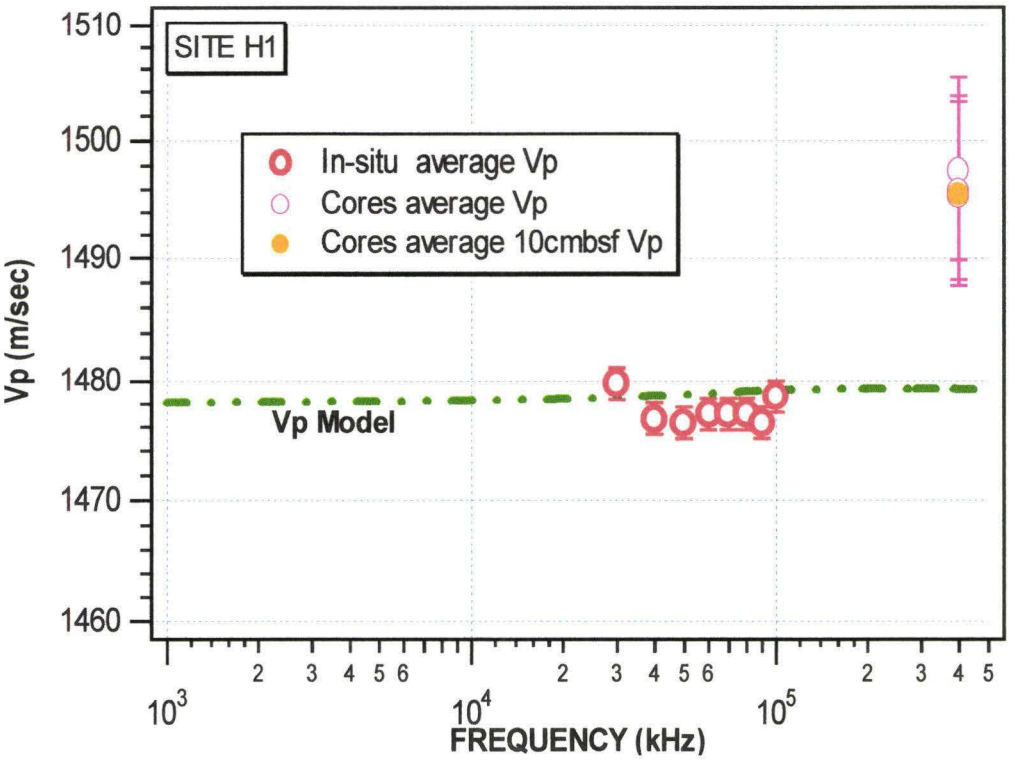

Figure 8.5

Model simulations for site H1 compressional wave velocity.

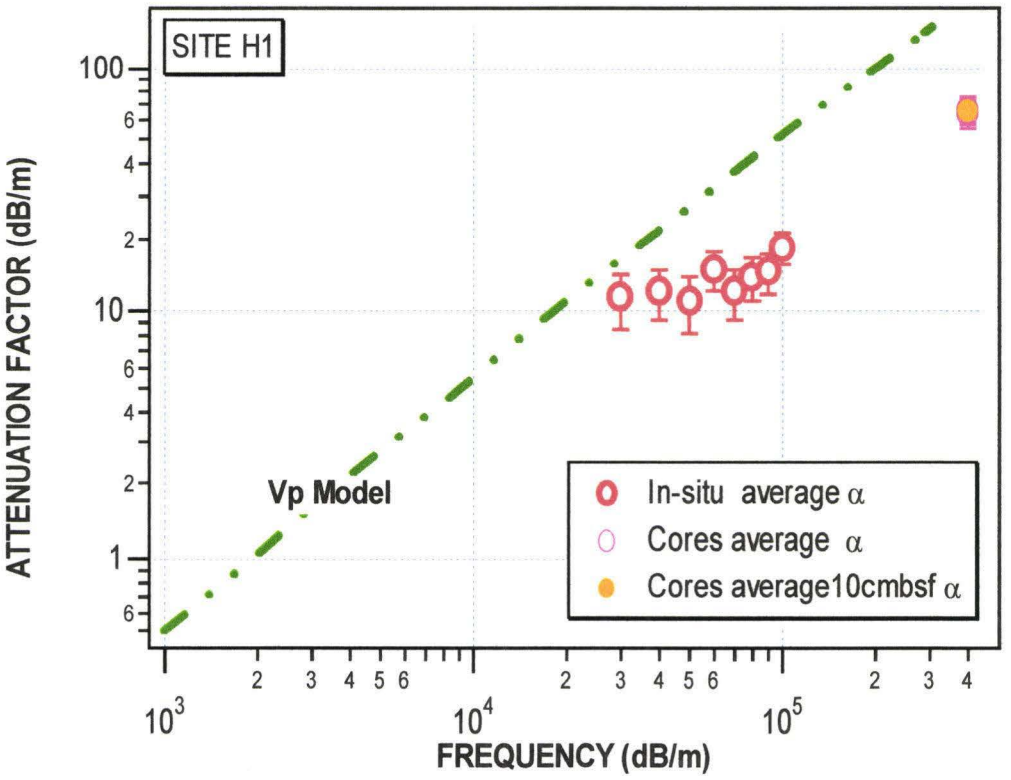

Figure 8.6

Model simulations for site H1 intrinsic attenuation factor.

8.2 Simulation Attenuation Data Comparison

In order to investigate the value of the exponent (n) in the frequency interval from 20 to 100 kHz, we compared the in-situ attenuation with both the simulated and Hamilton's values: for the latter ones, the proportionality parameter (k) was calculated at 50 kHz and predicted attenuation was calculated with linear dependence on the frequency. Table 8.2 shows all the computed values pertinent to the attenuation comparison for each site simulation.

Table 8.2.

Attenuation data comparison for each site simulation.

Site	In-Situ k	Simulated k*	Hamilton's k	In-Situ n	Simulated n*	Hamilton's n
H1	0.4000	0.0007	0.0002	0.32	0.97	1.00
H3	0.0160	0.0040	0.0010	0.56	0.51	1.00
H4	0.5500	0.0580	0.0010	0.43	0.51	1.00

*- referring to Vp Model

8.2.1 Site H4

A graphical comparison between attenuation factors for site H4 data is shown on Figure 8.7. The in-situ k parameter is equal to 0.55 dB/m-kHz (R^2=0.80), and the relationship exponent is about 0.43. The exponent for the simulated values of Vp and Core Models varies from 0.51 to 0.50, with proportionality factor between 0.08 and 0.06 dB/m-kHz respectively (both R^2=1). For the attenuation predicted with Hamilton's model, the proportionality constant is equal to 1.10E-03 dB/m-kHz.

8.2.2 Site H3

The same comparison for site H3 attenuation is plotted in Figure 8.8: again, in-situ and simulated attenuation show good accordance in their exponents (0.56 for in-situ, 0.51 and 0.49 for the Vp and Core Models) and in their slopes. The calculated values for Hamilton's theory have a higher slope (1.3E-03 dB/m-kHz). The slopes of the in-situ and simulated curves generally match and are clearly different from the Hamilton model, thus excluding an exponent equal to unity.

8.2.3 Site H1

In Figure 8.9 we observe that for H1 muds the modeled attenuation follows a linear dependence on the frequency, as required by both the Hamilton and Biot-Stoll models, since fine materials are linearly dependent only at high values of the frequency. There is a contradiction, though, with the other sites because the intrinsic modeled attenuation is higher than the effective one. A lower input permeability might lead to a better fit, but we still must consider the difficulty in calculating attenuation factors in loose and clayey material with very low attenuation over such small transducers spacing (0.30 m).

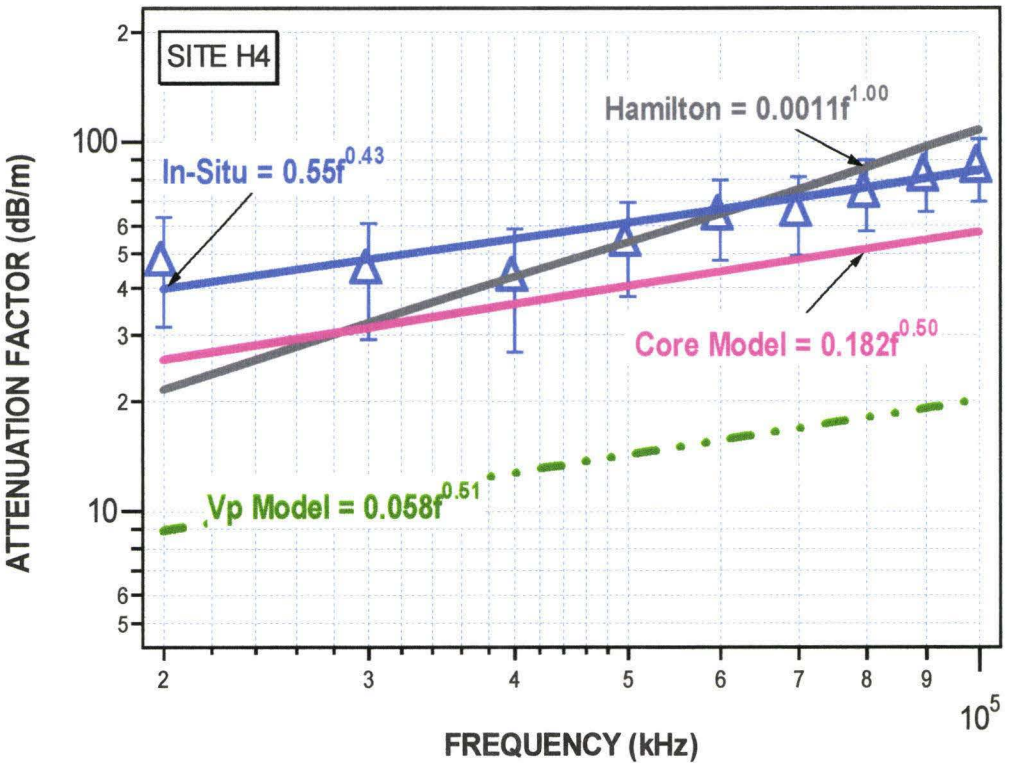

Figure 8.7

Site H4 attenuation data comparison.

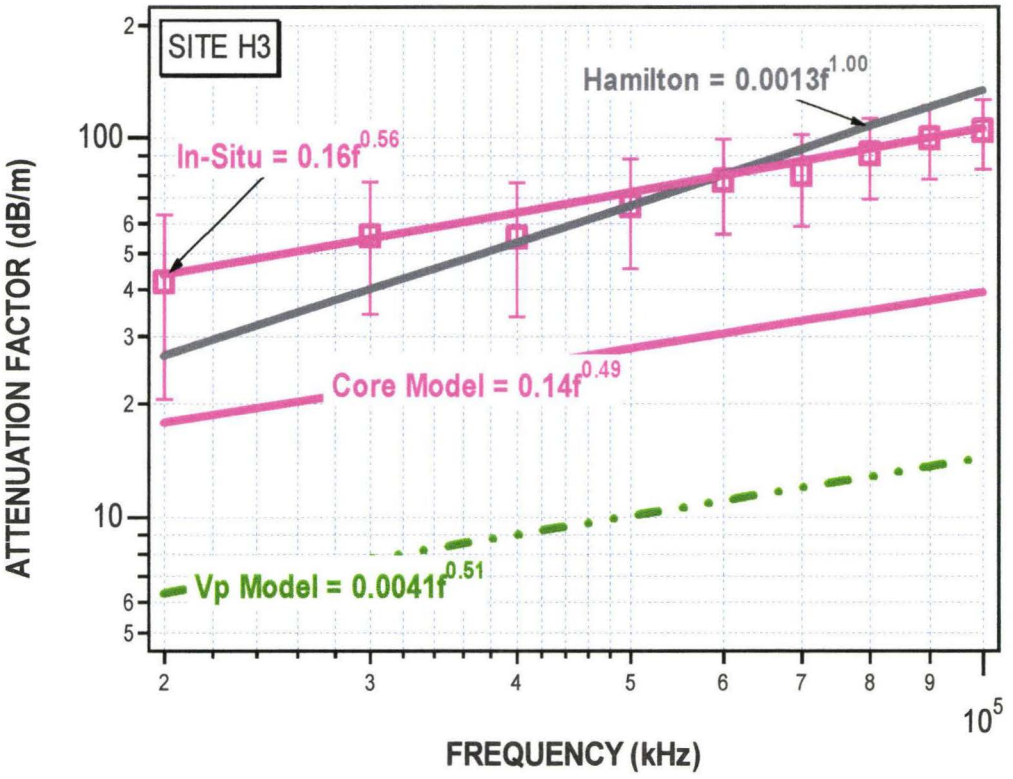

Figure 8.8

Site H3 attenuation data comparison.

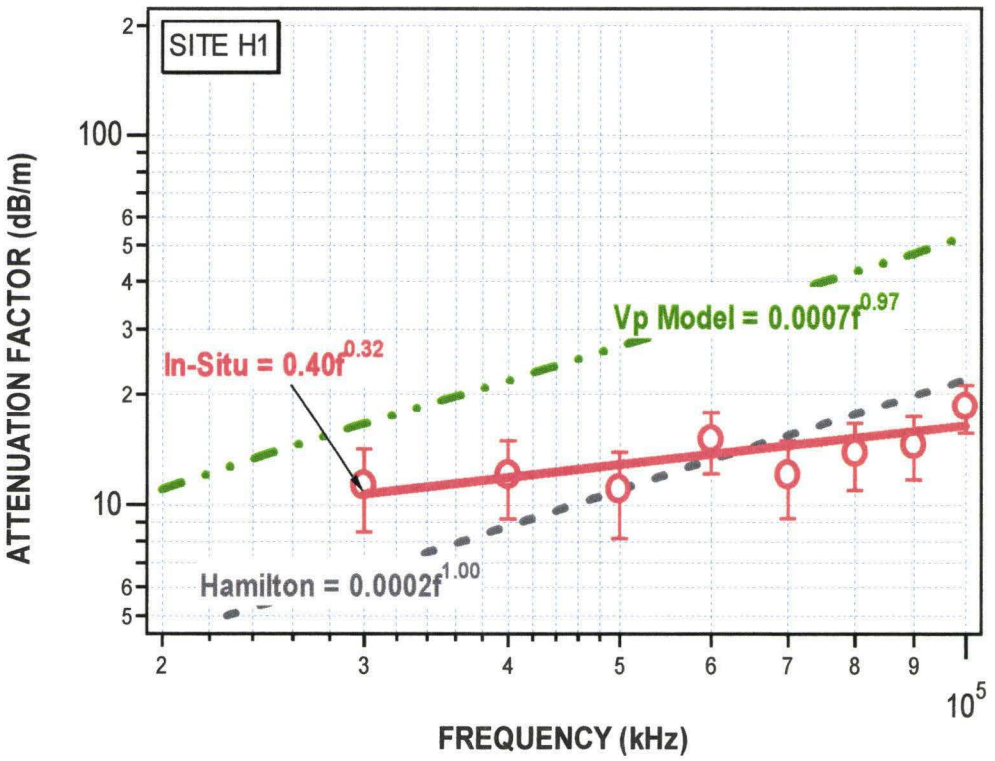

Figure 8.9

Site H1 attenuation data comparison.

8.3 Discussion on Simulation Results

As seen in Chapter 4, the term "scattering" defines very generally the energy lost in wave transformation from P-waves to S-waves, reflections at layer interfaces, objects with dimensions comparable to the wavelength, and so on.

A high percentage of "scattering" loss in H3 and H4 sands between the simulated Vp and Core Models' attenuation may be caused by the presence of shells, reef and shell fragments that seem to be abundant in Kaneohe Bay sediments. The high-energy environment found at sites H3 and H4 are related to hydrodynamic processes that may exert a strong influence on the fine scale geoacoustic response of these sandy sediments. The muds at site H1 show the lowest, if not even negligible, variation in geoacoustic properties. Fine scale homogeneity, both horizontal and vertical, can be assumed at this site, since the core depth and the transmitter-to-receiver distance are both around 0.30 m. The lagoonal low energy environment is more likely to be controlled by biological activity, rather than by hydrodynamic processes.

The interaction of hydrodynamic and biological processes is a control factor on sediment geoacoustic properties (Richardson, 1986). Bioturbation tends to stabilize the spatial variability of the sediment: tube dwelling species, observed in the cores, tend to exert this influence up to depth of 10 cmbsf, with seasonal recurrence.

Attenuation in sediment is strongly controlled by its permeability and pore space characteristics. In his previous works, Stoll (1977) showed the influence of possible different pore sizes on the attenuation response of coarse sands. This model calculates the average pore size and main grain size with the same standard empirical relationships we used to estimate core hydraulic properties. However, using the estimated permeability in the simulations led to one single point matching of the in-situ data only, thus missing the wave velocity dispersion over the frequency, the main focus of our modeling.

The best velocity fit for H4 is reached through the estimated average porosity and for its calculated average geometric permeability, whereas for H3 the required permeability input is equal to the lower estimated value. We believe the different sorting of these sands at the investigation depth affects the overall hydraulic characteristics: H3 sands are less sorted than H4 sands, so finer grains fill the pore space and decrease its permeability. The assumption of spherical grains and pores surely leads to overestimation of sediment permeability, especially in such poorly sorted materials.

The fact that the sediment properties are estimated from vertical cores takes us again to the problem of the lack of knowledge of the horizontal spatial variability of surficial sediment, as well as of the processes that affect their geoacoustic response. Generalizations about a sediment grain size distribution, sorting, structure, and compaction may lead to mistakes in the evaluation of the hydraulic properties and noteworthy miscalculation of the intrinsic attenuation.

CHAPTER 9

CONCLUSIONS AND RACCOMANDATIONS

New piezo-composite transducers allowed the collection of compressional wave velocities in three different kinds of sediment at Kaneohe Bay, in a continuous frequency range between 20 and 100 kHz. The corresponding effective attenuation was calculated, while the sediments' physical properties were determined from core analysis after sampling. Ultrasonic tests for compressional wave velocity and attenuation were performed. In-situ and core velocity dispersion is observed in the coarser sediments, primarily sandy materials, as predicted by the Biot-Stoll theory. In the coarser sediments, in-situ attenuation and frequency do not follow a linearly dependent relationship.

Our modeling showed that the Biot-Stoll based mathematical model may be useful in determining inversely the sediments main physical parameters from in-situ data, especially porosity, always assuming constraints about parameters that cannot be estimated a priori. The magnitude difference between simulated fit to the data and estimated values for permeability seems to increase with a decrease in sorting: this is evidence of how much the Biot-Stoll model depends on information on the sedimentologic characteristic of a modeled sediment.

This series of in-situ data represent a new element in sediment geoacoustic research, considering that for the first time we were able to examine the compressional wave velocity and attenuation response of different sediments continuously over different frequencies. Ideas and theories about these responses have been tested and proved, others discarded, and many are still not answered.

More tests are needed, over lower frequency intervals and in different marine environments, in order to deepen our knowledge on how sediment properties, and biological and physical processes at both large and small scales affect wave velocity and attenuation patterns. As for future research, we can consider two main work directions:

- The design and construction of transducers able to register signals at very low frequency. The detection of wave signals over a frequency range that corresponds to the wave velocity shift may be modeled with less uncertainty and more defined input parameters.

- In-situ acoustic tests in different experimental locations, differing as for sedimentary and biological processing involved both on low and large scale.

APPENDIX A

MODEL FLOW CHART

A.1 FLOW CHART ELEMENTS

ON-SCREEN MANUAL INPUT

PROCESS

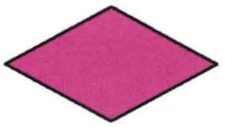

DECISION

ON-SCREEN OUTPUT

MEMORY/FILE STORAGE

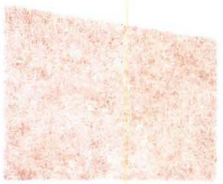

A.2 FLOW CHART

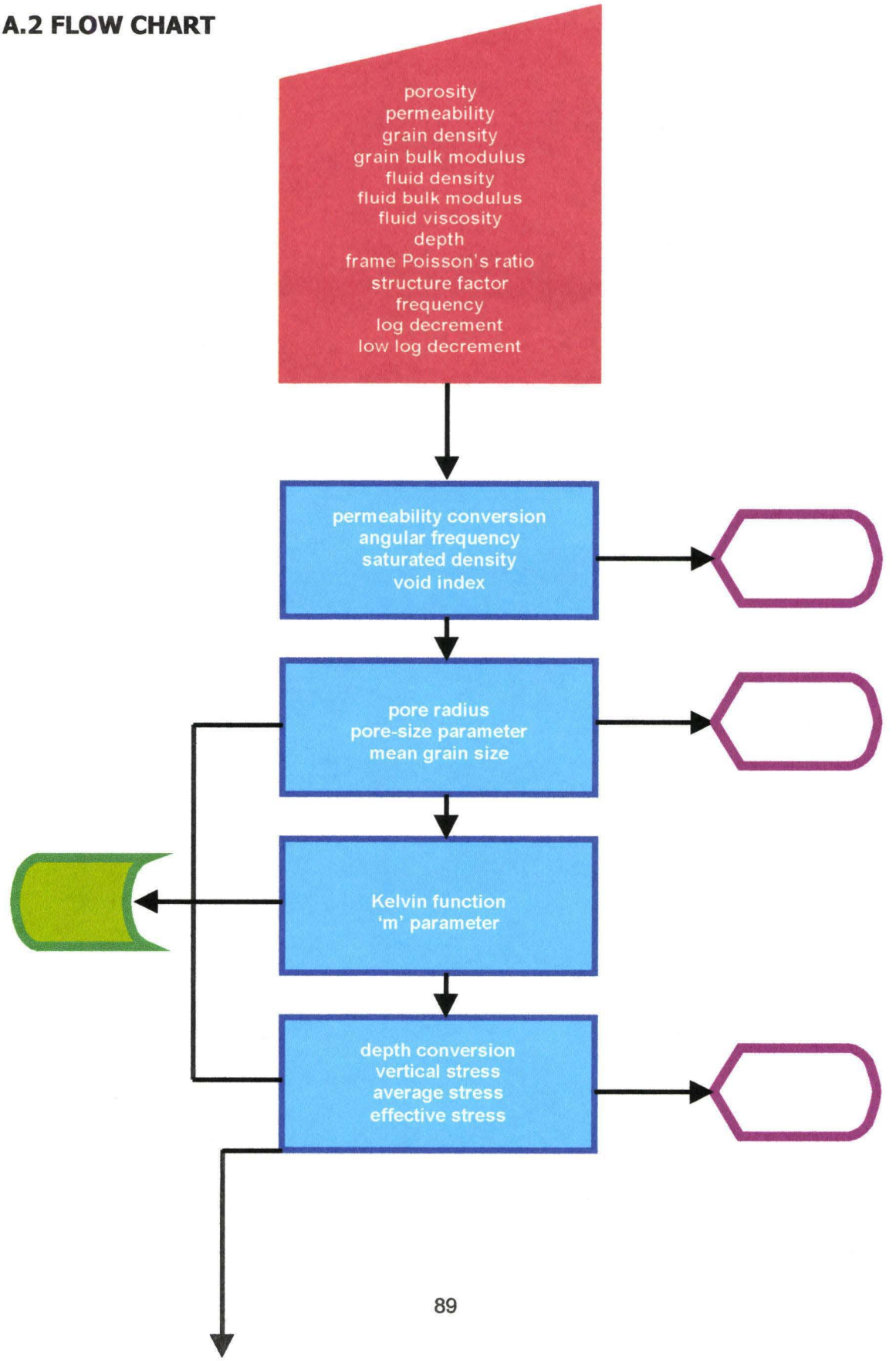

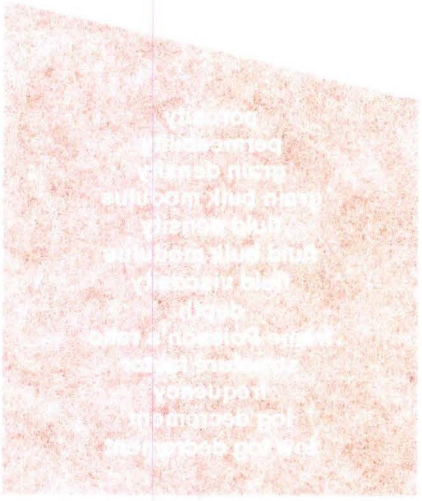

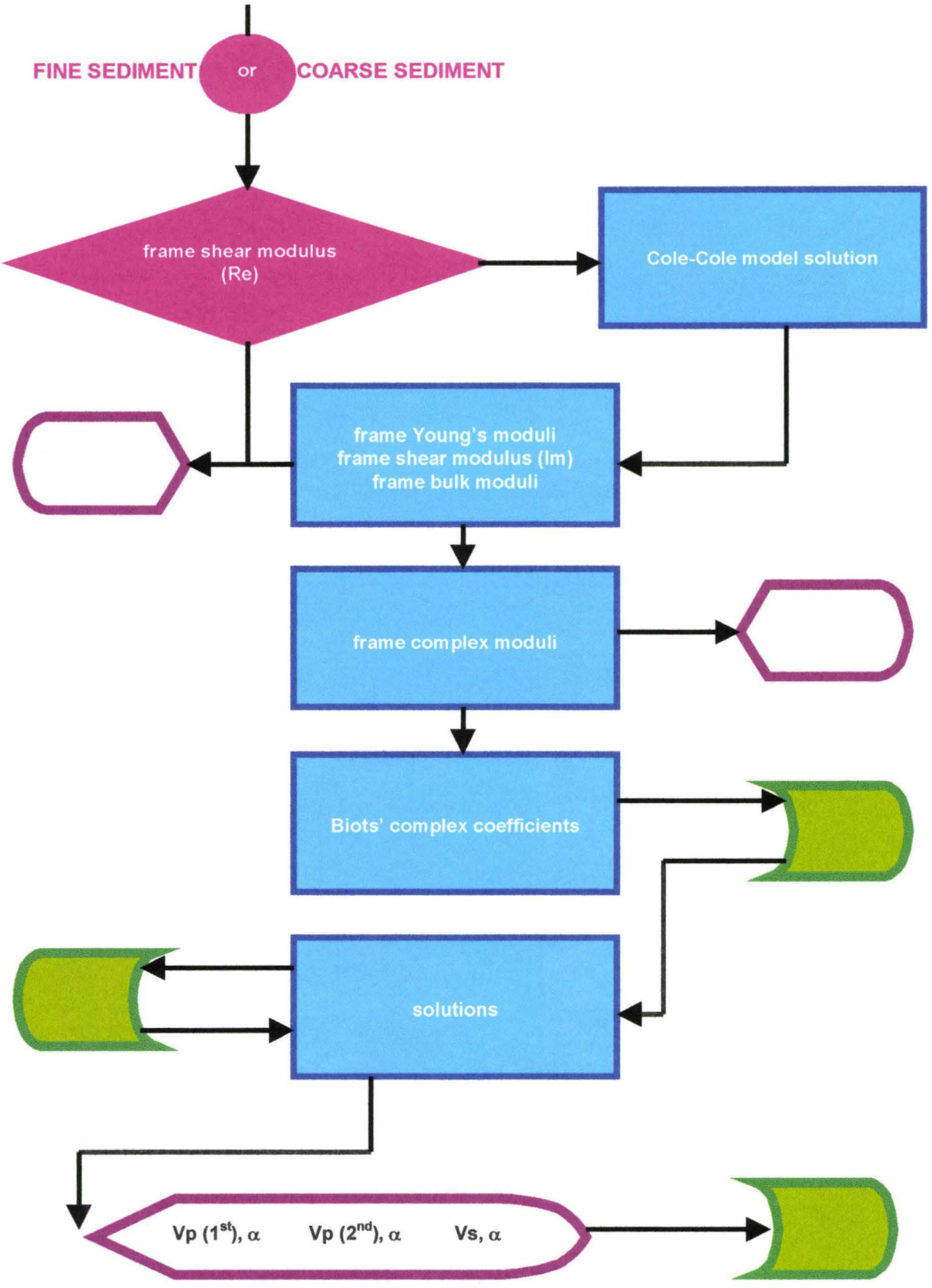
FINE SEDIMENT
or
COARSE SEDIMENT
frame shear modulus (Re)
Cole-Cole model solution
frame Young's moduli
frame shear modulus (Im)
frame bulk moduli
frame complex moduli
Biots' complex coefficients
solutions
Vp (1st), α
Vp (2nd), α
Vs, α

APPENDIX B

MODEL CODE

B.1 Model Language and Platforms

The model used in this research has been coded in Matlab 5.0 ™, a very powerful mathematical tool, under UNIX Sun 4.0 ™ and WINDOWS98 ™. After calculating the solutions to equation (20) and (21), the model stores the wavenumber data in three temporary data files (extension ".dat", carriage delimitation) for later calculations.

B.2 Save Text File

After wavenumber retrieval, phase velocities and corresponding intrinsic attenuation calculation and plotting, all data are saved into a text file (extension ".txt", carriage delimitation) for definitive storage use. The data column significance in the save "file.txt" is as follow:

Table B.1.

File.txt format

Frequency (Hz)	**Compressional Velocity 1st Kind** (m/sec)	**Compressional Attenuation Factor** (dB/m)	**Shear Velocity** (m/sec)	**Shear Attenuation Factor** (dB/m)

B.3 Model Code

```
%%%%%%%%%%%%%%%%%%%%%%%%%%%%%%%%%%%%%%%%%%%%%%%%%%%%%%%%%%%%%%%%%%%%%%%%%%%%%%%%
%          Stoll-Biot Model: Wave attenuation and Velocity Dispersion %
%                                  Stefano F. Baffi                   %
%                                  University of Hawaii               %
%                                                                     %
%                                  October 1998                       %
%                                                                     %
%%%%%%%%%%%%%%%%%%%%%%%%%%%%%%%%%%%%%%%%%%%%%%%%%%%%%%%%%%%%%%%%%%%%%%%%%%%%%%%%

%%%%%%%%%%%%%%%%%%%%%%%%%%%%%%%%%%%%%%%%%%%%%%%%%%%%%%%%%%%%%%%%%%%%%%%%%%%%%%%%
%1-FILES DELETION %%%%%%%%%%%%%%%%%%%%%%%%%%%%%%%%%%%%%%%%%%%%%%%%%%%%%%%%%%%%%%
%%%%%%%%%%%%%%%%%%%%%%%%%%%%%%%%%%%%%%%%%%%%%%%%%%%%%%%%%%%%%%%%%%%%%%%%%%%%%%%%
 clear all
 delete *.dat

%%%%%%%%%%%%%%%%%%%%%%%%%%%%%%%%%%%%%%%%%%%%%%%%%%%%%%%%%%%%%%%%%%%%%%%%%%%%%%%%
%2-VARIABLES DECLARATION %%%%%%%%%%%%%%%%%%%%%%%%%%%%%%%%%%%%%%%%%%%%%%%%%%%%%%%
%%%%%%%%%%%%%%%%%%%%%%%%%%%%%%%%%%%%%%%%%%%%%%%%%%%%%%%%%%%%%%%%%%%%%%%%%%%%%%%%
%phi----------porosity
%perm---------permeability [m^2]
%darcy--------permeability [darcy]
%mdarcy-------permeability [md]
%msec---------permeability [m/sec]
%cm-----------permeability [cm^2]
%rden---------grain density [kg/m^3]
%rmod---------grain bulk modulus [Pa]
%frho---------pore fluid density [kg/m^3]
%fmod---------pore fluid bulk modulus [Pa]
%rho----------sediment saturated density [kg/m^3]
%viscf--------pore fluid viscosity [Pa-sec]
%frmnu--------evaluated frame Poisson's ratio
%fac----------structure factor
%dep----------investigation depth [mbsf]
%depth--------investigation depth [feet]
%ifreq--------initial frequency [Hz]
%sfreq--------frequency step [Hz]
%ffreq--------final frequency [Hz]
%omega--------angular frequency [radians]
```

```
%egrat--------logarithmic decrement ratio
%low----------low logarithmic decrement ratio
%e-------------void ratio
%hr------------hydraulic radius [cm]
%a-------------poresize parameter [cm]
%mgs-----------mean grain size [m]
%phiunit-------mean grain size [phi]
%mpar----------m parameter
%ggrav---------specific densities difference
%overpsi-------vertical effective stress [psi]
%overpascal----vertical effective stress [Pa]
%averagepsi----average effective stress [psi]
%sigmapsi------effective stress [psi]
%sigmapascal---effective stress [Pa]
%gr------------frame real shear modulus [Pa]
%gi------------frame imaginary shear modulus [Pa]
%emodr---------frame real Young's modulus [Pa]
%emodi---------frame imaginary Young's modulus [Pa]
%br------------frame real bulk modulus [Pa]
%bi------------frame imaginary bulk modulus [Pa]
%cbulk---------frame complex bulk modulus [Pa]
%cshear--------frame complex shear modulus [Pa]
%D-------------Biot complex coefficient
%C-------------Biot complex coefficient [Pa]
%H-------------Biot complex coefficient [Pa]
%M-------------Biot complex coefficient [Pa]
%vpf-----------first kind compressional phase velocity [m/sec]
%vps-----------second kind compressional phase velocity [m/sec]
%vs------------shear phase velocity [m/sec]
%fca-----------first kind compressional attenuation [Nepers/m]
%sca-----------second kind compressional attenuation [Nepers/m]
%sa------------shear attenuation [Nepers/m]
%%%%%%%%%%%%%%%%%%%%%%%%%%%%%%%%%%%%%%%%%%%%%%%%%%%%%%%%%%%%%%%%%%%%%%
%%%%%%%%%%%%%%%%%%%%%%%%%%%%%%%%%%%%%%%%%%%%%%%%%%%%%%%%%%%%%%%%%%%%%%
%%%%%%%%%%%%%%%%%%%%%%%%%%%%%%%%%%%%%%%%%%%%%%%%%%%%%%%%%%%%%%%%%%%%%%
%%%%%%%%%%%%%%%%%%%%%%%%%%%%%%%%%%%%%%%%%%%%%%%%%%%%%%%%%%%%%%%%%%%%%%
%%%%%%%%%%%%%%%%%%%%%%%%%%%%%%%%%%%%%%%%%%%%%%%%%%%%%%%%%%%%%%%%%%%%%%
%%%%%%%%%%%%%%%%%%%%%%%%%%%%%%%%%%%%%%%%%%%%%%%%%%%%%%%%%%%%%%%%%%%%%%
%%%%%%%%%%%%%%%%%%%%%%%%%%%%%%%%%%%%%%%%%%%%%%%%%%%%%%%%%%%%%%%%%%%%%%
```

```
%%%%%%%%%%%%%%%%%%%%%%%%%%%%%%%%%%%%%%%%%%%%%%%%%%%%%%%%%%%%%%%%%%%%%%%%%%%%
%3-VARIABLES INPUT %%%%%%%%%%%%%%%%%%%%%%%%%%%%%%%%%%%%%%%%%%%%%%%%%%%%%%%%%
%%%%%%%%%%%%%%%%%%%%%%%%%%%%%%%%%%%%%%%%%%%%%%%%%%%%%%%%%%%%%%%%%%%%%%%%%%%%

%-------------------------------------------------------------------------
%Porosity
 disp(' ')
 phi=input('Please enter POROSITY {0-1} []:>');
%-------------------------------------------------------------------------

%Permeability
 disp(' ')
 perm=input('Please enter PERMEABILITY [m^2]:>');

%-------------------------------------------------------------------------

%Permeability Conversion
 cm=perm/1e-4;
 darcy=perm/9.869e-12;
 mdarcy=(darcy*1e3);
 msec=(darcy/1e5);
 disp(' ')
 disp(['             PERMEABILITY IS [cm^2] 'num2str(cm)])
 disp(' ')
 disp(['             PERMEABILITY IS [d] 'num2str(darcy)])
 disp(' ')
 disp(['             PERMEABILITY IS [md] 'num2str(mdarcy)])

%-------------------------------------------------------------------------

%Grain Density
 disp(' ')
 rden=input('Please enter GRAIN DENSITY [kg/m^3]:>');

%-------------------------------------------------------------------------

%Grain Bulk Modulus
 disp(' ')
 rmod=input('Please enter GRAIN BULK MODULUS [Pa]:>');

%-------------------------------------------------------------------------

%Pore Fluid Density
 disp(' ')
 frho=input('Please enter PORE FLUID DENSITY [kg/m^3]:>');

%-------------------------------------------------------------------------

%Pore Fluid Bulk Modulus
 disp(' ')
 fmod=input('Please enter PORE FLUID BULK MODULUS [Pa]:>');

%-------------------------------------------------------------------------
%Pore Fluid Viscosity
 viscf=1e-3;
```

```
 disp(' ')
 disp(['             PORE FLUID VISCOSITY [Pa sec] IS
'num2str(viscf)]);
%-------------------------------------------------------------------------
%Frame Poisson's Ratio
 disp(' ')
 frmnu=input('Please enter EVALUATED FRAME POISSON RATIO []:>');

%-------------------------------------------------------------------------
%Structure Factor
 disp(' ')
 fac=input('Please enter EVALUATED STRUCTURE FACTOR [1.00-3.00]:>');

%-------------------------------------------------------------------------
%Depth

 disp(' ')
 dep=input('Please enter DEPTH OF INVESTIGATION [mbsf]:>');

%-------------------------------------------------------------------------
%Frequency

 disp(' ')
 ifreq=input('Please enter INITIAL FREQUENCY  [Hz] :>');
 disp(' ')
 ffreq=input('Please enter FINAL FREQUENCY    [Hz] :>');
 disp(' ')
 sfreq=input('Please enter FREQUENCY STEP     [Hz] :>');

%-------------------------------------------------------------------------

%Log-decrement Ratio

 disp(' ')
 egrat=1input('Please enter LOGARITHMIC DECREMENT RATIO {1.00-1.500} []
:>');

%-------------------------------------------------------------------------
%Log-decrement Ratio

 disp(' ')
 low=input('Please enter LOW LOGARITHMIC DECREMENT RATIO {0.005-0.500}
[] :>');

%%%%%%%%%%%%%%%%%%%%%%%%%%%%%%%%%%%%%%%%%%%%%%%%%%%%%%%%%%%%%%%%%%%%%%%%
%4-SEDIMENT SATURATED DENSITY & VOID INDEX %%%%%%%%%%%%%%%%%%%%%%%%%%%%%
%%%%%%%%%%%%%%%%%%%%%%%%%%%%%%%%%%%%%%%%%%%%%%%%%%%%%%%%%%%%%%%%%%%%%%%%
 disp(' ')
 rho=((1-phi)*rden)+(phi*frho);
 disp(['             SATURATED SEDIMENT DENSITY [kg/m^3] IS
'num2str(rho)])

%-------------------------------------------------------------------------
%Void index

 e=phi/(1-phi);
```

```
 disp(' ')
 disp(['              VOID INDEX IS 'num2str(e)])

%%%%%%%%%%%%%%%%%%%%%%%%%%%%%%%%%%%%%%%%%%%%%%%%%%%%%%%%%%%%%%%%%%%%%%%%%%%%
%4-FREQUENCY %%%%%%%%%%%%%%%%%%%%%%%%%%%%%%%%%%%%%%%%%%%%%%%%%%%%%%%%%%%%%%
%%%%%%%%%%%%%%%%%%%%%%%%%%%%%%%%%%%%%%%%%%%%%%%%%%%%%%%%%%%%%%%%%%%%%%%%%%%%

 nfreq=(ifreq:sfreq:ffreq);
 npts=length(nfreq);
 omega= 2*pi*nfreq;

%-------------------------------------------------------------------------
%Pore Size Parameter and size

 hr=(sqrt((5*perm)/phi));
 disp(' ')
 disp(['              CALCULATED PORE RADIUS IS [cm] 'num2str(hr*100)])
 a=2*hr;
 disp(' ')
 disp(['              CALCULATED PORE SIZE PARAMETER "a" IS [cm]
'num2str(a)])
 mgs=(a/0.155)*100;
 disp(' ')
 disp(['              CALCULATED MEAN GRAIN SIZE IS [cm] 'num2str(mgs)])
 phiunit=-3.322*log10(mgs);
 disp(' ')
 disp(['              CALCULATED MEAN GRAIN SIZE IS [phi]
'num2str(phiunit)])

%%%%%%%%%%%%%%%%%%%%%%%%%%%%%%%%%%%%%%%%%%%%%%%%%%%%%%%%%%%%%%%%%%%%%%%%%%%%
%5-KELVIN FUNCTION %%%%%%%%%%%%%%%%%%%%%%%%%%%%%%%%%%%%%%%%%%%%%%%%%%%%%%%%
%%%%%%%%%%%%%%%%%%%%%%%%%%%%%%%%%%%%%%%%%%%%%%%%%%%%%%%%%%%%%%%%%%%%%%%%%%%%

 rz = sqrt(2);
 for n=1:npts
     z(n)=sqrt(nfreq(n).*2*pi*frho/viscf)*hr;
  if z(n)>8
    t1=1/rz-3/(8*z(n))-15/(64*rz*z(n)^2)-
45/(512*z(n)^3)+315/(8192*rz*z(n)^4);

t2=1/rz+1/(8*z(n))+9/(64*rz*z(n)^2)+39/(512*z(n)^3)+75/(8192*rz*z(n)^4)
;
    d4=1+1/(4*rz*z(n))+1/(64*z(n)^2)-33/(256*rz*z(n)^3)-
1797/(8192*z(n)^4);
    tr=t1/d4;
    ti=t2/d4;
  else
    ber=1;
    dber=0;
    sign=-1;
    for m=4:4:32
      den=1;
      for mm=2:2:m
        den=mm*mm*den;
      end
```

```
      ber=sign*z(n)^m/den+ber;
      dber=sign*z(n)^(m-1)/den*m+dber;
      sign=-sign;
    end
    bbei=0;
    ddbei=0;
    sign=1;
    for m=2:4:30
      den=1;
      for mm=2:2:m
        den=mm*mm*den;
      end
      bbei=sign*z(n)^m/den+bbei;
      ddbei=sign*z(n)^(m-1)/den*m+ddbei;
      sign=-sign;
    end
    tr=(bbei*ddbei+ber*dber)/(ber*ber+bbei*bbei);
    ti=(ber*ddbei-bbei*dber)/(ber*ber+bbei*bbei);
  end
  ffr(n)=(0.25*z(n)*(tr*(1-2*ti/z(n))+ti*tr*2/z(n)))/((1-
2*ti/z(n))^2+(2*tr/z(n))^2);
  fi(n)=(0.25*z(n)*(ti*(1-2*ti/z(n))-tr*tr*2/z(n)))/((1-
2*ti/z(n))^2+(2*tr/z(n))^2);
 kel(n)=ffr(n)+j*fi(n);
 end

%%%%%%%%%%%%%%%%%%%%%%%%%%%%%%%%%%%%%%%%%%%%%%%%%%%%%%%%%%%%%%%%%%%%%%%%%%%%
%6-"m" PARAMETER %%%%%%%%%%%%%%%%%%%%%%%%%%%%%%%%%%%%%%%%%%%%%%%%%%%%%%%%%%
%%%%%%%%%%%%%%%%%%%%%%%%%%%%%%%%%%%%%%%%%%%%%%%%%%%%%%%%%%%%%%%%%%%%%%%%%%%%

 mpar=fac*frho/phi;
 disp(' ')
 disp(['             THE "m" PARAMETER VALUE IS 'num2str(mpar)])

%%%%%%%%%%%%%%%%%%%%%%%%%%%%%%%%%%%%%%%%%%%%%%%%%%%%%%%%%%%%%%%%%%%%%%%%%%%%
%7-FRAME ELASTICS %%%%%%%%%%%%%%%%%%%%%%%%%%%%%%%%%%%%%%%%%%%%%%%%%%%%%%%%%%
%%%%%%%%%%%%%%%%%%%%%%%%%%%%%%%%%%%%%%%%%%%%%%%%%%%%%%%%%%%%%%%%%%%%%%%%%%%%

%-------------------------------------------------------------------------
%Vertical Stress

 depth=dep/0.3048;
 ggrav=rden/frho;
 overpsi=((1-phi)*(ggrav-1)*62.42796*depth)/144;
 overpascal=overpsi*6.894757e3;
 disp(' ')
 disp(['             VERTICAL EFFECTIVE STRESS [Pa] IS
'num2str(overpascal)])
 disp(' ')

%-------------------------------------------------------------------------
%Effective Stress

 if fac > 2
 averagepsi=(1/3)*(3*overpsi);
```

```
coeff=1630;
elseif fac <= 2
averagepsi=(1/3)*(overpsi+(overpsi/2)+(overpsi/2));
coeff=2630;
end
sigmapascal=averagepsi*6.894757e3;
disp(' ')
disp(['             EFFECTIVE STRESS [Pa] IS 'num2str(sigmapascal)])

%-------------------------------------------------------------------------
%Frame Shear Modulus (Re)

gr=(((coeff*(2.97-e)^2)/(1+e))*sqrt(averagepsi))*6.894757e3;
disp(' ')
disp(['             FRAME SHEAR MODULUS (Re) [Pa] IS 'num2str(gr)])

%-------------------------------------------------------------------------
%Shear Logarithmic Decrement (Viscous Losses Model)

alpha=0.2;amfac=0.16;peakfreq=10000;
tau=1/(2*pi*peakfreq);
Mr1=gr;
Mi1=low*Mr1/pi;
Mr2=Mr1*amfac;
A1A=1-alpha;
dn=1+2*(omega*tau).^A1A*sin(alpha*pi/2)+(omega*tau)*(2.*A1A);
Mr3=Mr2-(Mr2*(1+(omega.*tau).^A1A*sin(alpha*pi/2))./dn;
Mi3=Mr2*(omega.*tau).^A1A*cos(alpha*pi/2)./dn;
Mr=Mr1+Mr3;
Mi=Mi1+Mi3;
dec=Mi./Mr*pi;

%-------------------------------------------------------------------------
%Frame Shear Modulus (Im)

gdec=dec;
gi=gdec.*gr/pi;

%-------------------------------------------------------------------------
%Frame Young's Modulus (Re)

emodr=2*gr*(frmnu+1);

%-------------------------------------------------------------------------
%Frame Young's Modulus (Im)

emodi=egrat.*gi./gr.*emodr;

%-------------------------------------------------------------------------
%Frame Bulk Modulus (Re)

br=gr*((2+2*frmnu)/(3-6*frmnu));
disp(' ')
disp(['             FRAME BULK MODULUS (Re) [Pa] IS 'num2str(br)])
```

```
%-------------------------------------------------------------------------
%Frame Bulk Modulus (Im)

 bi=(3*gr*gr.*emodi-emodr.*emodr.*gi)./(3*gr-emodr)./(3*gr-emodr)/3;
%-------------------------------------------------------------------------
%Complex Moduli

 cbulk=br+i*bi;
 cshear=gr+i*gi;

%-------------------------------------------------------------------------
%D Coefficient

 D=rmod*(1+phi*(rmod/fmod-1));

%-------------------------------------------------------------------------
%H Coefficients

 H=((rmod-cbulk).^2./(D-(cshear)))+cbulk+(4*(cshear)/3);

%-------------------------------------------------------------------------
%C Coefficients

 C=rmod*(rmod-(br+i*bi))./(D-(br+i*bi));

%-------------------------------------------------------------------------
%M Coefficients

 M=rmod^2./(D-(cbulk));

%%%%%%%%%%%%%%%%%%%%%%%%%%%%%%%%%%%%%%%%%%%%%%%%%%%%%%%%%%%%%%%%%%%%%%%%
%8-WAVE NUMBERS AND ATTENUATION COEFFICIENTS %%%%%%%%%%%%%%%%%%%%%%%%%%%
%%%%%%%%%%%%%%%%%%%%%%%%%%%%%%%%%%%%%%%%%%%%%%%%%%%%%%%%%%%%%%%%%%%%%%%%

h=waitbar(0,'PLEASE WAIT FOR COMPRESSIONAL WAVE SOLUTIONS');
 for n=1:npts
 ac=C.^2-(H.*M);
 bc=(H*mpar.*omega.^2)-
((H*i.*omega.*kel(n)*viscf)/perm)+(M*rho.*omega.^2)-
(2*C*frho.*omega.^2);
 cc=((frho^2-
mpar*rho).*omega.^4)+omega.^2.*((rho*i*omega.*kel(n)*viscf)/perm);
 q=sqrt(roots([ac(n) bc(n) cc(n)]))';
     fid=fopen('comp.dat','a+');
     fprintf(fid,'%e    %e\n',abs(real(q)));
     fid=fopen('calpha.dat','a+');
     fprintf(fid,'%e    %e\n',abs(imag(q)));
 waitbar(n/npts);
 end
 close(h)

%-------------------------------------------------------------------------

as=((i.*omega.*kel(n)*viscf)/perm).*cshear-(mpar*(omega).^2).*cshear;
```

```
cs=((mpar*rho-frho^2).*omega.^4)-
omega.^2.*((rho*i*omega.*kel(n)*viscf)/perm);
h=waitbar(0,'PLEASE WAIT FOR SHEAR WAVE SOLUTIONS');
for n=1:npts
    w=roots([as(n) 0 cs(n)])';
    fid=fopen('shear.dat','a+');
    fprintf(fid,'%e    %e\n',abs(real(w)));
    fid=fopen('salpha.dat','a+');
    fprintf(fid,'%e    %e\n',abs(imag(w)));
waitbar(n/npts)
end
close(h)

%%%%%%%%%%%%%%%%%%%%%%%%%%%%%%%%%%%%%%%%%%%%%%%%%%%%%%%%%%%%%%%%%%%%%%%%%%%%
%9-WAVE VELOCITIES %%%%%%%%%%%%%%%%%%%%%%%%%%%%%%%%%%%%%%%%%%%%%%%%%%%%%%%%
%%%%%%%%%%%%%%%%%%%%%%%%%%%%%%%%%%%%%%%%%%%%%%%%%%%%%%%%%%%%%%%%%%%%%%%%%%%%

load comp.dat;
load shear.dat;

%-------------------------------------------------------------------------
%Wave Numbers

wnpf=comp(:,2)';
wnps=comp(:,1)';
snp=shear(:,1)';

%-------------------------------------------------------------------------
%Calculated Velocities

vpf=omega./wnpf;
vps=omega./wnps;
vs=omega./snp;

load *.txt %in-situ datafiles

%%%%%%%%%%%%%%%%%%%%%%%%%%%%%%%%%%%%%%%%%%%%%%%%%%%%%%%%%%%%%%%%%%%%%%%%%%%%
%10-ATTENUATION PARAMETERS %%%%%%%%%%%%%%%%%%%%%%%%%%%%%%%%%%%%%%%%%%%%%%%%
%%%%%%%%%%%%%%%%%%%%%%%%%%%%%%%%%%%%%%%%%%%%%%%%%%%%%%%%%%%%%%%%%%%%%%%%%%%%

load calpha.dat;
load salpha.dat;
fca=calpha(:,2)'*8.686;
sca=calpha(:,1)'*8.686;
sa=salpha(:,1)'*8.686;

%%%%%%%%%%%%%%%%%%%%%%%%%%%%%%%%%%%%%%%%%%%%%%%%%%%%%%%%%%%%%%%%%%%%%%%%%%%%
%11-PHASE VELOCITIES AND ATTENUATION PLOTS %%%%%%%%%%%%%%%%%%%%%%%%%%%%%%%%%
%%%%%%%%%%%%%%%%%%%%%%%%%%%%%%%%%%%%%%%%%%%%%%%%%%%%%%%%%%%%%%%%%%%%%%%%%%%%

%-------------------------------------------------------------------------
%Compressional Waves

fig1=figure('Name','COMPRESSIONAL WAVES OUTPUT','NumberTitle','off');
figure(fig1)
```

```
subplot(2,1,1)
semilogx(nfreq,vpf,f1,v1,'*');
grid on
ylabel('m/sec')
title('First Kind Compressional Wave Velocities');
subplot(2,1,2);
loglog(nfreq,fca,f1,af1,'*')
grid on
ylabel('dB/m')
xlabel('Log Frequency');
title('First Kind Compressional Wave Attenuation');
%figure
%subplot(2,1,1)
%semilogx(nfreq,vps);
%grid on
%ylabel('m/sec')
%title('Second Kind Compressional Wave Velocities');
%subplot(2,1,2)
%loglog(nfreq,sca)
%grid on
%ylabel('dB/m');
%xlabel('Log Frequency');
%title('Second Kind Compressional Wave Attenuation');

%-------------------------------------------------------------------------
%Shear Waves
fig2=figure('Name','SHEAR WAVES OUTPUT','NumberTitle','off');
figure(fig2)
subplot(2,1,1)
semilogx(nfreq,vs);
grid on
ylabel('m/sec')
title('Shear Wave Velocities');
subplot(2,1,2);
loglog(nfreq,sa);
grid on
ylabel('dB/m');
xlabel('Log Frequency');
title('Shear Wave Attenuation');

%%%%%%%%%%%%%%%%%%%%%%%%%%%%%%%%%%%%%%%%%%%%%%%%%%%%%%%%%%%%%%%%%%%%%%%%%%%
%12-SAVE DATA AGAIN %%%%%%%%%%%%%%%%%%%%%%%%%%%%%%%%%%%%%%%%%%%%%%%%%%%%%%
%%%%%%%%%%%%%%%%%%%%%%%%%%%%%%%%%%%%%%%%%%%%%%%%%%%%%%%%%%%%%%%%%%%%%%%%%%%

A=[nfreq' vpf' fca' vs' sa'];
save test.txt A -ascii;

%%%%%%%%%%%%%%%%%%%%%%%%%%%%%%%%%%%%%%%%%%%%%%%%%%%%%%%%%%%%%%%%%%%%%%%%%%%
%13-DATA OUTPUT %%%%%%%%%%%%%%%%%%%%%%%%%%%%%%%%%%%%%%%%%%%%%%%%%%%%%%%%%%
%%%%%%%%%%%%%%%%%%%%%%%%%%%%%%%%%%%%%%%%%%%%%%%%%%%%%%%%%%%%%%%%%%%%%%%%%%%

fig3=figure('Name','MODEL DATA OUTPUT','NumberTitle','off');
figure(fig3)
```

```
 lbl1=uicontrol('Style','text','Units','normalized','Position',[0.05
0.8 0.5   0.1],'HorizontalAlignment','left','BackgroundColor',[0.8 0.8
0.8],'String','Void Index','FontWeight','bold');


data1=uicontrol('Style','text','Units','normalized','Position',[0.7 0.8
0.2 0.1],'HorizontalAlignment','left','BackgroundColor',[0.8 0.8
0.8],'String',num2str(e),'FontWeight','bold');

 lbl2=uicontrol('Style','text','Units','normalized','Position',[0.05
0.7 0.5 0.1],'HorizontalAlignment','left','BackgroundColor',[0.8 0.8
0.8],'String','Saturated Density     [kg/m3]','FontWeight','bold');

 data2=uicontrol('Style','text','Units','normalized','Position',[0.7
0.7 0.2 0.1],'HorizontalAlignment','left','BackgroundColor',[0.8 0.8
0.8],'String',num2str(rho),'FontWeight','bold');

 lbl3=uicontrol('Style','text','Units','normalized','Position',[0.05
0.6 0.5 0.1],'HorizontalAlignment','left','BackgroundColor',[0.8 0.8
0.8],'String','"m" Parameter','FontWeight','bold');

 data3=uicontrol('Style','text','Units','normalized','Position',[0.7
0.6 0.2 0.1],'HorizontalAlignment','left','BackgroundColor',[0.8 0.8
0.8],'String',num2str(mpar),'FontWeight','bold');

 lbl4=uicontrol('Style','text','Units','normalized','Position',[0.05
0.5 0.5 0.1],'HorizontalAlignment','left','BackgroundColor',[0.8 0.8
0.8],'String','Pore-Size Parameter','FontWeight','bold');

 data4=uicontrol('Style','text','Units','normalized','Position',[0.7
0.5 0.2 0.1],'HorizontalAlignment','left','BackgroundColor',[0.8 0.8
0.8],'String',num2str(a),'FontWeight','bold');

 lbl5=uicontrol('Style','text','Units','normalized','Position',[0.05
0.4 0.5 0.1],'HorizontalAlignment','left','BackgroundColor',[0.8 0.8
0.8],'String','Pore Radius   [cm]','FontWeight','bold');

 data5=uicontrol('Style','text','Units','normalized','Position',[0.7
0.4 0.2 0.1],'HorizontalAlignment','left','BackgroundColor',[0.8 0.8
0.8],'String',num2str(hr),'FontWeight','bold');

 lbl6=uicontrol('Style','text','Units','normalized','Position',[0.05
0.3 0.5 0.1],'HorizontalAlignment','left','BackgroundColor',[0.8 0.8
0.8],'String',...
'Mean Grain Size   [cm]','FontWeight','bold');

 data6=uicontrol('Style','text','Units','normalized','Position',[0.7
0.3 0.2 0.1],'HorizontalAlignment','left','BackgroundColor',[0.8 0.8
0.8],'String',num2str(mgs),'FontWeight','bold');

 lbl7=uicontrol('Style','text','Units','normalized','Position',[0.05
0.2 0.5 0.1],'HorizontalAlignment','left','BackgroundColor',[0.8 0.8
0.8],'String','Dynamic Permeability   [darcy]','FontWeight','bold');
```

```
 data7=uicontrol('Style','text','Units','normalized','Position',[0.7
0.2 0.2 0.1],'HorizontalAlignment','left','BackgroundColor',[0.8 0.8
0.8],'String',num2str(darcy),'FontWeight','bold');

 lbl8=uicontrol('Style','text','Units','normalized','Position',[0.05
0.1 0.5 0.1],'HorizontalAlignment','left','BackgroundColor',[0.8 0.8
0.8],'String','Dynamic Permeability   [cm/sec]','FontWeight','bold');
 data8=uicontrol('Style','text','Units','normalized','Position',[0.7
0.1 0.2 0.1],'HorizontalAlignment','left','BackgroundColor',[0.8 0.8
0.8],'String',num2str(msec),'FontWeight','bold');

 lbl9=uicontrol('Style','text','Units','normalized','Position',[0.05
0.0 0.5 0.1],'HorizontalAlignment','left','BackgroundColor',[0.8 0.8
0.8],'String','Mean Grain Size [phi]','FontWeight','bold');

 data9=uicontrol('Style','text','Units','normalized','Position',[0.7
0.0 0.2 0.1],'HorizontalAlignment','left','BackgroundColor',[0.8 0.8
0.8],'String',num2str(phiunit),'FontWeight','bold');
```

REFERENCES

Barbagelata A., Richardson M. D., Miaschi B., Muzi E., Guerrini P., Troiano L., Akal T., 1991.

"ISSAMS: An In Situ Sediment Acoustic Measurement System" - Shear Waves In Marine Sediments

Bathen K. H., 1968.

"A Descriptive Study of the Physical Oceanography of Kaneohe Bay, Oahu, Hawai'i" - University of Hawai'i Technical Report 14

Berryman J. G., 1980.

"Confirmation of Biot's Theory" - Applied Physics Letters 37

Biot M. A., 1941.

"General Theory of Three-Dimensional Consolidation" - Journal of Applied Physics 12

Biot M. A., 1956a.

"Theory of Propagation of Elastic Waves in a Fluid-Saturated Porous Solid. I Low Frequency Range" - Journal of the Acoustic Society of America 28

Biot M. A., 1956b.

"Theory of Propagation of Elastic Waves in a Fluid-Saturated Porous Solid. II Higher Frequency Range" - Journal of the Acoustic Society of America 28

Birch F. et al., 1960a.

"The Velocity of Compressional Waves in Rocks to 10 kbar: Part I" - Journal of Geophysical Research 65

Birch F. et al., 1960b.

"The Velocity of Compressional Waves in Rocks to 10 kbar: Part II" - Journal of Geophysical Research 66

Brunson B. A., Johnson R. K., 1980.

"Laboratory Measurements of Shear Wave Attenuation in Saturated Sands" - Journal of the Acoustic Society of America 68

Brunson B. A., 1983.

"Shear Wave Attenuation in Unconsolidated Laboratory Sediments" - NORDA Tech. Note 159

Bryan G. M., 1984.

"A Compaction Model for Compressional Wave Velocity" - Journal of the Acoustic Society of America 76

Bryiant W. R., Hottmann W., Trabant P., 1975.

"Permeability of Unconsolidated and Consolidated Marine Sediments, Gulf of Mexico" - Marine Geotechnics 1

Chave E. H. et al., 1973.

"A Historical sketch of the Kaneohe Bay Region" - Atlas of Kaneohe Bay: A Reef Ecosystem under Stress, University Sea Grant Program TR-02-71

Cole B. F., 1965.

"Marine Sediment Attenuation and the Ocean Bottom Reflected Sound" - Journal of the Acoustic Society of America 38

Donaldson E. C., Tiab D., 1996.

"Petrophysics" - Petroleum Engineering, Gulf Publishing Company

Dutta N. C., Ode H., 1979.

"Attenuation and Dispersion of Compressional Waves in Fluid-Filled Porous Rocks with Partial Gas Saturation (White Model): Part I Biot Theory" - Geophysics 44

Fan P. F., 1975.

"Sediment of Kaneohe Bay, Oahu, Hawai'i" - Consultant Reports, U.S. Army Corps of Engineers Appendix II

Frazer L. N., Wilkens R. H., 1997.

"Changes in Attenuation with Depth in an Ocean Carbonate Section: Ocean Drilling Program Sites 806 and 807, Ontong Java Plateau" - Journal of Geophysical Research 102-B2

Fu S. S., Wilkens R. H., Frazer L. N., 1998.

"Hamilton's Parameters and the Acoustic Properties of Coral Sands, Waikiki, Hawai'i" - Accepted for Publication on Journal of the Acoustic Society of America

Gassman F., 1951.

"Elastic Waves Through a Packing of Spheres" - Vierteljahrsschrift Naturforschenden Gesellschaft in Zurich, Zurich 96

Gentilman R. L., Fiore D. F., Path H. T., French K. W., Bowen L. J., 1994.

"Fabrication and Properties of 1-3 PZT Polymer Composites" - Ceramic Transactions 43

Hamilton E. L., 1970.

"Sound Velocity and Related Properties of Marine Sediments, North Pacific" - Journal of Geophysical Research 75

Hamilton E. L., 1972.

"Compressional Wave Attenuation in Marine Sediments" - Geophysics 37

Hamilton E. L., 1975.

"Acoustic and Related Properties of the Seafloor: Density and Porosity Profiles and Gradients" – NUC Technical Paper 459

Hamilton E. L., 1980.

"Geoacoustic Modeling of the Seafloor" - Journal of the Acoustic Society of America 68

Hampton L. D., 1967.

"Acoustic Properties of Sediment: an Update" - Journal of the Acoustic Society of America 42

Hardin B. O., Richart F. E. Jr., 1963.

"Elastic Wave Velocities in Granular Soils" - Journal of Soil Mechanics Foundation Division ASCE 89

Hardin B. O., Black W. L., 1968.

"Vibration Modulus of Normally Consolidated Clay" - Journal of Soil Mechanics Foundation Division ASCE 94

Hollet K. J., 1997.

"Shoaling of Kaneohe Bay, Oahu, Hawai'i, in the Period 1927 to 1976, Based on Bathymetric, Sedimentological and Geophysical Studies" - Master of Science in Geology and Geophysics Thesis, University of Hawai'i at Manoa

Hovem J. M., Ingram J. D., 1979.

"Viscous Attenuation of Sound in Saturated Sand" - Journal of the Acoustic Society of America 66

Jackson M. L., Levelt T. W. M., Syers J. K., Rex R. W., Sherman G. D., Uehara G., 1971.

"Geomorphological Relationships of Tropo-Spherically Derived Quartz in the Soils of the Hawaiian Islands" - Soil Society American Proceedings 35

Kibblewhite A. C., 1989.

"Attenuation of Sound in Marine Sediments: a Review with Emphasis on New Low-Frequency Data" - Journal of the Acoustic Society of America 86

Lambe T. W., Whitman R. V., 1970.

"Soil Mechanics", Wiley & Sons, New York

Lewis D.C., 1984.

"Practical Sedimentology", Hutchinson Ross Publishing Company

Macdonald G. A., Abbot A. T., 1970.

"Volcanoes in the Sea: the Geology of Hawai'i' - University of Hawai'i Press

Moberly R., 1963a.

"Rate of Denudation in Hawai'i" - Journal of Geology 71

Moberly R., 1963b.

"Amorphous Marine Muds from Tropically Weathered Basalts" - American Journal of Science 261

Moberly R., Campbell J. F., 1969.

"Hawaiian Shallow Marine Sand Inventory" - University of Hawai'i, National Science Foundation Sea Grant Program GH-28

Ogushwitz P. R., 1985a.

"Applicability of the Biot Theory I: Low-Porosity Materials" - Journal of the Acoustic Society of America 77

Ogushwitz P. R., 1985b.

"Applicability of the Biot Theory II: Suspensions" - Journal of the Acoustic Society of America 77

Ogushwitz P. R., 1985c.

"Applicability of the Biot Theory III: Wave Speed versus Depth" - Journal of the Acoustic Society of America 77

Rex R. W., Syers J. K., Jackson M. L., Clayton R. N., 1969.

"Eolian Origin of Quartz in Soils of Hawaiian Islands and in the Pacific Pelagic Sediments" - Science 163

Richardson M. D., 1983.

"The Effects of Bioturbation on Sediment Elastic Properties" - Bulletin Societe Geologique de France 25

Richardson M. D., 1986. "Implications for High Frequency Acoustic Propagation and Scattering" - Geo-Marine Letters

Richardson M. D., 1993.

"On the Use of acoustic Impedance Values to Determine Sediment Properties" - Proc. I. O. A. 15-2

Roy K. J., 1970.

"Change in Bathymetric Configuration, Kaneohe Bay, Oahu" - University of Hawai'i , Hawai'i Institute of Geophysics Technical Report 70-15

Schon J. H., 1996.

"Physical Properties of Rocks: Fundamentals and Principles of Petrophysics" - Handbook of Geophysical Exploration, Pergamon 18

Shumway G., 1970.

"Sound Speed and Absorption Studies of Marine Sediments" - Journal of the Acoustic Society of America 47

Spencer J. W. Jr., Cates M. E., Thompson D. H., 1994.

"Frame Moduli of Unconsolidated Sands and Sandstones" – Geophysics 59

Stearns H. T., Vaksvik K. N., 1935.

"Geology and Groundwater Resources of the Island of Oahu, Hawai'i" - Division of Hydrography, State of Hawai'i

Stearns H. T., 1940.

"Supplement to Geology and Groundwater Resources of the Island of Oahu, Hawai'i" - Division of Hydrography, State of Hawai'i

Stearns H. T., 1966.

"Geology of the State of Hawai'i"

Stoll R. D., Bryan G., 1970.

"Wave Attenuation in Saturated Sediments" - Journal of the Acoustic Society of America 47

Stoll R. D., 1974.

"Acoustic Waves in Saturated Sediments" - Physics of Sound in Marine Sediments

Stoll R. D., 1977.

"Acoustic Waves in Ocean Sediments" - Geophysics 42

Stoll R. D., 1980.

"Theoretical Aspects of Sound Transmission in Sediments" - Journal of the Acoustic Society of America 68

Stoll R. D., 1985.

"Marine Sediment Acoustics" - Journal of the Acoustic Society of America 77

Stoll R. D., 1989.

"Sediment Acoustic" - Lectures Notes in Earth Science 26

The MathWorks, Inc., 1997. MATLAB v5.0

Toskoz M. N., Johnston D. H., 1981a.

"Definitions and Terminology" - Seismic Wave Attenuation Edition

Toskoz M. N., Johnston D. H., 1981b.

"Attenuation of Seismic Waves in Dry and Saturated Rocks" - Seismic Wave Attenuation Edition

Tullos F. N., Reid A. C., 1969.

"Seismic Attenuation of Gulf Coast Sediments" - Geophysics 34

Urik R. J., 1947.

"A Sound Velocity Method for Determining Compressibility of Finely Subdivided Substances"- Journal of Applied Physics

Zhou J. et al., 1987a.

"Geoacoustic Parameters in a Stratified Sea Bottom from Shallow Water Acoustic Propagation" - Journal of the Acoustic Society of America 82

Zhou J. et al., 1987b.

"Effect of Frequency Dependence of Sea-Bottom Attenuation on the Optimum Frequency for Acoustic Propagation in Shallow Water" - Journal of the Acoustic Society of America 82

White J. E., 1975.

"Computed Seismic Speeds and Attenuation in Rocks with Partial Gas Saturation" - Geophysics 40

Winkler K., Nur A., 1981.

"Pore Fluids and Seismic Attenuation" - Seismic Wave Attenuation Edition

Wood, A. B. Weston D. E., 1964.

"The Propagation of Sound in Mud" - Acustica 14